UNIVERSITY OF SOUTHAMPTON

FACULTY OF ENVIRONMENTAL AND LIFE SCIENCE

OCEAN AND EARTH SCIENCES

Determining the controls on flow behaviour, bedform development and stratigraphic architecture from detailed surveys and monitoring of active submarine channels

By

DANIELA VENDETTUOLI

Thesis for the degree of Doctor of Philosophy

March 2021

University of Southampton

Faculty of Environmental and Life Sciences

Ocean and Earth Science

Thesis for the degree of Doctor of Philosophy

Determining the controls on flow behaviour, bedform development and stratigraphic architecture from detailed surveys and monitoring of active submarine channels

By Daniela Vendettuoli

Abstract

Seafloor-hugging flows, known as turbidity currents, transport sediment from shallow to deep water via submarine channels. These flows carry globally important volumes of sediment, and transport organic carbon, oxygenated waters, nutrients and contaminants that accumulate within submarine channels and at their downslope terminal lobes or submarine fans. The often-powerful nature of turbidity currents poses a significant hazard to critical seafloor infrastructure. Previous studies have largely relied upon the study of ancient deposits or scaled-down measurements of laboratory-scale flows to understand turbidity currents. Several conceptual models exist, but it remains unclear as to whether turbidity currents show a distinct behaviour at different scales, or if a continuum of behaviour exists from small to large events. Recent technological advances allow us to investigate these issues. The advent of Autonomous Underwater Vehicles enables mapping of the seafloor at unprecedented detail, repeat surveys record previously-unseen seascape changes, while Acoustic Doppler Current Profilers record the range of internal structures observed in field-scale turbidity currents for the first time. In this thesis, I use high-resolution data acquired in several modern offshore systems to analyse turbidity current behaviour across various spatial and temporal scales. First, a global analysis of direct velocity measurements of turbidity currents reveals two end-member modes of turbidity current behaviour that range from: i) a sudden peak in velocity that decays exponentially, lasting minutes to hours; to ii) sustained flow that lasts for days. I show that a continuum exists between these flow modes; likely controlled by the proportion of sand or mud within the flow. Second, an extensive (65 x 50 km) and detailed (5 m bin size) seafloor survey offshore East Africa, reveals a variety of bedforms within two deep-sea canyons. Morphometric analysis reveals a continuum from small-scale (10s m wavelength) crescentic bedforms to large-scale (kms wavelength) sediment waves. This continuum is in contrast with a previous global study, but that study did include such high-resolution deep-

water data. Previous studies may have missed an intermediate scale of bedform due to the decreasing resolution with increasing water depth-related. Small to medium-scale bedforms may be more common in the deep sea than currently thought. Third, I analyse repeat mapping of an active submarine delta to reveal how turbidity currents build stratigraphy. As a result of the reworking caused by repeated flows, the completeness of the stratigraphy record over three months is found to be 10% on average. The stratigraphic record is dominated by large events. Large slope failures are more likely to be preserved than smaller bedforms, while erosion is dominated by rare, but powerful turbidity currents that can obscure the record of smaller flows.

I conclude that a continuum in turbidity current behaviour exists across various scales of flow, from small fjord channel systems to the largest submarine channels on the planet. The mode of flow is dominantly controlled by the grain size of the sediment available in the system. The continuum in bedform scales reflects both the downstream evolution of turbidity currents, as they expand due to mixing with ambient seawater and entrainment of seafloor sediment, and modifications caused by seafloor morphology. What becomes recorded in stratigraphy does not show a gradual continuum, however, and instead appears to be strongly biased by larger but infrequent events. These findings from modern systems provide new insights to inform the understanding of ancient depositional records and have implications for assessing seafloor hazards and understanding deep-sea sediment transport in general.

Table of Contents

List of Figures

List of Tables

Research Thesis: Declaration of Authorship

Print name: Daniela Vendettuoli

Title of thesis:

Determining the controls on flow behaviour, bedform development and stratigraphic architecture from detailed surveys and monitoring of active submarine channels

I declare that this thesis and the work presented in it is my own and has been generated by me as the result of my own original research.

I confirm that:

This work was done wholly or mainly while in candidature for a research degree at this University;

Where any part of this thesis has previously been submitted for a degree or any other qualification at this University or any other institution, this has been clearly stated;

Where I have consulted the published work of others, this is always clearly attributed;

Where I have quoted from the work of others, the source is always given. With the exception of such quotations, this thesis is entirely my own work;

I have acknowledged all main sources of help;

Where the thesis is based on work done by myself jointly with others, I have made clear exactly what was done by others and what I have contributed myself;

Part of this work has or will be published in peer-reviewed scientific journals: see ”Publication” section

Date: March 2021

Publications

Journal publications arising from this thesis

*Note: * indicates submitted manuscripts*

D. Vendettuoli, M.A. Clare, J.E. Hughes Clarke, A. Vellinga, J. Hizzett, S. Hage, M.J.B. Cartigny, P.J. Talling, D. Waltham, S.M. Hubbard, C. Stacey, D.G. Lintern. Daily bathymetric surveys document how stratigraphy is built and its extreme incompleteness in submarine channels. Earth and Planetary Science Letters, Volume 515, 2019, 231-247

***D. Vendettuoli**, M. A. Clare, E.J. Sumner, M.J.B. Cartigny, P.J. Talling, J. Wood, L.P. Bailey, M. Azpiroz - Zabala, C.K. Paull, R. Gwiazda, J.P. Xu, C. Stacey, D.G. Lintern, S.M. Simmons, E.L Pope and S. Hage. Global monitoring data shows grain size controls turbidity current structure. Geophysical Research Letters, In Review.

Other Journal publications

Englert, R.G.; Hubbard, S.M.; Cartigny, M.J.B.; Clare, M.A.; Coutts, D.S.; Hage, S.; Hughes Clarke, J.; Jobe, Z.; Lintern, D.G.; Stacey, C.; **Vendettuoli, D**.; Normandeau, A. Quantifying the three-dimensional stratigraphic expression of cyclic steps by integrating seafloor and deep-water outcrop observations. Sedimentology, 2020.

S. Hage, M.J.B. Cartigny, M.A. Clare, E.J. Sumner, **D. Vendettuoli**, J.E. Hughes Clarke, S. M. Hubbard, P.J. Talling, D. G. Lintern, C. D. Stacey, R.G. Englert, M.E. Vardy, J.E. Hunt, M. Yokokawa, D.R. Parsons, J. L. Hizzett, M. Azpiroz-Zabala and A. J. Vellinga. How to recognise crescentic bedforms formed by supercritical turbidity currents in the geologic record: Insights from active submarine channels. Geology, 2018, 46 (6), 563–566

*Ye Chen, Parsons, D.R., Simmons, S.M., Williams, R., Cartigny, M.J.B, Hughes Clarke, J.E., Stacey, C.D., Hage, S., Talling, P.J., Azpiroz-Zabala, M., Clare, M.A., Heijnen, M.S., Heerema, C.J., Pope, E.L., Hizzett, J.L., Hunt, J.E., Lintern, d.G., Sumner, E.J., Vellinga, A.J., **Vendettuoli, D**. Knickpoints and crescentic bedform interactions in submarine channels. Sedimentology, 68 (4), 1358-1377.

Acknowledgements

Life is an extraordinary journey that we make in the lives of the people we meet - those we leave behind and those we decide to carry on with. The past ten years of my life have been really challenging. Started to question the meaning of my it and its purpose; got all the answers in the most difficult times The toughest of all was about the value of my life – how much it is worth?

During this journey, I have learned that the value of our life depends upon the value of the people we decide to share it with. Victory cannot ever be achieved only by because we need people to build and share it with, as a happy person is the one that is never alone during victories and defeats.

So, this section is about all those people who supported and helped me achieving this important goal. Many are the reasons I need to thank them for; here there are just few of them.

Firstly - I want to thank the Professor Peter Talling, because he was the one who opened the gate for all this to manifest in my life. And of course, for his immense contribute to my growth as student and researcher

Dr Michael Clare – my main supervisor for being always there. His support has been like a lantern in the dark to me. No matter how lost I was or how tough it was. Mike has always supported me,never through judgments – rather always smiling and using words of encouragements. A true mentor.

Dr Matthieu Cartigny – my supervisor. A person always in good moods and supportive. His good attitude has been very inspirational for me as well as his unshakable convictions in my abilities.

Dr Esther Sumner – my supervisor. Very supportive and always smiling.

Dr James Hunt – for the technical support, encouragement and kind words.

Age, James, Maria, Sophie, Lewis, Maarten - all part of this extraordinary journey. Thank you for your help, collaboration, and friendship.

I would also like to take this opportunity to thank my examiners, Dr Domenico Chiarella and Professor Ivan Haigh, for their valued comments/suggestions and time taken to read my thesis and conduct the examination. I appreciate the corrections they asked me to carry out which helped me in bringing out the value of my work even more than before. I have taken their comments and suggestions when updating my thesis. The whole PhD process for me has been one extensive learning experience and the same is true for the final examination.

Dr Raja Naeem Akram – one of my closest friends with who I have learned to value my life. Friendship is the most precious of all the treasures in life. And Raja, is a true friend.

Finally, I wish to thank all my friends and relative who during this last very challenging year supported me.

Emancipation is never an easy way to build up. And true happiness can only be achieved if

we become truly emancipated persons.

Chapter 1
Introduction

1.1 Rationale

Turbidity currents are subaqueous density flows that travel downslope due to the higher density of the sediment they carry in suspension compared to the ambient water (Daly, 1936; Middleton and Hamp,1976) (Figure 1.1 Panel A). They are amongst the most important sediment transport processes and form the some of the largest sedimentary bodies on our planet (Talling et al., 2012). Understanding the behaviour of these sediment-laden flows is important because it modulates the efficiency and extent transport of sediment, organic carbon and pollutants to the deep-sea, and dictates the nature of impacts to critical seafloor infrastructure such as telecommunication cables (Galy et al., 2007; Carter et al., 2014; Pohl et al., 2020; Zhong and Peng, 2021). In fact, one of the first lines of evidence for the existence of turbidity currents was a series of faults along sequential seafloor telecommunications cables in 1929, following a large earthquake-triggered submarine landslide that generated a long run-out turbidity current (Figure 1.1 Panel B; Stevenson et al., 2018). The importance of understanding this and similar events is heightened nowadays; particularly given our increased reliance on the network of subsea telecommunications cables that spans the world's oceans (Carter et al., 2014).

As turbidity currents are notoriously difficult to observe directly (Inman et al., 1976; Carter et al., 2014; Pope et al., 2017; Talling et al., 2015; Clare et al., 2017) (Figure 1.1 Panel A), we often rely on inferences made from studies of ancient deposits from outcrops of sediment cores, laboratory-scale physical experiments and numerical models to better understand them (e.g. Bouma, 1964; Kuenen, 1966; Middleton and Hampton, 1976; Mohrig and Marr, 2003; Baas et al., 2005; Covault et al., 2016). Deposit-based studies, such as outcrops provide valuable information on the deposits of turbidity currents (turbidites); however, the link to formative processes remains speculative, as different flow types may produce similar deposits (Covault et al., 2016; Stevenson et al., 2018; Hubbard et al., 2020). Laboratory-scale experiments provide an important aide to understand the inner mechanics of turbidity currents, but there are scaling issues, some of which, but not all, can be overcome concurrently (Sequeiros et al., 2012; Talling et al., 2012; Imran et al., 2017; de Leeuw et al., 2018). Numerical modelling has tended to use depth-averaged models, which omits the natural vertical velocity and structure of the flows (Kostic, 2014). Even with recent advances in computing power, complex 3-D numerical modeling necessarily makes a number of assumptions, especially with regards to sediment erosion, that are based on laboratory-scale observations, due to a paucity in field-scale flow measurements (e.g. Talling et al., 2012; Vellinga et al., 2016; Azpiroz-Zabala et al., 2017; Salinas et al., 2021).

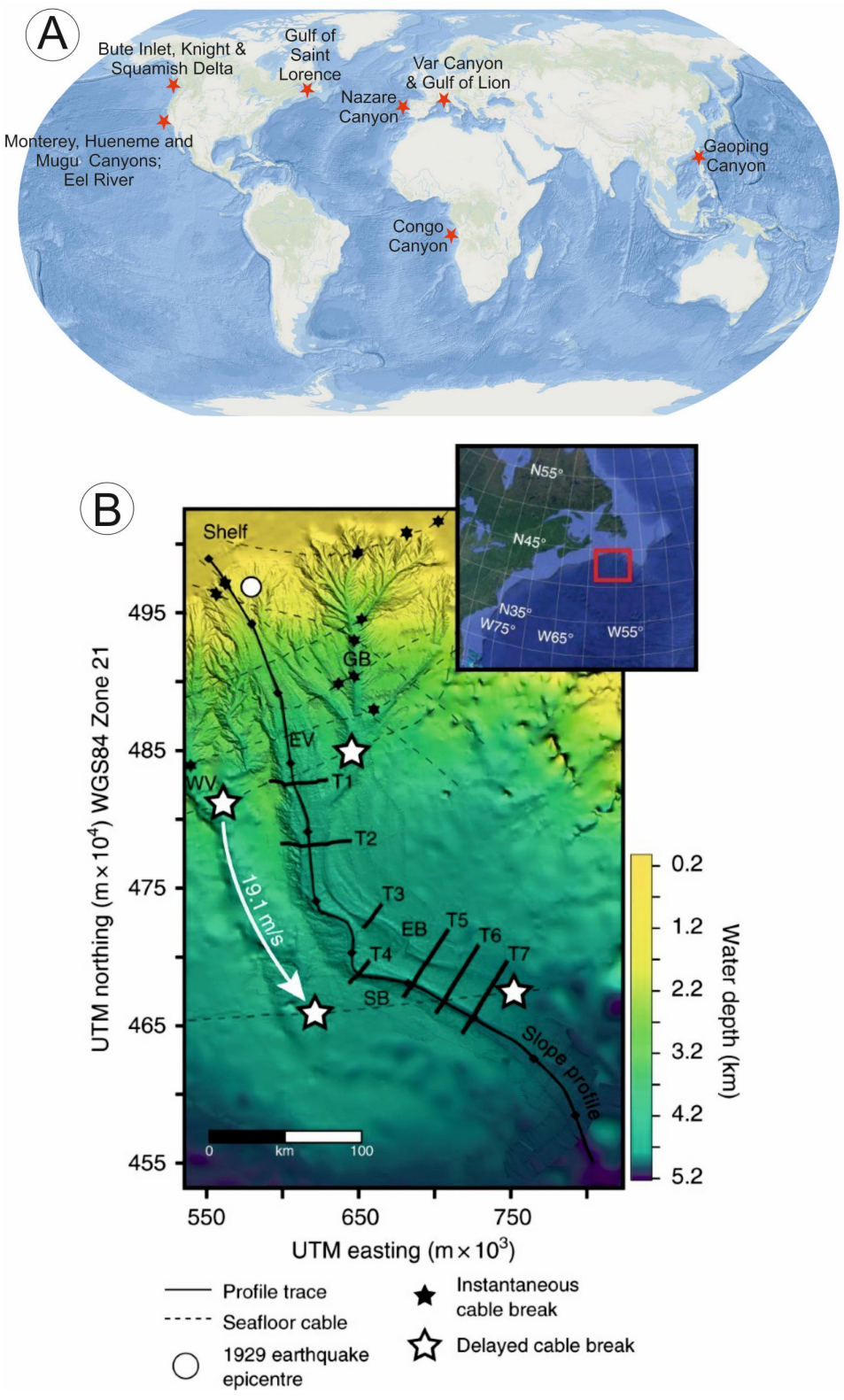

Figure 1.1 A: global map showing the location of published studies that have reported direct measurements of turbidity currents (see Table 1.1). B: Main pathway of the 1929 Grand Banks turbidity current. It is labeled as 'Slope profile' and was triggered by a Magnitude 7.3 earthquake. The timing of cable breaks indicated a maximum flow velocity of 19 m/s for this event (from Stevenson e t al., 2018)

Recent advances in remote sensing technology have enabled the first detailed direct measurements of field-scale turbidity currents, however (e.g. Paull et al., 2002; Xu et al., 2004; Khripounoff et al., 2012; Xu et al., 2013; Hughes Clarke, 2016; Azpiroz-Zabala et al., 2017; Paull et al., 2018). It is therefore an exciting time as, these and future measurements in modern, active systems, provide new opportunities to fill key but outstanding knowledge gaps; one of which is to link flow observations with their most recent deposits (e.g. Symons et al., 2017). The records of past turbidity currents, in the form of their deposits, and the bedforms that they create on the seafloor, will remain important archives for understanding the behaviour of turbidity currents (e.g. Bouma, 1964; Kuenen, 1964; Zeng et al., 1991; Piper and Normark, 2009; Hubbard et al., 2014 ; Postma and Cartigny, 2014; Maier et al., 2019).

1.2 Sites studied in this thesis

So far no one has compared different dataset acquired with different techniques and from different sites worldwide to build up a general understanding of how flow behave, interact with the seafloor and sculp the stratigraphic record.

However, there is now sufficient flow monitoring data available to begin considering more general questions about the dynamics of turbidity currents across multiple systems. In Chapter 2, I analyse high-resolution depth-resolved velocity measurements, because I aim to assess the diversity and commonalities in the maximum velocity structure of turbidity currents that were recorded using downward-looking Acoustic Doppler Current Profilers (ADCP), at seven different physiographic systems worldwide from 60 m to 2,300 m water depth (Figure 2.1).

To study the interaction between turbidity currents and seafloor, I present in Chapter 3 an unusually detailed and extensive AUV bathymetry dataset - 5 m across a large area, with inset surveys of even higher resolution - to analyse the geometric characteristics of sediment waves along two major canyons crossing the continental slope offshore Mozambique. Because the extension of this survey spans from shallow (~60m water depth) to deep water (~3000m water depth), in this study I explore the physical controls on the distribution of the different scales of bedform, its continuity and implications for flow behaviour in the deep sea. This study also allows me to fill in a previously data gap in bedform dimensions identified by Symons et al., 2016 and revise their previously proposed model of flow behaviour.

To observe and measure active flows, in Chapter 4 I study the Squamish delta that has proven to be an ideal test site due to the high frequency of turbidity currents (more than 100 per year). During recent years it has been the site of repetitive multibeam echo-sounder survey programs which aimed to monitor the temporal evolution of the prodelta morphology and to capture the spatial pattern of seabed changes, as the delta grows. I, therefore, took advantage of the 93 repeated high-resolution hydrographic surveys (Hughes Clarks et. al., 2011) to study the highly active system from source to lobe that, in a very compact area, features three channels (northern, central and southern) which initiate from a delta-lip and extend to depositional lobes at approximately 150 m water depth. This study highlights how the three submarine

major channels at Squamish delta acted as a conduit for recurrent turbidity current activity shaping the seafloor by localised erosion and deposition.

1.3 Structure of the thesis

This present chapter provides the rationale and context for the three specific research questions listed below, and address in Chapter 2to Chapter 4. The science chapters are presented in this thesis in their 'journal format'. Chapter 2 is currently under review in *Geophysical Research Letters*. Chapter 3is in preparation for submission to *Marine Geology*. Chapter 4has been published in *Earth and Planetary Science Letters*. In the following chapters, I analyse the available and different datasets collected around the world, spanning shallow water fjord systems to full ocean-depth submarine channels, acquired using systems including Acoustic Doppler Current Profilers (ADCP) to measure the velocity of active turbidity currents (Chapter 2), and multibeam echo sounders deployed from an Autonomous Underwater Vehicle (AUV; Chapter 3) and from a research vessel (Chapter 4). These datasets were collected by various organisations, to which they are attributed in the relevant chapters. Together, Chapters 2, 3 and 4 enable a better understanding of turbidity currents behavior because they provide new insights into the factors that influence flow processes (Chapter 2), and explain how turbidity currents interact with the seafloor (Chapter 3) and the deposits they leave behind (Chapter 4). Finally, Chapter 5outlines a summary of the main conclusions with suggestions for future work.

1.4 Thesis aims

This thesis takes advantage of several new high-resolution data sets from modern systems that document how turbidity currents behave at field-scale, how they sculpt the seascape and build stratigraphic records over relatively short timeframes (i.e. days to months).These direct field observations bridge a gap between turbidity current behaviour and their deposits and help to answer the overarching thesis aim.

Overarching aim: Is there a continuum in turbidity current behaviour across spatial and temporal scales?

To answer this aim, I considered three main aspects of turbidity currents. First, I investigated if direct measurements of turbidity currents worldwide reveal whether distinct flow modes occur, or if there is a continuum in behaviour between end-member states. Second, unusually high-resolution seafloor data are used for the morphometric analysis of bedforms in deep-sea channels, offshore Mozambique, to determine if a continuum exists in the scale of flows that sculpted the seafloor. Finally, 93 daily repeated seafloor surveys performed at the highly active Squamish submarine delta, British Columbia, allow me to investigate whether all scales of flow are equally recorded in the resultant stratigraphy, or if infrequent, but larger events

bias that preservation. I now discuss the three main research questions addressed in Chapter 2 to 4.

Question 1 (Chapter 2): *Is there a continuum in the velocity structure of turbidity currents, and what controls that behaviour?*

Chapter 2 Motivation: There are numerous models for how turbidity currents behave (e.g. Bagnold, 1962; Middleton, 1966; Parker et al., 1986; Cantero et al., 2012; Azpiroz-Zabala et al., 2017; Symons et al., 2017; Heerema et al., 2020), each having very different implications for understanding shallow to deep sea sediment, carbon and pollutant flux, and the nature of geohazards that affect seafloor infrastructure. The advent of direct monitoring of turbidity currents has provided the chance to measure flow behaviour at field-scale, but to date no one has synthesised the measurements that have been made at multiple sites. These are the issues that underpin the motivation for this chapter – maximizing the value of flow measurements at multiple sites to investigate, for the first time, the diversity of monitored turbidity current behaviour and what the physical controls are on that behaviour.

Stimulated by advances in monitoring technology, the number of studies that make direct measurements of turbidity currents at field-scale has grown rapidly over the past decade (Figure 1.2; Clare et al., 2020 and references therein). Several of these studies have proposed new models for how turbidity currents behave. For instance, Azpiroz-Zabala et al. (2017) identified that turbidity currents in the deep-sea Congo Canyon, West Africa, can be driven by a fast-moving (2-3 m/s) frontal cell, in contrast with previous models that were based on laboratory-scale flows. Symons et al. (2017), and subsequently Paull et al. (2018), demonstrated how fast-moving (up to 7 m/s) turbidity currents in the Monterey Canyon, California, include a dense near-bed layer that can also outrun the rest of the flow. Hughes Clarke (2016) reached a similar conclusion from measurements of smaller flows that reaches velocities of the order 2-3 m/s on the Squamish submarine delta in British Columbia, Canada, where the dense near-bed part of the flow causes localised erosion on the steeper lee side of bedforms. In contrast, Sumner and Paull (2014) observed a much slower-moving (<1 m/s) turbidity current in the Mendocino Canyon, demonstrating that more sluggish and dilute flows exist. So, are these new models for flow behaviour distinct or is there a continuum of flow modes between end member states? To date, no studies have collated measurements to provide a quantitative comparison and understand how flows vary across different systems.

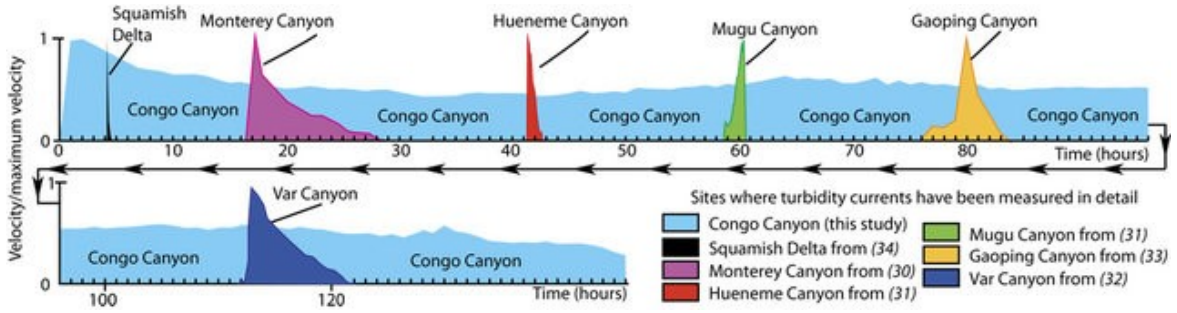

Figure 1.2 Comparison of tubidity currents in different settings. These flows have been measured in the ocean from Azpiroz-Zabala et al. (2017). The flows in the Congo Canyon last significantly longer (days) than those measured elsewhere (minutes to days).

Chapter 2aims to address this issue and provides the first global comparison of the first available measurements of turbidity current to understand whether there are distinct types of flow, or instead if a continuum exists between end-members. I compare the temporal evolution of the maximum velocity of turbidity currents detected at different systems worldwide that range from active channels in fjords, deep-sea channels offshore from major rivers, to shelf-incising canyons where sediment is delivered by littoral (along-shelf) transport. First, the chapter discusses what flow modes exist for turbidity currents in these disparate settings. Second, the chapter investigates the physical controls on the observed flow behaviour. Previous studies have suggested that system type and the initial trigger may control the type of turbidity current (Mulder et al., 2001; Mohrig and Marr, 2003; Goldfinger et al., 2007; Howarth et al., 2021), while others have proposed that grain size of the sediment available for transport may be more responsible (e.g. Hiscott, 1994; Baas et al., 2005;). Determining the physical controls on flow behaviour, and if this behaviour is dependent or independent of the type of system and trigger, will provide valuable information for future studies where acquisition of direct monitoring data is logistically or financially prohibitive. For instance, this will inform the nature of hazard posed to critical seafloor infrastructure such as telecommunications cables and pipelines and will aid with understanding the transport and burial of particles such as organic carbon and pollutants (including microplastics) (e.g. Galy et al., 2007; Kane et al., 2019; Hage et al., 2020; Pohl et al., 2020;).

Question 2 (Chapter 3): *Is there a continuum in the dimensions of bedforms created on the seafloor by turbidity currents, and what are we currently missing from deep-sea surveys?*

Chapter 3 Motivation: Bedforms are the building blocks of many sedimentary systems (Covault et al., 2014). Often we lack direct measurements of flows, such as those in Chapter 2. Morphometric analysis of bedforms therefore provides a valuable proxy understanding of flow behaviour. The variability of bedform morphologies and scales can provide key insights into the diversity of flow behaviour; in particular whether there is a continuum in magnitude of flows, or whether distinct modes of flow exist. Previous global analysis of seafloor bedforms indicated that turbidity currents show distinct behaviour that either gives rise to dune-scale or much larger bedforms with km-scale wavelengths, but was hindered by the lack

of high-resolution seafloor data in deep water. In Chapter 3I analyse a dataset that fills this resolution gap to tackle this question that has important implications for understanding what we may be missing from existing, low resolution seafloor surveys and in turn motivates a need for acquiring new high resolution bathymetric data in active submarine depositional systems worldwide.

A global analysis of seafloor bedforms created by turbidity currents identified two clusters in scales, between which there was a statistically-significant gap (Symons et al., 2017; Figure 1.3 Panel A). These clusters included small-scale (tens of metres wavelength) bedforms that are restricted to confined (canyon or narrow channel) settings and large-scale (kms wavelength) sediment waves and scours that were observed at the distal reaches of channels and on unconfined slopes.

Symons et al. (2017) and other previous studies largely used ship-based multibeam echosounder surveys that provide digital elevation models of the seafloor from which bedforms can be identified and measured. The resolution of such ship-based systems is a function of water depth; hence, in greater water, the ability to recognise smaller features is diminished. In Chapter 4, I use an exceptionally detailed seafloor survey with a consistent resolution (made possible through the use of an AUV to map the seafloor at a constant resolution independent of water depth) to investigate whether the gap in bedform dimensions of Symons et al. (2017) is real, or an artifact caused by data resolution in deeper waters (Hughes Clarke, 1998). I analyse data acquired over a 65 x 50 km area, which ranges from 60 to 2,800 m water depth from two submarine canyons offshore Mozambique, East Africa. I use a bedform measurement algorithm to objectively quantify bedform morphometry and to determine if a continuum in bedform scales exists.

Recent high resolution seafloor surveys have started to identify that steep steps in submarine canyons (known as knickpoints) can dominate the erosion observed in active submarine canyons (Heijnen et al., 2020; Guiastrennec-Faugas et al., 2020), but were not previously recognised in the global analysis of Symons et al. (2017). I therefore analyse similar features in the data from offshore Mozambique and explore where knickpoints sit on the global spectrum of bedforms. Finally, I discuss the implications of variable resolution bathymetric data for the identification of bedforms in deep-sea settings and how AUV-based studies provide the means to fill fundamental gaps in our understanding of how submarine channels are built and maintained, and to better constrain the nature of particulate transport into the deep sea.

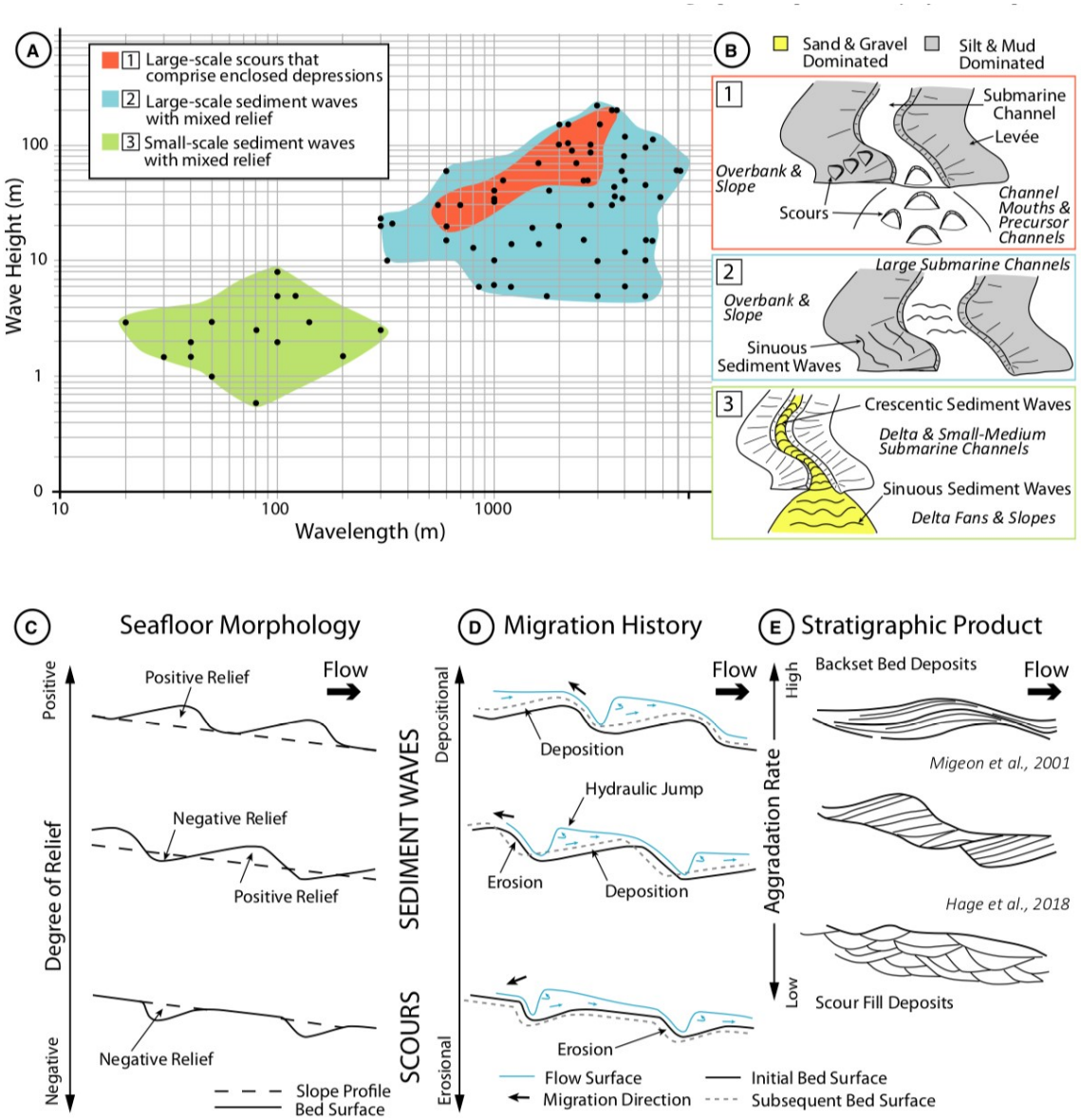

Figure 1.3 (A) Graph showing the scale of the three main bedform groups differentiated by Symons et al. (2016). (B) Sketches highlighting additional characteristics associated with each bedform group including planform geometry, composition and common location within turbidite-dominated environments. 1: large-scale scours that comprise enclosed depression; 2: large-scale sediment waves with mixed relief; 3: small-scale sediment waves with mixed relief (refer to insert A); (C) to (E) Linkages between seafloor features, sedimentary processes and stratigraphic products established from observations in modern environments. (C) Morphology of features interpreted to be cyclic steps on the seafloor, often referred to as sediment waves and scours. (D) Flow–seafloor interactions and migration for cyclic step bedforms in (C). (E) Stratigraphic products of these processes based on repeat bathymetry data (Hage et al., 2018) and seismic profiles (Migeon et al., 2001). Parts (A) to (E) from Englert, Vendettuoli et al. (2020) after Symons et al., 2016.

Question 3 (Chapter 4): *How do turbidity currents build stratigraphy and how faithfully does that stratigraphy preserve a record of past flow activity?*

Chapter 4 Motivation: Bedforms are a valuable proxy for inferring flow behaviour (Chapter 3), however, successive turbidity currents can rework these seafloor deposits, thus obscuring

or obliterating their expression in the depositional record. It is therefore important to understand how stratigraphy is built (and removed) by such repeated flows, whether certain magnitude events are disproportionately responsible for eroding or building stratigraphy, and how to interpret deposits in active submarine channel systems. This chapter aims to fill this knowledge gap in one unusually well-surveyed system, where multiple seafloor surveys (that image seafloor bedforms created by turbidity currents) are analysed to determine when and how stratigraphy is built, and erased by successive turbidity currents. No other submarine system has been so well surveyed (i.e. as many times), hence this study takes advantage of a unique dataset and provides motivation for such an approach to be performed in other active systems.

Understanding processes from their depositional record is complicated because successive events can rework or erase previous deposits. This is particularly challenging for turbidity currents, which can be extremely vigorous (e.g. Paull et al., 2018; Figure 1.4). Therefore, environments dominated by turbidity currents, such as submarine canyons and channels, only partially record their deposits. But precisely how incomplete these deposits are remains unclear. A number of previous studies have explored the concept of *stratigraphic completeness* (e.g. Sadler, 1981; Strauss and Sadler, 1989). Stratigraphic completeness is defined as the proportion of accumulated deposit thickness preserved over a given time period. This completeness can be affected by a range of factors that include external allogenic controls (e.g. sea level changes and tectonic influence) and internal, autogenic controls that are related to the sediment transport process itself (Barrell, 1917; Paola et al., 2018; Strauss and Sadler, 1989). It is important to understand stratigraphic completeness because deposits continue to provide a source of information on past turbidity current activity for both modern and ancient systems that is routinely used in geohazard assessments and to understand past fluxes of sediment and organic carbon (e.g. Kane et al., 2017; Jobe et al., 2018; Englert et al., 2020).

In subaerial environments, repeat satellite or aerial photogrammetric surveys enable monitoring of river and delta evolution, assessment of their stratigraphic completeness, and thus calibration of deposit- or laboratory-based models (Moody and Meade, 2014; Schwenk et al., 2017). In submarine systems stratigraphic completeness has previously been based on interpretation of depositional sequences (e.g. Trabucho-Alexandre, 2014), laboratory-scale or numerical modeling (e.g. Sylvester et al., 2011; Straub and Esposito, 2013) or through analogue with terrestrial systems such as rivers (e.g. Durkin et al., 2018) and thus lacks field-scale calibration. Such field-scale calibration is challenging, particularly in deep in marine systems, as acquisition of seafloor elevation data requires expensive and time-consuming multibeam bathymetric surveys (Hughes Clarke, 2012).

In Chapter 4, I take advantage of repeat bathymetric surveys that were performed at a timescale (every week day) appropriate to detect the frequency of >100 turbidity currents over four months at the very active Squamish submarine delta, British Columbia. Previous studies have revealed how different scales of event affect the Squamish submarine delta, including relatively large-scale delta lip collapses (involving volumes of up to 150,000 m^3) and smaller-scale upstream-migration of crescentic bedforms by much smaller turbidity currents (Hughes Clarke, 2016; Clare et al., 2016; Hizzett et al., 2018). Here, I ask whether all scale of flows

play an equal role, or are some magnitudes of event disproportionately efficient at becoming preserved or instead removing the stratigraphic record of others? Such detailed repeat surveys do not exist for any other site worldwide, hence this provides a unique opportunity to understand the influence of repeated turbidity currents on the stratigraphic record.

Links Between Thesis Objectives and Application: The combination of these three chapters provides a link between the direct measurement of turbidity currents (Chapter 2), the morphology of bedforms that arise from different scales and types of turbidity current (Chapter 3), and the stratigraphy is built by successive turbidity currents (Chapter 4). It is rare that flow monitoring, seafloor surveys and stratigraphic records (e.g. core, seismic data) are all available for a system; hence, this thesis presents a novel combination of analyses and datasets that provide useful and broad process-based sedimentological insights, with implications for a range of applications, in particular for geohazard assessments. Geohazard assessments for seafloor infrastructure such as telecommunications cables and pipelines requires an understanding of the frequency, magnitude (e.g. extent, velocity) and nature of turbidity currents (Bruschi et al., 2006). This thesis provides new insights into the global variability in flow velocity and duration, in particular in Chapter 2 identifying the physical controls on flow behaviour (i.e. grain size and slope gradient), which can now be used to inform pipeline and cable routes (e.g. avoid steep slopes and systems with coarse grain sizes, or design pipelines to withstand prolonged, low velocity impacts in muddy low relief systems). Determining the nature of larger turbidity currents (i.e. larger than those recorded during relatively short monitoring windows) also requires consideration in such hazard assessments. The nature of past flows can be inferred from bedform morphmetrics, but as shown in Chapter 3 this may require high-resolution (e.g. AUV) bathymetric datasets. This new contribution shows how certain types of bedform (and hence types of flow that formed them) may be missing from bathymetric datasets that were acquired in deep water from vessel-mounted systems. An important message to take from this study is the value of such high resolution datasets to better understand the variability of turbidity current activity. To assess the likely frequency of turbidity currents, geohazard assessments often analyse sediment cores, using age dating techniques to determine the emplacement time of event deposits (e.g. Hunt et al., 2013, Goldfinger et al., 2007). However, if successive flows erode sediment, this will affect the completeness of these sedimentary records. It is therefore important to assess whether certain events are better recorded than others, and which settings are better recorders of past geohazard activity. Chapter 4 provides the first attempt anywhere to do this in an active turbidity current system, concluding that many parts of the submarine channel systems on the Squamish delta feature very poorly preserved stratigraphy and are thus unsuitable for reconstruction of past event frequency and magnitude. However, large landslide events are better preserved, and guidance for future sampling is provided (e.g. levees and distal lobe provide the greatest stratigraphic completeness).

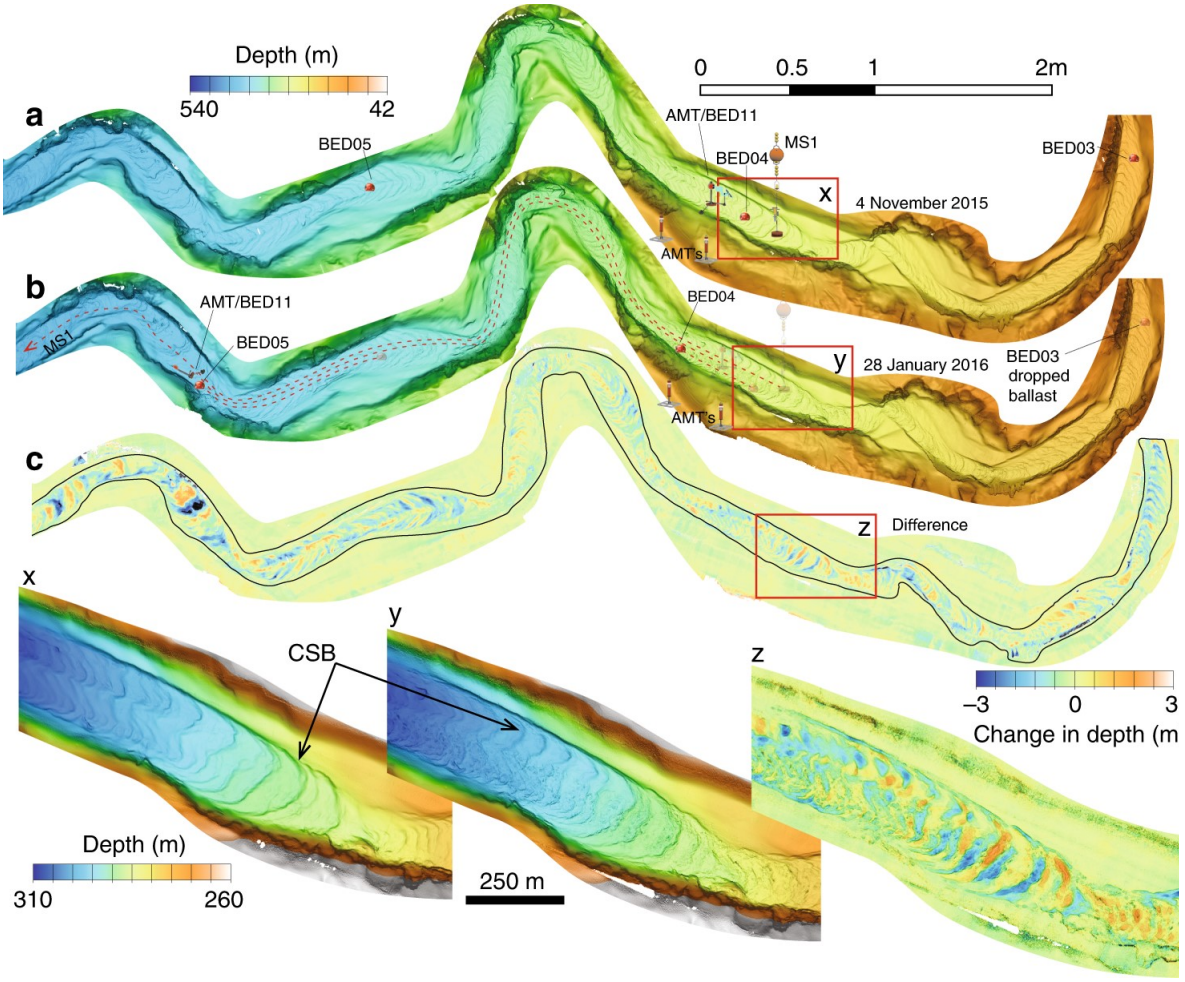

Figure 1.4 Repeat mapping using an AUV shows changes changes in seafloor morphology in Monterey Canyon (from Paull et al., 2018). A) Bathymetric surveys for the upper canyon collected with an AUV between 42 and 540 m water depths on 4 November 2015 and B) on 28 January 2016, before and after a powerful (c. 7 m/s) turbidity current. C) Changes in seafloor elevation between surveys a and b. X, Y, and Z are enlarged sections of A, B, and C, respectively. CSB refers to crescentic bedforms

1.5 Turbidity currents on the modern seafloor

The following section provides further context for these three questions, primarily focusing on the different tools and techniques used in this study.

1.5.1 Multibeam bathymetric surveys to identify and characterise turbidity current pathways and bedforms

Seafloor and lake-bed surveys that started as a series of simple point soundings, provided some of the first observations of subaqueous canyons and channels (e.g. Forel, 1888; Heezen et al., 1964; Girardclos et al., 2012). In subsequent decades, advances in seafloor surveying included the development of single-beam and subsequently multi-beam bathymetric systems; the latter of which can create detailed 3D models of the seafloor (Hughes Clarke, 2018). Such surveys are now routinely used to identify the primary pathways of turbidity currents, including submarine canyons, channels and lobes, and where resolution permits, to image their building blocks in the form of terraces, levees and bedforms (Paull et al., 2011; Conway et al., 2012; Covault et al., 2014). These seafloor features provide valuable information about past flows and have been used to make inferences on the likely thickness, velocity, and nature of turbidity currents creating them (e.g. Nakajima, 2002; Spinewine et al., 2009; Stow et al., 2009; Sequeiros, 2012; Cartigny et al., 2012; Kostic, 2014; Postma and Cartigny, 2014; Stevenson et al., 2018). Other seafloor surveys include the use of side scan sonar, which provides a measure of the reflectivity of the seafloor, and hence its sediment composition (e.g. Damuth et al., 1988; Clark et al., 1992).

As already mentioned, the spatial resolution of multibeam bathymetric sonars is a function of their height above the seafloor. Therefore, where such systems are deployed from surface vessels, their resolution decreases in increasing water depth. Horizontal and vertical resolution of multibeam sonar systems is ~ 3.5–20% of water depth and ~ 0.2–0.8% of water depth respectively (Hughes Clarke, 1998; Symons et al., 2016). To tackle this issue, Autonomous Underwater Vehicles are growing in use, as they can dive a set distance above the seafloor to ensure a consistent and much higher resolution of data. These surveys have started to provide a much clearer picture of the geomorphology that exists within submarine canyon and channel systems, such as the presence of dune-scale bedforms, canyon flank collapses, and major scours at their distal reaches, where they transition to a submarine lobe (e.g. Huvenne et al., 2011; Paull et al., 2013; Covault et al., 2014; Tubau et al., 2015; Carvajal et al., 2017; Maier et al., 2017). Such surveys tend to be limited in spatial extent, however, which means that these high-resolution observations are limited to small sections of canyons and channels (Figure 1.5 and Figure 1.6). Chapters 3 and 4 provide high-resolution multibeam bathymetric surveys that cover extensive reaches of submarine canyon and channel systems. In particular, Chapter 3 analyses an AUV survey covering an area of a 50 x 65 km from offshore Mozambique with a horizontal resolution of at least 5 m x 5 m. This detailed survey enables

characterisation of two major canyons along at least 60 km of their length, as well as a variety of bedforms and scours that have been created by turbidity currents that passed through these canyons.

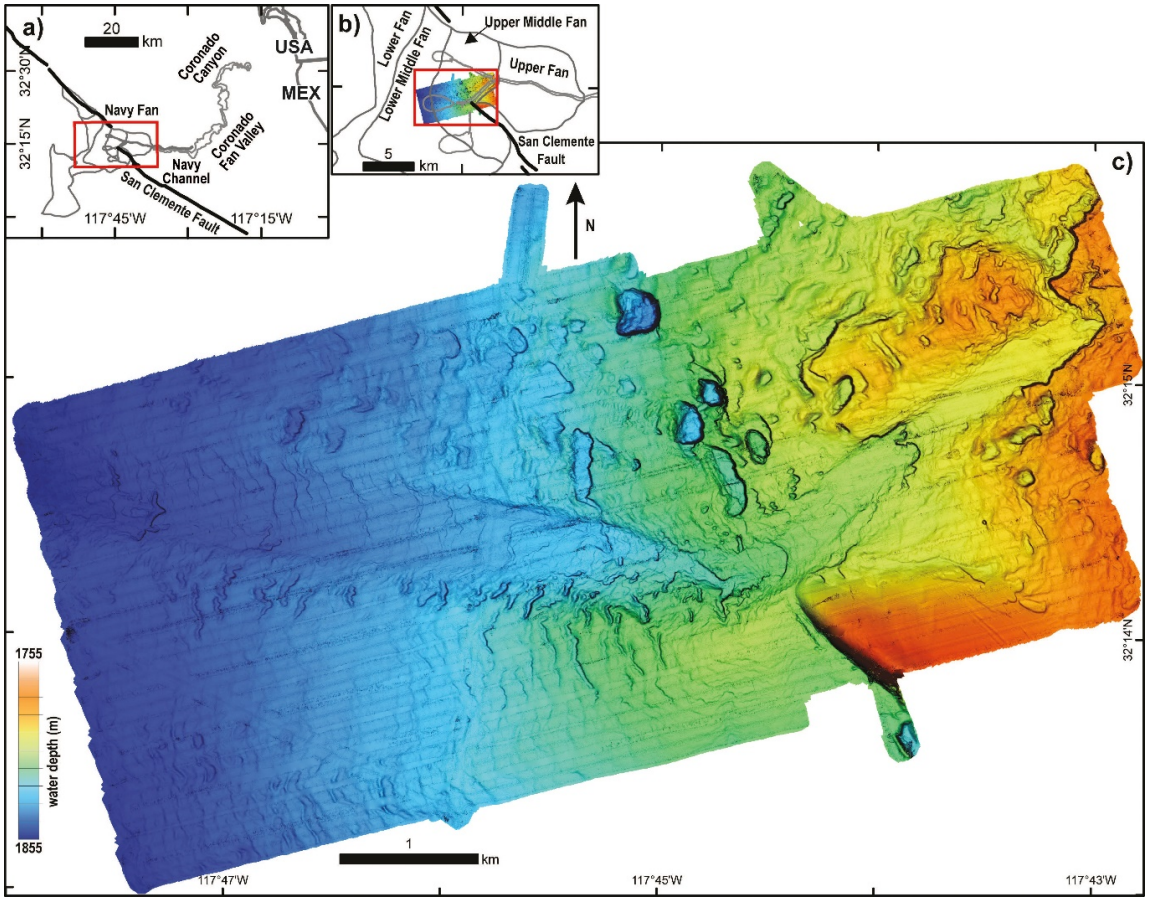

Figure 1.5 AUV bathymetric survey showing detail on the Nazy Fan, offshore Mexico (from Carvajal et al., 2017)

1.5.2 Repeated surveys to determine how turbidity currents interact with the seafloor

In recent years, successive seafloor surveys performed at the same location have started to show how turbidity currents interact with the seafloor, revealing areas of erosion and deposition and providing a better link to sedimentological processes. Such repeated surveys are still relatively rare, but are growing in their application as detailed in Table 1.1, which provides a summary of previous bathymetric mapping in areas of active submarine landslides and turbidity currents. These surveys are generally limited to fewer than six in total, and span periods of months to years (or even decades), and as a result they tend to provide a time-averaged view of how flows interact with the seafloor.

In some cases, however, the effects of individual turbidity currents can be identified from these repeat surveys. Isolating the effect of individual events either occurs in instances where

turbidity currents are relatively infrequent or where the rapidity of surveys was sufficient. This either comes down to planning (e.g. in cases where the triggering mechanisms are well known, such as the Squamish delta where a combination of elevated Spring and Summer river discharge and low tides are known to trigger flows; Hage et al., 2019), luck or a combination of both. One such example comes from the Kaikōura Canyon, offshore New Zealand, where a repeat seafloor survey was performed a few days after a large magnitude earthquake that triggered a powerful turbidity current (Mountjoy et al., 2018; Figure 1.6). Another, where triggers were not known *a priori* is the Monterey Canyon, where an AUV survey was performed before and then shortly after a turbidity current that was measured using an array of moored seafloor instruments (Paull et al., 2018; Figure 1.4).

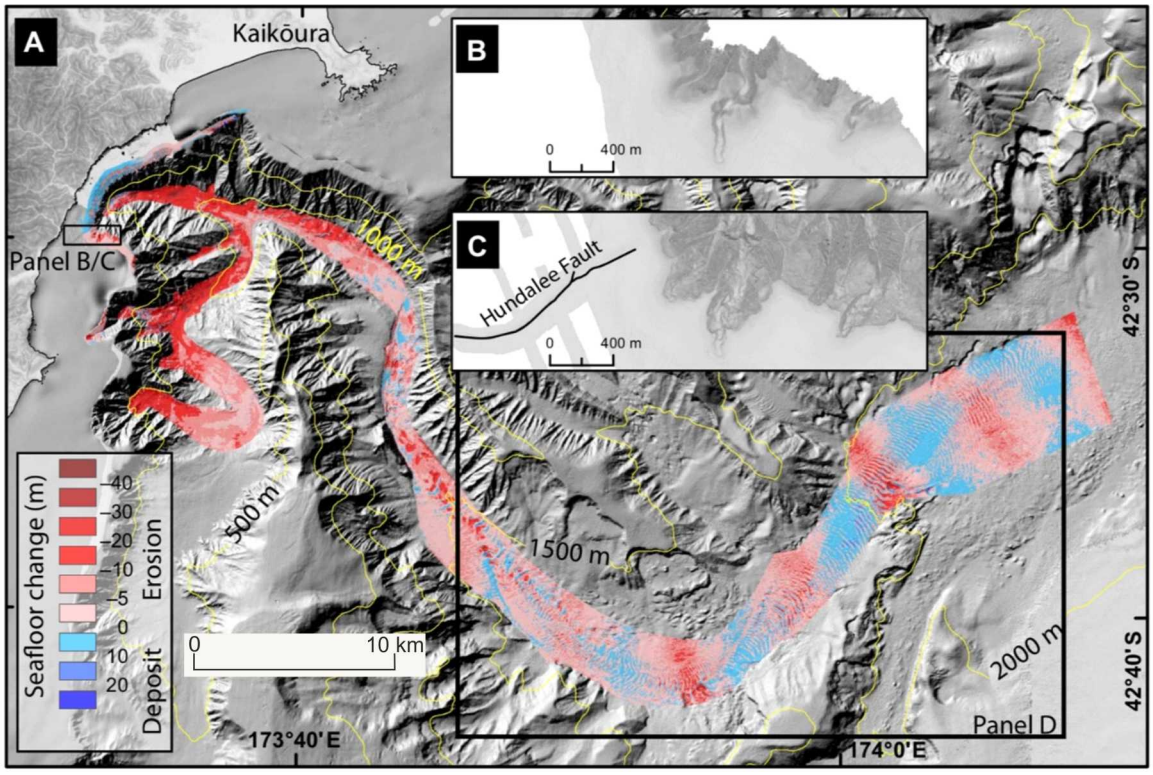

Figure 1.6 Differential elevation map of the Kaikoura Canyon, New Zealand after the magnitude 7.8 2016 earthquake, revealing significant erosion in the head of the canyon (from Mountjoy et al., 2018).

Of specific relevance to this thesis are repeated high-resolution hydrographic surveys at the Squamish Delta, British Columbia, which record the change in seafloor following successive flows (Hughes Clarke et al., 2012; Clare et al., 2016). These surveys were performed during the Spring and Summer in 2011 for 93 consecutive weekdays (Hughes Clarke et al., 2012; Clare et al., 2016). These surveys not only allow for the identification of how the seafloor is changing, but also for the determination how stratigraphy is built across the entirety of three active submarine channels (Figure 1.7). This data forms the basis of the analysis in Chapter 4.

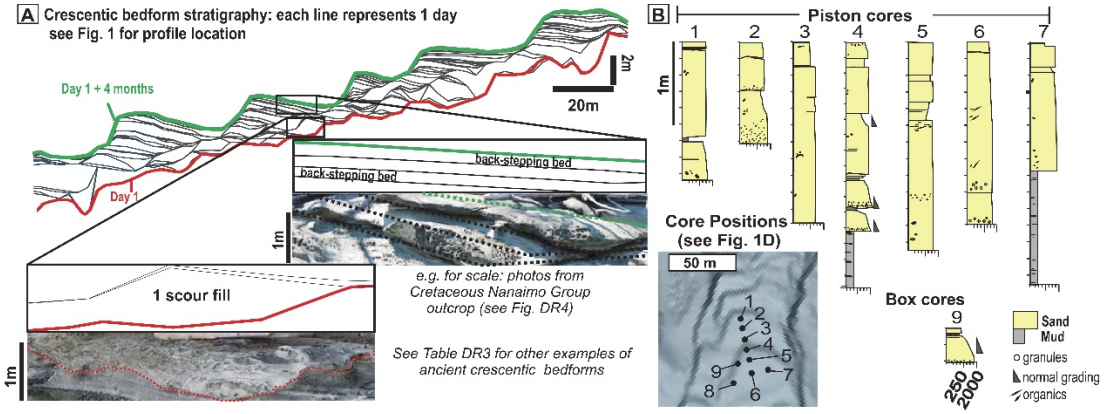

Figure 1.7 A) The stratigraphy built over 93 consecutive week days in a proximal part of a channel in the Squamish prodelta, British Columbia. B) Sediment cores used to link the repeated seafloor surveys to sedimentological facies. This figure was based on analysis performed in Chapter 4 (as published in Hage, Vendettuoli et al., 2018).

Table 1.1 Summary of previous repeat bathymetric mapping in areas of active submarine landslides and turbidity currents

Repeated bathymetric surveys	Location and water depth [m]	Frequency of flows/landslide [if known]	Processed observed	Reference
5 x annual surveys (2008-2004) 1 x annual survey (2009)	Oguue' River submarine delta, Gabon [55 m]	10s/year	Submarine landslide	Biscara et al. (2012)
2 x annual survey (in 2009 and 2004)	Begawan Solo submarine delta, East Java [30 m]	-	Turbidity currents	Syahnur and Java (2016)
Survey every 6-24 months (from 2004 to 2009); survey every week day (during Spring and Summer 2011 and 2012); single survey for 6 days (June 2013); 1 x annual survey (2015) *5 x surveys a day for 6 days (2015)	Squamish submarine delta, British Columbia, Canada [<200m] *Central Channel at Squamish Delta [60 m]	10s ÷ 100s/year	Delta-lip collapses, turbidity currents and bedform migration	Hughes Clarke et al. (2012, 2014), Clare et al. (2016), Hughes Clarke (2016), Hizzett et al. (2018), Hage et al. (2018), this work;
Repeat surveys every 15 minutes for 10 days	Westerschelde Estuary, the Netherlands [20 m]	10s ÷ 100s/year	Dredging-induced slope failure, bedform migration	Mastbergen et al. (2016)
6 x annual surveys (1967, 1974, 1991, 1999, 2006 and 2011)	Offshore Nice, France [300 m]	10s ÷ 100s/year	Submarine landslide	Kelner et al. (2016)

2 x annual surveys (September 2002 and February 2005); 2 x surveys (March 25, 2003 and March 26, 2006); 1 x annual survey (September 2003); 2 x surveys (September 2004 and November 2004);	Monterey Canyon, California, USA [300 m]	10s ÷ 100s/year	Submarine landslide, bedforms migration	Smith et al. (2007); Xu et al. (2008); Paull et al. (2010)
1 x annual surveys (1891); 1 x annual survey (between December 2012 and November 2013); 4 x surveys (1986, 2000, 2008, 2012)	Lake Geneva, Western Europe [<300 m]	~10s ÷ 100s/flows	Turbidity currents, mass transport events	Silva et al. (2018); Corella et al. (2016)
1 x annual survey (2007); 1 x annual survey (2012)	Lower St. Lawrence Estuary, Eastern Canada [350 m]		Turbidity currents, bedform migration	Normandeau et al. (2014)
2 x annual surveys (2005 and 2008); 1 x annual survey (2010)	Knight, Bute and Toba Inlets, British Columbia, Canada [up to 400 m]	10s/year	Slope failure, turbidity currents	Conway et al. (2012);
2 x annual surveys (between 2005 and 2007)	Fiumara Mouths, Western Messina Strait, Italy [up to 2000 m]	~100s/year	Hyperpycnal flows, landslides	Casalbore et al. (2011)
2 x surveys (2016)	Kaikoura Canyon, New Zealand [2000 m]	~100s/year	Canyon flushing	Mountjoy et al. (2018)
1 x annual survey (1994, 2001, 2003, 2005); 2 x surveys (May 2006 and September 2006)	Fraser River Delta, Western Canada [up to 110 m]	~ 10s/year	Turbidity currents, slope failure	Hill et al. (2008); Lintern et al. (2018)

1.5.3 Advances in direct monitoring of turbidity currents in the ocean

Advances in technology, particularly over the past decade, have enabled the first high-resolution direct measurements of turbidity currents to be made, which is transforming our understanding of how these flows behave, interact with the seafloor and the nature of their resultant deposits (Hughes Clarke et al., 2011, 2014; Cooper et al., 2013; Talling, 2014; Clare et al., 2016; Hughes Clarke, 2016). These new data provide valuable calibration for numerical modelling (e.g. Talling et al., 2015), and improved quantification of aspects such as the triggers and frequency of flows (e.g. Bailey et al., 2021), and ascertain their effectiveness at transporting and burying organic carbon (e.g. Hage et al., 2020). However, turbidity currents

have only been monitored in a handful of places worldwide, and direct monitoring datasets that include several flows are valuable. So far, the direct monitoring of turbidity currents has primarily been focused in setting such as lakes, fjords and relatively shallow ocean water (Table 1.1), although studies in deeper water have started to be performed (e.g. Azpiroz-Zabala et al., 2017) (Figure 1.8).

A range of new tools is now available for measuring turbidity currents. For instance, water column imaging using multi-beam sonars has shown how turbidity currents interact with bedforms and erode the seafloor (Hughes Clarke, 2016). Acoustic Doppler Current Profilers (ADCP) provide depth and time-resolved measurements of current velocity and acoustic backscatter that provides insights into suspended sediment concentrations and the temporal and vertical variations in flow structure (Hughes Clarke et al., 2014; Simmons et al., 2020). In Chapter 2, I focus specifically on the analysis of ADCP data acquired from seven systems worldwide. I choose sites where detailed measurements of flow velocity have been made to compare the temporal evolution in maximum flow velocity across sites that include coastal fjords to the deep sea Congo Canyon, and that are supplied by sediment in different manners.

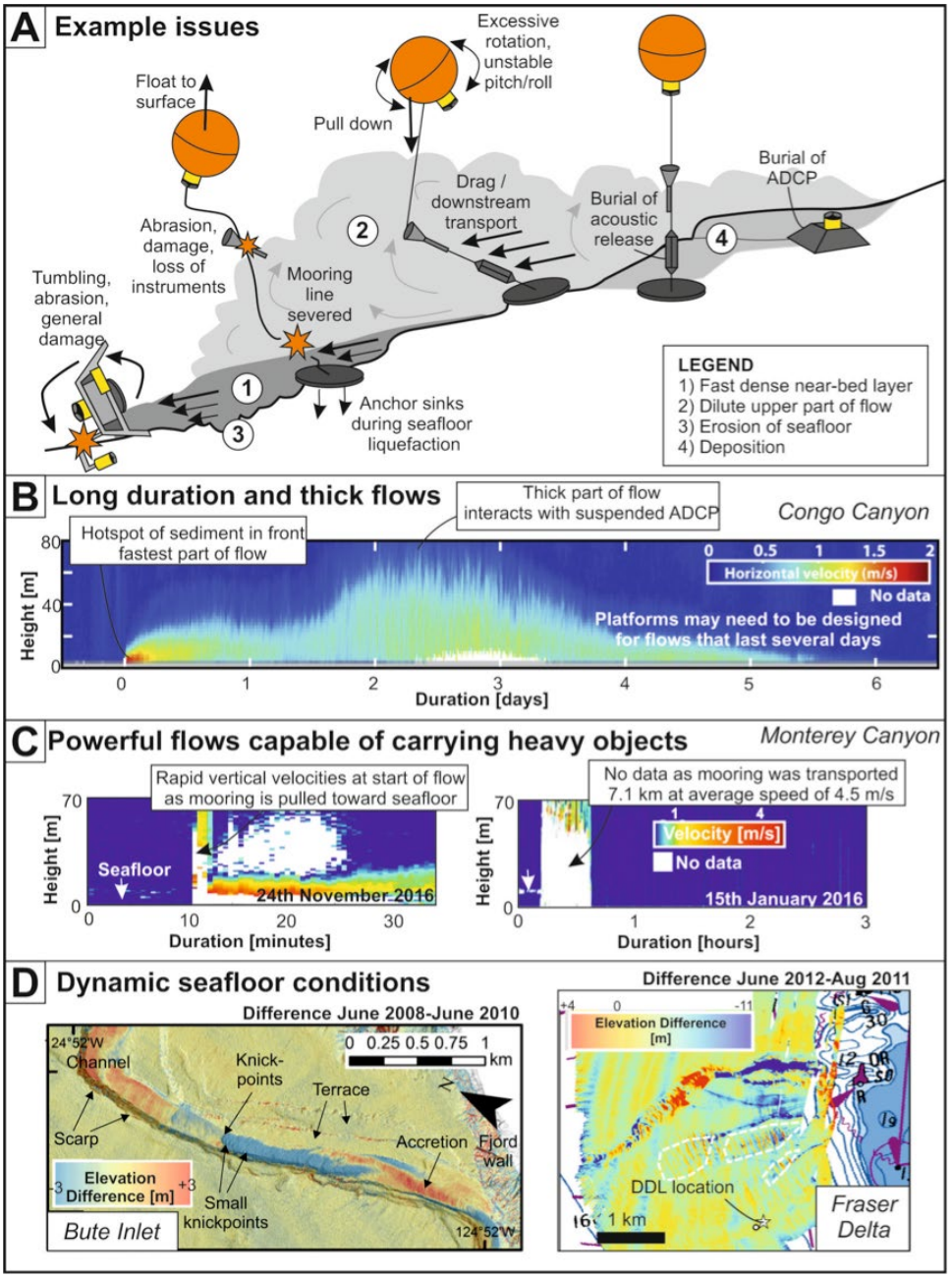

Figure 1.8 Overview of some of the new data types generated by recent monitoring of turbidity currents and the seafloor change they create (from Clare et al., 2020). a) Some of the issues involved in measuring powerful turbidity currents that have impacted previous studies. (b) An example of one of the long-duration turbidity currents measured in the deep-water Congo Canyon that may attain thicknesses of 80 m (modified from Azpiroz-Zabala et al. 2017a). (c) Two turbidity current events measured at the shallowest water mooring in the Monterey coordinated canyon experiment in Monterey Canyon. On the left is a flow that pulled the instruments and buoyancy towards the seafloor at the start of the event due to enhanced drag early on. On the right is the record from an ADCP that was transported by a flow at several m/s; hence, no reliable data were recorded during the flow. This mooring was transported 7.1 km down-canyon and then broke free from its anchor and was released to the sea surface. (d) Repeat multibeam echo-sounder seafloor surveys illustrating how active turbidity currents can both erode and deposit at the seafloor. The location of the Delta Dynamics Laboratory (DDL) is labelled on the Fraser Delta (right).

Table 1.2 Overview of previous direct monitoring studies of turbidity currents in submarine canyons and channels with reference to different types of sediment supply (modified by Bailey et al. ,2021)

Sediment supply	Site	Flows	Period	Triggers	Reference
River-fed fjords	Knight Inlet, Canada	39	17 months	Elevation in freshet river discharge.	Bornhold et al., 1994
	Bute Inlet, Canada	35	13 months		
	Squamish Prodelta, Canada	106	147 days	System active during river discharge >300 m3/s. Tidal drawdown or rapid sedimentation trigger.	Clare et al., 2016; Hizzett et al., 2018
River-fed canyons	Congo Canyon, offshore Angola	6	4 months	Elevated river discharge but not flood peaks.	Azpiroz-Zabala et al., 2017
	Gaoping Canyon, offshore Taiwan	23	3.5 years	Flow initiates following typhoon elevation of river discharge.	Zhang et al., 2018
		2	2 months	Typhoon-triggered hyperpycnal flows.	Liu et al., 2012
		Cable Breaks		River flooding, tropical cyclones and earthquakes.	Hsu et al., 2008; Carter et al., 2012; Pope et al., 2017
	Gulf of Lions canyon system, Mediterranean	6	4 months	Dense shelf water cascading, storms, river flooding and trawling.	Canals et al., 2006
	Var Canyon, Mediterranean	8	2 years	Hyperpycnal flows during river flooding and some local storms.	Khripounoff et al., 2009
Littoral drift-fed canyons	Eel River Shelf and Canyon, offshore California	11	83 days	Storms, not directly linked to river floods.	Puig et al., 2004
	Hueneme & Mugu Canyons, offshore California	6	6 months	Storms. The same storm event is capable of triggering flows in both canyons simultaneously.	Xu et al., 2010
	Monterey Canyon, offshore California	4	11 months	Coincident with elevation in storm activity.	Xu et al., 2004
		10	16 & 26 months		Paull et al., 2003, 2010
	Nazare Canyon, offshore Portugal	3	22 months	Storm waves with potential contribution from flooding north of the canyon head.	Martín et al., 2011

Sediment supply	Site	Flows	Period	Triggers	Reference
Sediment starved canyon	Gulf of St. Lawrence, East Canada	4	27 months	Sustained storms resuspend sediment in canyon heads.	Normandeau et al., 2020

Chapter 2
Identification of controls on turbidity current structure based on direct monitoring

This chapter forms a paper currently in review in *Geophysical Research Letters*:

D. Vendettuoli, M. A. Clare, E.J. Sumner, M.J.B. Cartigny, P.J. Talling, J. Wood, L.P. Bailey, M. Azpiroz-Zabala, C.K. Paull, R. Gwiazda, J.P. Xu, C. Stacey, D.G. Lintern, S.M. Simmons, E.L Pope and S. Hage (In review, Geophysical Research Letters). Global monitoring data shows grain size controls turbidity current structure.

Author contributions: I led on the analysis and processing of the data, designed the study, and wrote the manuscript. M.J.B. and L.P.B. assisted with processing the ADCP data. M.A.C., E.J.S. and M.J.B.C. provided the main editorial support on the manuscript. Other authors provided access to ADCP data and all the authors commented on the final version of this manuscript.

Abstract

The first detailed measurements from active turbidity currents have been made in the last few years, at multiple sites worldwide. These data allow us to investigate the factors that control the structure of these flows. By analyzing the temporal evolution of the maximum velocity of turbidity currents at different sites, we (1) aim to understand whether there are distinct types of flow, or if a continuum exists between end members; and (2) to investigate the physical controls on the different types of observed flow. Our results show that the evolution of the maximum velocity of turbidity currents falls between two end-members. Either the events show a rapid peak in velocity followed by an exponential decay or, flows continue at a plateau-like, near constant velocity. Our analysis suggests that rather than triggers or system input type, flow structure is primarily governed by the grain size of the sediment that is available for incorporation into the flow.

2.1 Introduction

Until recently, few direct measurements existed for powerful sediment avalanches on the seafloor, known as turbidity currents. It is important to understand these flows, as they play a key role in sediment and nutrient transfer to the deep sea, thereby affecting global geochemical cycling (Schlunz et al., 2000; Talling, 2014; Rabouille et al., 2017). Turbidity currents are challenging to measure because they occur on the seafloor, can be destructive (Inman et al.,

1976; Talling et al., 2013; Xu et al., 2010; Paull et al., 2018) and pose a hazard to critical seafloor infrastructure (Carter et al., 2014). Furthermore, their recurrence is poorly constrained due to limited understanding of their preconditioning and triggering mechanisms; hence predicting turbidity currents remains an open challenge (Talling et al., 2013; Bailey, 2021). Despite these issues the last decade has seen a growth in the seafloor monitoring of turbidity currents (Clare et al., 2020 and references therein); providing the first detailed insights into the structure of these flows. These monitoring studies have led to several new models for turbidity current dynamics (e.g. Azpiroz-Zabala et al., 2017; Symons et al., 2017; Heerema et al., 2020), that test aspects of previous influential models (e.g. Bagnold, 1962; Middleton, 1966; Parker et al., 1986; Cantero et al., 2012)

2.1.1 Can we determine the factors that control flow behaviour?

Many classification systems exist for turbidity currents, based upon either their deposits or scaled-down laboratory experiments (e.g. Lowe, 1979b; Postma, 1986; Mulder and Cochonat, 1996; Haughton et al., 2009; Talling et al., 2012). The nature of triggers and flow initiation has been suggested as a strong control on the structure of turbidity currents. For instance, Mulder et al. (2003) proposed that flows in muddy river-fed systems differ from those in more dilute river-fed settings or littoral drift-fed canyons. In such classifications, initiation through a rapid slope collapse may form a short-lived, unsteady surge, while sustained sediment input (such as during sediment-laden river flood discharge to the ocean) may result in a prolonged, more steady flow (e.g. Middleton and Hampton, 1976; Kneller and Branney, 1995; Khripounoff et al., 2012). Others suggest that flow behavior relates to physiographic controls such as canyon or channel morphology (Xu et al., 2010), shelf gradient (Talling et al., 2007), or the particle size and density present in the system (e.g. Stow and Bowen, 1980; Lowe, 1982; Mutti et al., 2003; Hodson et al., 2010).

2.1.2 Can we build up a general understanding on how turbidity currents behave?

There are fundamental gaps in understanding of how the structure of turbidity currents varies, and the physical controls on that variability. In the past, a lack of detailed monitoring data has limited the ability to test models using data from full-scale turbidity currents. Previous flow monitoring studies have typically focused on data-sets from individual canyons, and have focused on the characteristics of site-specific flows (e.g. Talling et al., 2013, Clare et al., 2020 and references therein). However, there is now flow monitoring data from different sites worldwide, which allows consideration of general questions about the dynamics of turbidity currents. For example, why do some flows maintain a fixed velocity for several days, while other flows rapidly accelerate but then dissipate within minutes to hours? What internal or external factors determine flow behavior?

2.1.3 Aims

For the first time, in this study we take advantage of detailed turbidity current monitoring data from recent surveys worldwide to understand the physical controls on turbidity current structure. Specifically, the first aim is to document the variability in turbidity current structure, especially duration and temporal evolution of velocity. We analyse whether there are distinct types of flow, or if a continuum exists between end members. Second, we investigate the physical controls on the different types of observed flow structures, including system type, triggers, flow initiation and grain size. We compare turbidity currents in systems linked to muddy and sandy rivers, and systems fed by longshore drift. The range of systems varies from small fjord-head channels to large deep-sea submarine canyons.

2.2 Data

To assess the diversity in the structure of turbidity currents, we analyse the first available high-resolution depth-resolved velocity measurements of turbidity currents relative to seven sites worldwide. These sites span a wide range of environments, including bedload dominated fjord-head delta systems, river-fed deep-sea canyons, and littoral-fed deep-sea canyons. In all but one of the datasets, flow velocities were recorded using downward-looking Acoustic Doppler Current Profilers (ADCPs), at sites from 60 m to 2,300 m water depth. In one dataset (from offshore West Papua), a single-point current meter was used (Table 2.1 and Table 2.2). We now briefly introduce the different systems to provide context for later discussion (Figure 2.1).

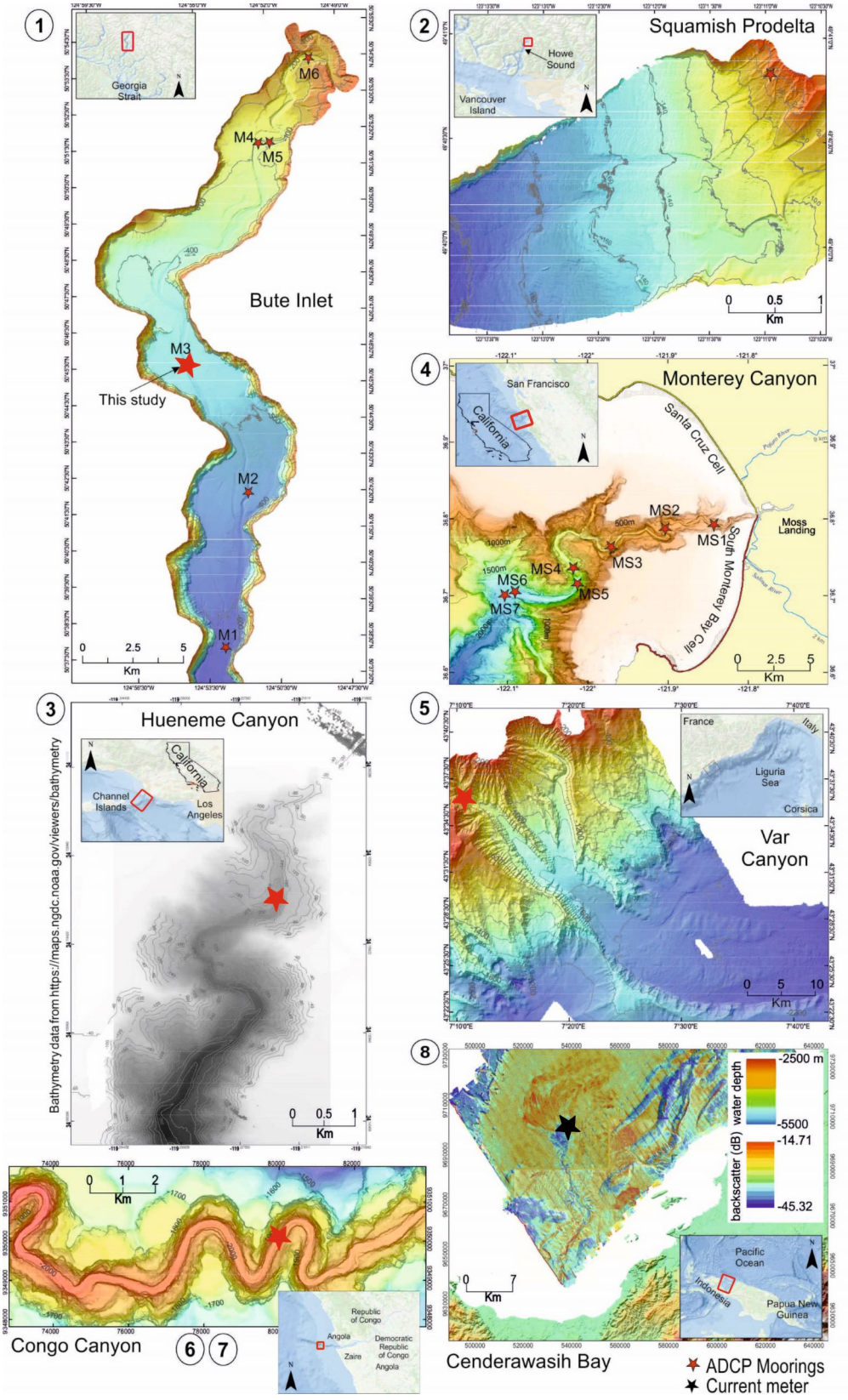

Figure 2.1 Sites where turbidity currents have been monitored in action and analysed in our study. Bute Inlet and Squamish Delta (British Columbia) are representative of fjord-head systems. Hueneme and Monterey canyons (California), represent littoral drift-fed submarine systems. Var canyon (north west Mediterranean Sea), Congo canyon (offshore Angola) and Cenderawasih Bay (West Papua) are representative of deep-sea submarine systems directly linked to the rivers activity (see also Table 2.1and Table 2.2)

Table 2.1 Physical parameters of the physiographic submarine systems analyzed in this study

Systems	Extend of the system	ADCP deployed at	Sediments supply	Sediment discharge into the systems	Monitoring data utilized in our study
Congo Canyon	350 km with 3,000 m water depth	2000m water depth @85m above seabed	River flood/ canyon wall slumping	43 x 10^9 kg yr^{-1} (Bongo-Passi, 1984)	Cooper et al., 20013 & 2016
Var Canyon	16 km within ~2,000 m water depth	1280m water depth @35 above seabed	River flood/ hyperpycnal flow/ canyon wall slumping	1.63 x 10^6 t yr^{-1}	Khripounoff et al., 2012
Hueneme Canyon	10 km within 500 m water depth	184	Littoral drift-fed submarine systems/ hyperpycnal flow	3-6 x 10^6 t yr^{-1}	Xu et al., 2010
Squamish Delta	2 km within 150 m water depth	60m water depth @	Bed-load dominated fjord-head delta systems	600-700 m^3/s (Hickin, 1989)	Hughes Clarke 2016
Bute Inlet	40 km within 600 m water depth	400m water depth @27m above seabed	Bed-load dominated fjord-head delta systems	*1.7 × 10^6 to yr^{-1} *amount of sediments delivered to the canyon head (Syvitski et al., 1988)	Hage et al., 2020
Monterey Canyon	153 km within 3,600 m water depth	From 300m to 1800m water depth @30m above seabed?	Littoral drift-fed submarine systems	300,000 m^3 yr^{-1} (Smith et al., 2005)	Paull et al., 2018.
Cendera-wasih Bay	60 km within 1,600 m water depth	<2000	River flood/ hyperpycnal flow	Not known	Wood, 2013

Table 2.2 Technical specification of the survey considered in this study for each mooring at each location

Systems	Date	Flows	ADCP	Sampling rate	Vertical Bin size	Background velocity	Moorings coordinate (longitude - latitude)
Squamish Delta							
	15-Jun-16	Flow 1	600KHz	Every 3.6 second	0.5 m	0.35 (m/s)	
Bute Inlet							
	10-Jun-16	Flow 1	614KHz	10-seconds	1 m	0.22 (m/s)	-124.914;
Mooring 3	11-Jul-16	Flow 2		samples		0.17 (m/s)	50.76245
	11-Jul-16	Flow 3				0.21 (m/s)	-124.918;
							50.76194
							-124.911;
							50.76307
Monterey Canyon							
Mooring 1	1-Dec-15	Flow 1	300KHz	30-seconds	2 m	0.27 (m/s)	-121.845;
	7-Jan-16	Flow 3		samples		0.43 (m/s)	36.79328
	1-Sep-16	Flow 8				0.39 (m/s)	
	24-Nov-16	Flow 9				0.38 (m/s)	
	9-Jan-17	Flow 10				0.49 (m/s)	
	20-Jan-17	Flow 11				0.39 (m/s)	
	21-Jan-17	Flow 12				0.57 (m/s)	
	23-Jan-17	Flow 14				0.36 (m/s)	
	3-Feb-17	Flow 15				0.65 (m/s)	
	18-Feb-17	Flow 16				0.54 (m/s)	
Mooring 2	24-Nov-16	Flow 9				0.46 (m/s)	-121.903;
	9-Jan-17	Flow 10				0.44 (m/s)	36.78827
	3-Feb-17	Flow 15				0.55 (m/s)	
	18-Feb-17	Flow 16				0.53 (m/s)	
Mooring 3	16-Jan-16	Flow 4				0.48 (m/s)	-121.97;
(This study)	1-Sep-16	Flow 8				0.48 (m/s)	36.76497
	9-Jan-17	Flow 10				0.44 (m/s)	
	3-Feb-17	Flow 15				0.53 (m/s)	
	18-Feb-17	Flow 16				0.44 (m/s)	
Mooring 4	16-Jan-16	Flow 4				0.41 (m/s)	-122.016;
							36.7358
Mooring 5	16-Jan-16	Flow 4				0.45 (m/s)	-122.013;
	1-Sep-16	Flow 8				0.51 (m/s)	36.71496
Mooring 7	16-Jan-16	Flow 4				0.38 (m/s)	-122.098;
							36.70162
Congo Canyon							
	4-Dec-09	Flow 1	300KHz	5-seconds	2 m	0.34 (m/s)	-5.8666; 11.209
	23-Dec-09	Flow 2		samples		0.34 (m/s)	
	26-Dec-09	Flow 3				0.32 (m/s)	
	9-Jan-10	Flow 4				0.33 (m/s)	
	16-Jan-10	Flow 5				0.33 (m/s)	
	26-Jan-10	Flow 6				0.34 (m/s)	

	8-Feb-10 10-Feb-10 26-Feb-10 10-Mar-10	Flow 7 Flow 8 Flow 9 Flow 10				0.31 (m/s) 0.32 (m/s) 0.34 (m/s) 0.35 (m/s)		
Hueneme Canyon								
	5-Dec-07	Flow 1	300KHz	30 one-second pings every 5 minutes	2 m	0.0005 (m/s)	-119. 226; 34.131	
Var Canyon								
Var Canyon	5-Feb-09 8-Feb-09	Flow 1 Flow 2	300KHz	1 current vertical profile every 30 minutes bins at 10 elevation	3 m	0.07 (m/s) 0.09 (m/s)	7.24; 43.57	
Cenderawasih Bay								
Cenderawasih Bay	10-Sep-12	Flow 1	300KHz	600 pings spaced every 2 seconds in 20 minutes intervals		0.009 (m/s)	135.36; 2.68	

Table 2.3: Lithological characterization of the core logs represented in Figure 2 - Panel C in the main text

Grainsize	Study area	Description	Reference
Sand-rich end members	Squamish Prodelta	Structureless sand, poorly graded, with layers of amalgamated sand toward the top.	Hage et al., 2018
	Hueneme Canyon	Fine and very fine sand, to silt and locally lens of clay.	Xu et al., 2010
	Monterey Canyon	Poorly sorted intervals containing coarse gravel or multi-coloured clay clasts near their base, overlain by fining-upward sand with sand-supported rounded cobbles and angular clay chips floating within the sand.	Paull et al., 2010
	Var Canyon	Coarse silt to very fine sand with interbedded thin layers of fine sand.	Klauche et al., 2000
Sand and mud- rich members	Bute Inlet	Sand beds, including associated mud top, from 10 cm to 1 m thickness. Mud, including associated mud top and organic debris, interbedded to layers of sand from 10 to 50 cm thickness.	Hage et al., 2019; 2020
	Cenderawasih Bay	Mud and woody organic debris locally interbedded by very thin layers of sand.	Orange et al., 2010
Mud-rich end members	Congo Canyon	Mud locally interbedded by very thin layers of sand. Often present laminations typically plane-parallel, in some cases, sub-parallel.	Azpiroz-Zabala et al., 2017

In the following sections (2.2.1 to 2.2.3) we briefly describe the different sites presented in our study grouping them per similar physiographic characteristics.

2.2.1 Bedload dominated fjord-head delta systems

Howe Sound and Bute Inlet in British Columbia (Figure 2.1) are relatively deep and steep-sided fjords, which host active submarine channels that are fed by one or more rivers at their heads (Gales et al., 2019). Squamish Prodelta is located at the mouth of the Squamish River in Howe Sound, where it connects to three submarine channels that reach water depths of c.200 m (Hughes Clarke, 2016). Here, we analyse ADCP measurements, collected in 2015 (Hage et al., 2018), that recorded 300 m downstream of the delta-lip, at a water depth of 60

m. In Bute Inlet, the Homathko and Southgate Rivers connect to a submarine channel that extends, ~40 km to ~600 m water depth (Prior et al., 1986). Turbidity currents were measured in 2016 using an ADCP located ~20 km downstream of the delta lip in 480 m water depth. Sediment cores in the axes of both channels generally recovered massive sands, although mud-caps are common in cores in Bute Inlet (Zeng et al., 1991; Vendettuoli et al., 2019; Hage et al., 2019; 2020) (Figure 2.5 Panel D).

2.2.2 River-fed deep-sea submarine canyons

The Congo Canyon, located offshore Angola (Figure 2.1), is directly connected to the Congo River and its head is located within the seaward end of the estuary (Savoye et al., 2009). Flows were recorded between 2009 and 2010 by an ADCP deployed at 2,000 m water depth (Cooper et al., 2013; Azpiroz-Zabala et al., 2017). Deposits on the canyon floor consist of laminated sediments mainly composed of clay and silt, organic matter, with a minor component of sand (Dennielou et al., 2017; Azpiroz-Zabala et al., 2017) (Figure 2.5 Panel D). The Var submarine canyon (Figure 2.1) is located in the northwest Mediterranean Sea, at the outflow of the Var River (Khripounoff et al., 2009). Turbidity currents were recorded from 2005-2008 by an ADCP located at 1,200 m water depth (Khripounoff et al., 2009). Sediment traps from the same location recovered fine to very-fine sand (Khripounoff et al., 2012) (Figure 2.5 Panel D). A sinuous submarine canyon extends from the Wanggar River delta in Cenderawasih Bay, West Papua (Figure 2.1), to ~1,600 m water depth. Near-bed velocity data were collected in 2012 using an Aanderaa RCM-9 single-point current meter positioned 10.3 m above the seabed at a location 10 km outside of the channel lobe axis in 1520 m water depth (Wood, 2013). Sediment cores recovered a range of grain sizes including sand (within the main channel axis) but were dominated by mud and woody organic debris (Orange et al., 2010) (Figure 2.5 Panel D), particularly in the lobe fringes where the current meter was located.

2.2.3 Oceanographically-fed submarine canyons

Monterey Canyon offshore California is fed by long-shore drift (Figure 2.1), with negligible river input (Paull et al., 2005). While the canyon extends to 3,600 m water depth, we focus on turbidity currents recorded in the upper 50 km length of Monterey Canyon measured by an array of ADCPs deployed from 2016-2018 in water depths between 200 m and 1850 m (Paull et al., 2018; Heerema et al, 2020). Sediment cores from the floor of Monterey Canyon dominantly sample coarse grained sand and gravels (Paull et al., 2005; Maier et al., 2019) (Figure 2.5 Panel D). Hueneme Canyon, offshore Southern California (Figure 2.1), is also an efficient trap for sands transported by littoral drift, although, the Santa Clara River is also an important source of sediment input (Xu et al., 2010). Turbidity currents were recorded by an ADCP located at 188 m water depth, where sediment traps mainly captured fine sand (Xu et al., 2010) (Figure 2.5 Panel D).

2.3 Methodology

We characterise the structure of each turbidity current using for each measurement the temporal evolution of the maximum velocity and the total flow duration We primarily use ADCP data in our analysis because the depth-resolved velocity measurements allow us to plot the maximum velocity despite the height of the velocity maximum changing through time. Raw ADCP data at Squamish Prodelta, Bute Inlet, Congo Canyon and Monterey Canyon permit such detailed velocity analysis (Figure 2.2).

We then compare our results with measurements from published data that do not permit us to be as precise, because flow velocity was only reported at fixed heights within the water column (i.e. ADCP measurements in Var and Hueneme Canyons and fixed current meter in Cenderawasih Bay; Table 2.2), but still provide a valid comparison with different system types.

2.3.1 Ensuring consistent identification of the start and end of turbidity currents

For each of the individual flow time series, we identified the starting point of turbidity currents. The start of a flow is straightforward to recognise, as it is the point in time that features a rapid increase in the downstream velocity. Defining the end of a turbidity current is more difficult. To be consistent among the datasets, we apply a cut off at the point where downstream flow velocity is less than the average background velocity, plus or minus one standard deviation. We define background velocity as the ambient range of velocities that precedes the start of each event (Figure 2.3).

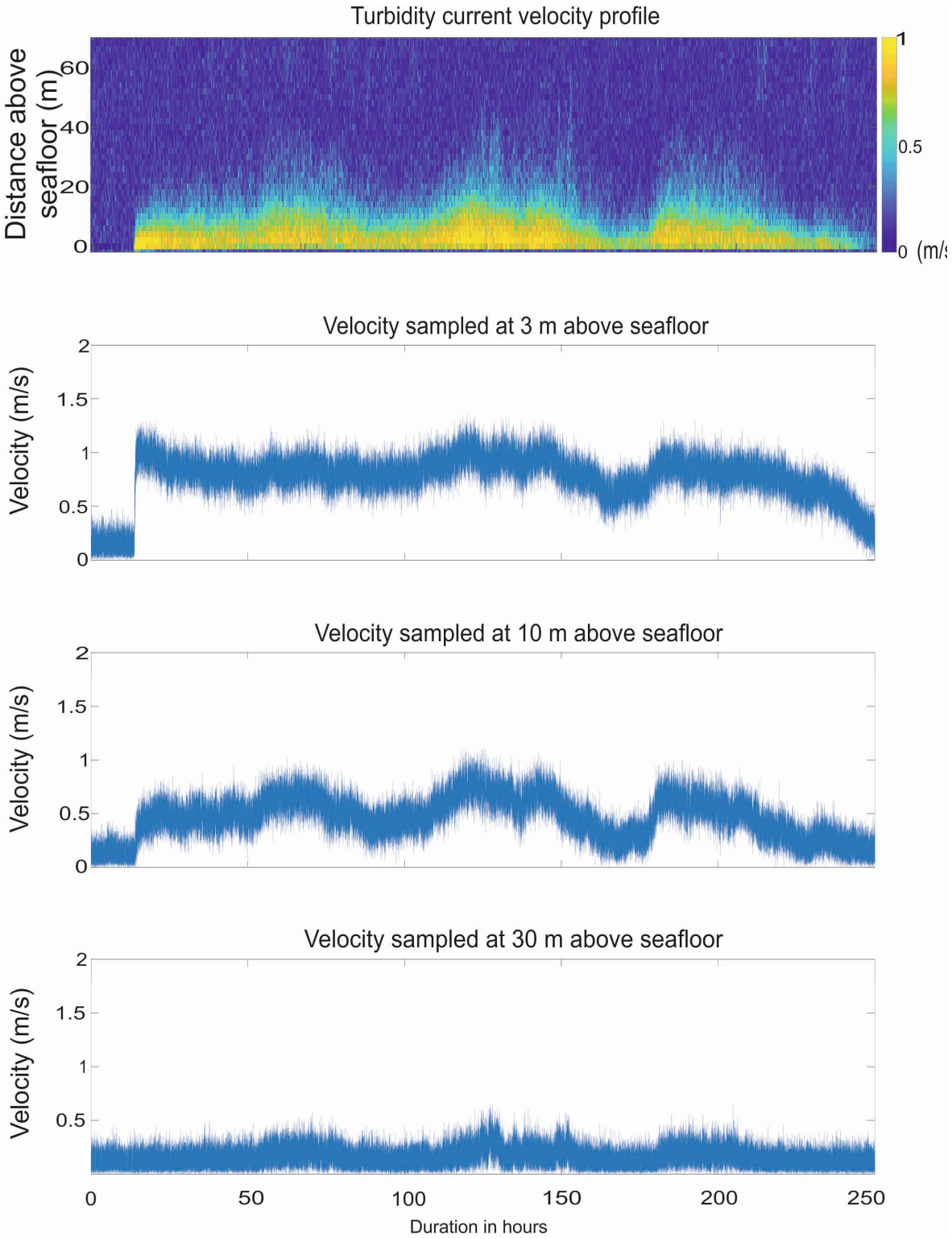

Figure 2.2: Example of velocity profiles measured using ADCP and extracted at different heights of the water column. Here we see Flow 01 from the Congo Canyon dataset (see Figure 2.4– Panel 6 in the main text and Table 2.1and Table 2.2)

2.3.2 Standardising the sampling frequency of velocity measurements

The temporal resolution of the data varies among the different sites depending on the configuration of the monitoring instruments (i.e. from every 1 second at Squamish Prodelta to every 30 minutes in Var Canyon; Table 2.2). In order to standardise the datasets, we sub-sampled the velocity of all of the events detected at each location relative to flow duration such that all datasets have 50 measurements regularly-spaced over the total duration of each flow (Figure 2.3).

This methodology means that the velocity-time plots of flows that were initially sampled with a higher resolution will be artificially smoothed to some degree. Our intention here, however, is to examine broad trends in velocity evolution over time. Therefore, it is important to ensure we provide a consistent comparison among all of the individual flows and across the different settings (Figure 2.4).

2.3.3 Normalised time-velocity plots

In order to compare trends in the temporal evolution of flow velocity, we plot normalised time-velocity graphs. In these plots, the velocity of each individual event is normalised relative to its peak velocity, with time normalised to total flow duration (Figure 2.5– Panel A). We also correlate the normalised velocity-time plots of turbidity current with the slope gradient relative to each physiographic system (Figure 2.5 Panel B).

2.3.4 Calculation of bed shear stress

To investigate the role of grain size on the structure of the turbidity currents, we estimate the bed shear stress using this formula:

$$U^*=Umax\ K\ [\ln (hmax/(0.1\ D90))]-1$$

Where, Umax is the maximum flow velocity (m/s), K is the Van Karman constant of 0.4, hmax is the height of the maximum velocity (m), and D90 is the ninetieth percentile of the grain size distribution in microns (Figure 2.6- Panel B).

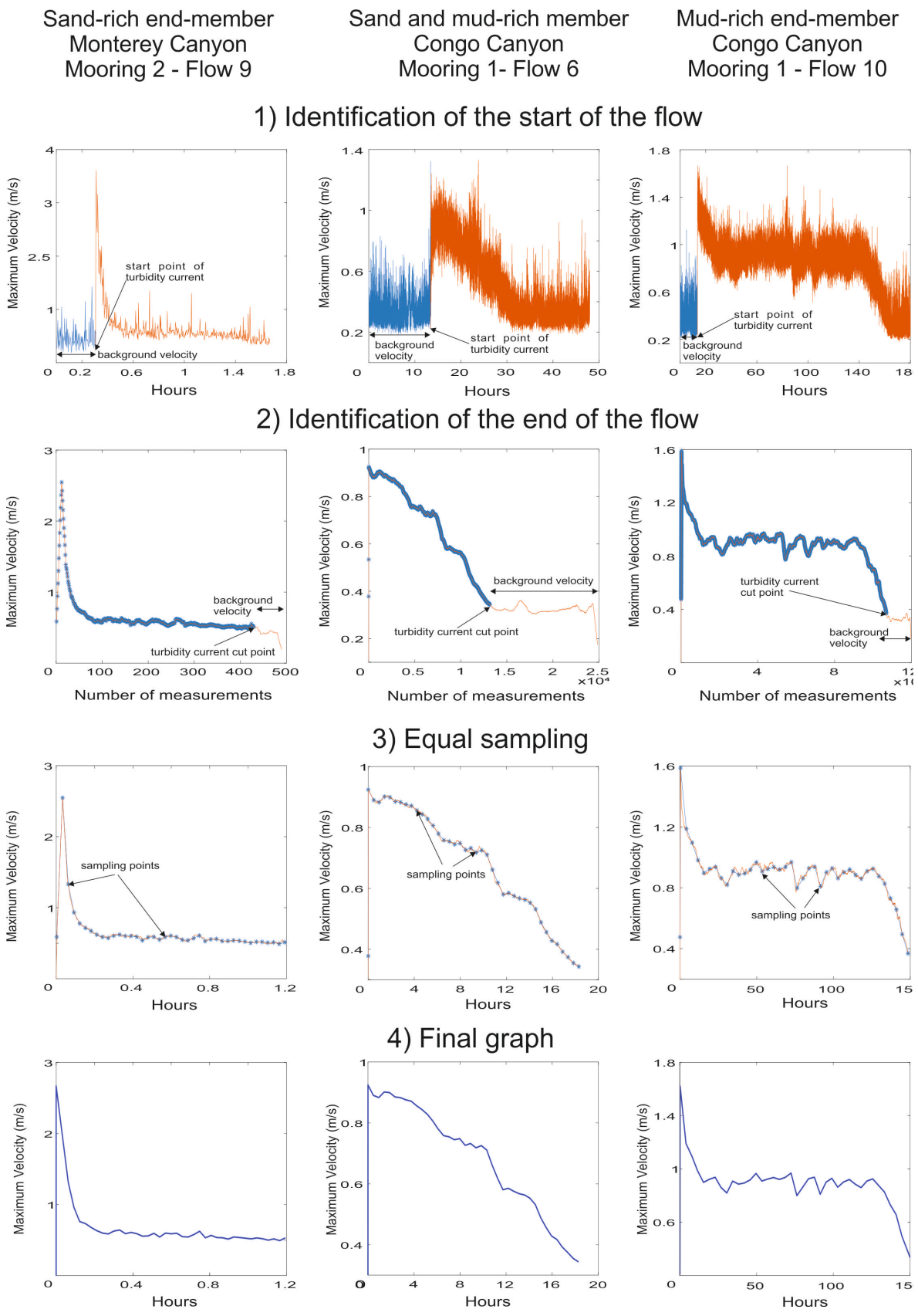

Figure 2.3: Schematic illustration of the methodology developed and applied to identify the turbidity currents analysed in this study. Events, ultimately, are plotted as graphs of time versus maximum velocity. Refer to the main text for the specification of our methods

2.4 Results

Here we describe the main results of our analysis.

2.4.1 Two end-members in turbidity current structure

Our results show that the velocity evolution of all of the turbidity currents analysed in our study fall between two end-members (Figure 2.5- Panel C).

The first end-member is characterised by flows that feature a rapid, near instantaneous, peak in velocity followed by an exponential decay. These events last from 42 minutes to 20 hours, and their peak velocity varies from 0.25 m/s to >6 m/s. The second end-member is represented by turbidity currents that initially show a similar trend (i.e. an increase in velocity followed by an exponential decrease that lasts up to 30% of the total flow duration). However, instead of continuing the exponential decay, these flows display a flat area of near-constant velocity (Figure 2.5 Panel C). Durations for this second type of flow are markedly longer, lasting for ~8 days (from 6 minimum to 10 days as maximum), with constant flat velocities lasting for ~110 hours (from a minimum of 70 hours to a maximum of 150 hours). The peak velocities it is ~2.25 m/s (minimum of 1.5 m/s to a maximum of 3 m/s), reducing to ~0.75 m/s (from a minimum of 0.5 m/s to a maximum of 1 m/s) in the flatten part of the flow. The near-constant velocity of such areas are characterised by bed shear stresses in the range of ~0.012 m/s (from a minimum of 0.008 to a maximum of 0.016 m/s) (Figure 2.5 Panel C).

2.4.2 Spectrum of flow behavior between the two end-member types

Normalised time-velocity plots (Figure 2.5 Panel A) suggest that there is a continuous spectrum of behavior between these two end members. Short-lived (minutes to hours) turbidity currents, which occur in sandy systems (e.g. Squamish Prodelta, Monterey Canyon), have behavior that is closest to the first end-member (i.e. rapid increase, followed by a swift exponential decay in velocity). Longer duration (days to weeks) turbidity currents in mud-rich systems (e.g. Congo Canyon) show a constant, more stable velocity in their latter stages that characterizes the second end member. Flows that show intermediate behavior between these two end-members come from sites with mixed grain sizes (e.g. Cenderawasih Bay, Bute Inlet). Such events feature a rapid increase of the maximum velocity followed by an sudden decay that lasts for about 30% of the entire flow duration. Once the velocity reaches 2/3 of its maximum, the decay then precedes until its minimum and flattens to zero. The duration of such flows varies from 27 minutes to up to 2 days and the maximum velocity ranges from 0.18 m/s to 1 m/s (Figure 2.6).

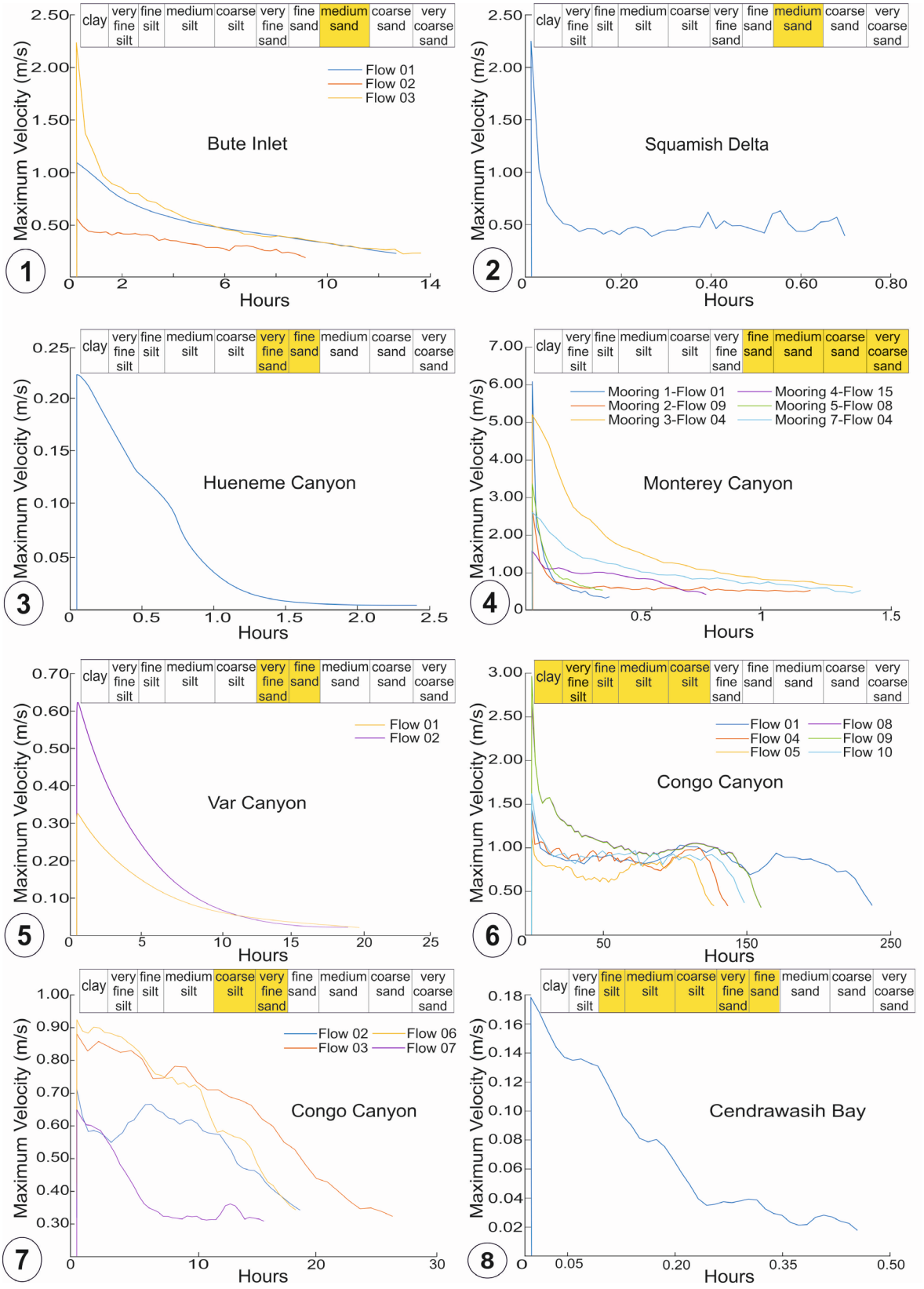

Figure 2.4: Maximum velocity versus time plotted for the different turbidity currents events detected at the different sites worldwide with the indication of the grainsize transported down-slope. The ADCP is moored to an anchor positioned to a fixed location; the measurements, therefore, are relative to the velocity of turbidity currents being detected at a single point along the continental shelf and/or channel thalweg. The ADCP measures water currents with sound by transmitting "pings" of sound at a constant frequency into the water within discrete time intervals. As the sound waves travel, they deflect off particles

suspended in the moving water, and reflect back to the instrument. The local decreases and increases of the velocities showed in our graph is due to local conditions within the water column that is sampled by the ADCP while a turbidity current is travelling down-slope. Each of the single lines shown in the graphs are relative to the general trend of the maximum velocity of the single events that have been detected during the monitoring campaign by each ADCP.

2.5 Discussion

Here we discuss the two end-members in turbidity current structure existing in nature, and which physical processes might determine where a particular flow lies on the spectrum between end-members.

2.5.1 Flow structure is independent of triggering mechanisms and system physiography

Turbidity current structure has previously been attributed to several factors, such as the physiography of the system (Xu et al., 2010; Talling et al., 2007; Stow and Bowen, 1980; Lowe, 1982), or the mechanism that triggered and initiated the flow (Middleton and Hampton, 1976; Kneller and Branney, 1995; Khripounoff et al., 2012). Here, we find that the flows from the different sites can show a very similar behavior, despite marked differences in how flows were triggered or initiated, and in the nature of sediment supply to the system. For instance, once normalised, the flow structure in littoral drift-fed systems (i.e. Monterey and Hueneme Canyons, offshore California) is similar to river-fed systems (i.e. Squamish Prodelta and Var Canyon; Figure 2.5 Panel A), conforming closely to the first end member scenario (rapid increase in velocity followed by exponential decay) (Figure 2.5 Panel C). Similar turbidity current structures were formed in the Squamish Prodelta, which were initiated by both delta-lip collapses or settling from a surface (homopycnal) plume (Hizzett et al., 2018; Hage et al., 2019), and flows in the Var Canyon caused by plunging (hyperpycnal) sediment-laden river floodwater (Khripounoff et al., 2012). The velocity-structure of these various turbidity currents were also comparable to flows measured in Monterey and Hueneme Canyons, caused by storm wave resuspension and slope failures preconditioned by rapid sediment accumulation (Xu et al., 2010; Paull et al., 2018) (Figure 2.5 Panel A),. Therefore, a wide range of triggers, flow initiation and physiographic systems can lead to very similar flow structure.Within a single physiographic system, however, multiple flow structures are possible. For example, flows in Congo Canyon are bimodal (Simmons et al., 2020); as some flows are fast with long durations, whereas others are slow with short durations (Figure 2.4 Panel 6 and 7 and Figure 2.6). However, flows from the same source area can also evolve in different ways, depending on their erosional capability and the grain sizes of sediment available on the canyon floor (Hage et al., 2019; Heerema et al., 2020), or there may be differences in distance to the source of these flows (Simmons et al., 2020).

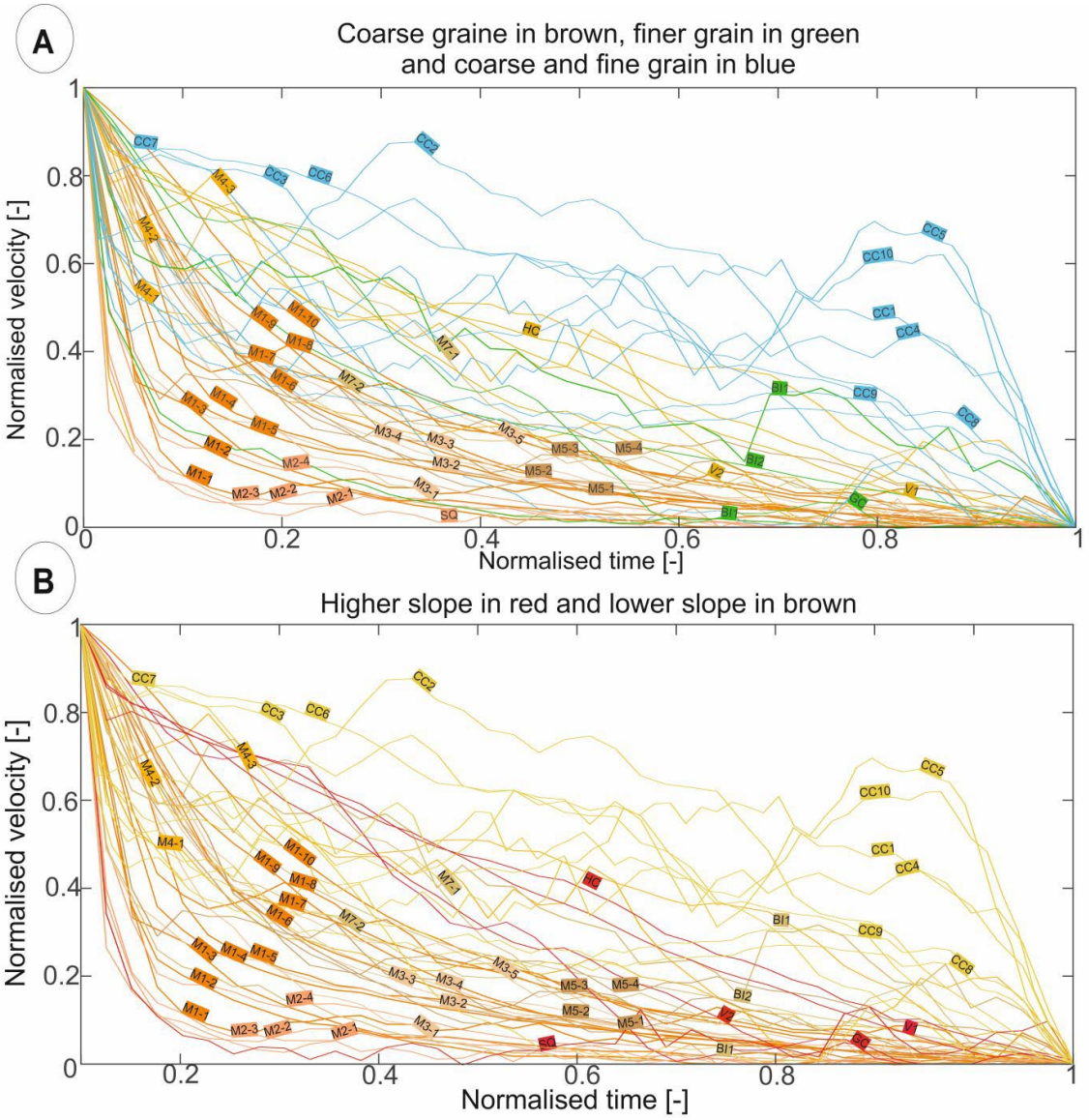

SQ= Squamish Prodelta
HC= Hueneme Canyon
MC= Monterey Canyon
GC= Cendrawasih Bay
VC= Var Canyon
BI= Bute Inlet
CC= Congo Canyon

Example:
M1-9= Monterey Canyon, Mooring 1, Flow 9
BI1= Bute Inlet, Flow 1

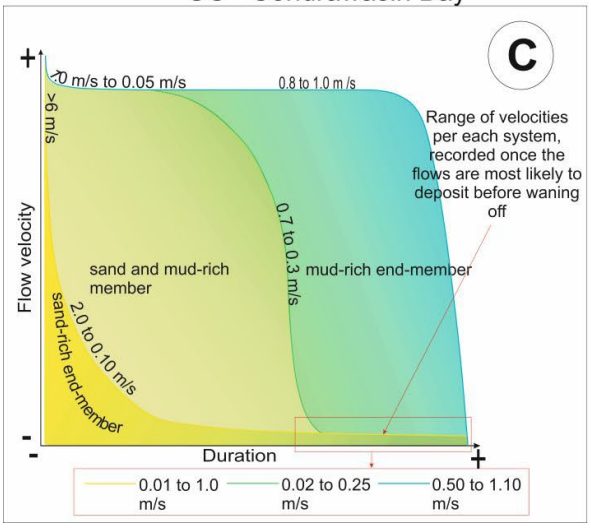

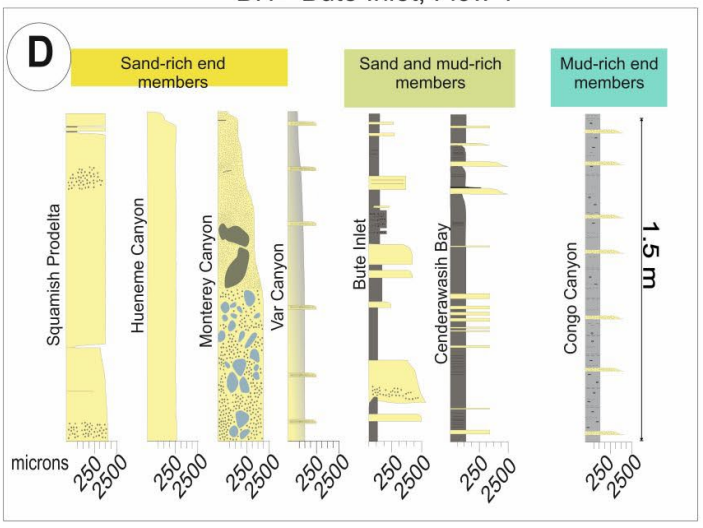

Figure 2.5: A) Normalised time-velocity plots for all of the turbidity currents studied in this chapter with the colour coded relative to the grain-size of the sediment flushed down each system; B) Normalised time-velocity graph of the same turbidity currents events with the colour coded linked to the steepness of the slope of the single systems C) Schematic layout of the main end-member turbidity currents as defined in this study. Numbers within the plot indicate the value of the maximum velocity detected from the ADCPs along the different portions of the flows; D) core logs sampled at the different physiographic systems used in this study to infer the grain-size of the sediments transported down-system by turbidity currents (see Table 2.3 for the description of such core logs and the reference to their study)

2.5.2 Does grain size control velocity-time profiles and if so why?

The normalised graphs shown in Figure 2.5 Panels A and B feature of two end members within the entire spectrum of flows that we have analysed in our study. The figure also shows other flows that seem to fall in between such end-members, and this leads us to believe that there may be a continuum among flow behaviour. We are aware, however, that our study is based on the available data that primarily focus on siliciclastic environments; hence, we provide future motivation that data from under-represented systems (e.g. muddy and carbonate-dominate systems) should be integrated in future.

Rather than triggers or system input type, our results suggest that flow structure is strongly influenced by the grain size of the sediment that is available for incorporation into the flow. The slope along which turbidity currents flow down-system seems also to exercise a strong influence in how flows behave (Figure 2.5 Panels B and C). Sand-dominated systems (e.g. Squamish Prodelta, Monterey, Hueneme, and Var Canyons; Figure 2.5 Panel D) feature a higher slope gradient (Figure 2.5 Panel B) and exhibit behavior closest to the first end-member. They feature short-duration (minutes to hours) flows, and often show the highest peak velocities (up to 6 m/s) (Figure 2.6). On a higher slope, sand settles out of suspension more quickly than mud; therefore, these sandy flows decelerate more rapidly. Such deceleration in turn drives further loss of sediment – resulting in an exponential decay in flow velocity. Mud-dominated systems feature a lower slope and, in our graph, (e.g. Congo Canyon; Figure 2.5 Panel D) they occur at the opposite end of the spectrum. These flows generally have lower velocities and a lower slope that allows flow to be sustained for several hours to days (Figure 2.6 Panel A).

Muddier sediment is much easier to keep in suspension, and hence slow near-uniform velocities could suspend mud leading to the long duration of the flows (Azpiroz-Zabala et al., 2017). The initial peak in velocity is likely to be due to a relative higher concentration of sediment in the frontal part of the flow, which is dominantly composed of sand (Simmons et al., 2020). We propose that flow behavior that falls between the two end-members (e.g. Bute Inlet, Cenderawasih Bay; Figure 2.5 Panel D) relates to the ratio of mud and sand within the flow and to the slope gradient relative to each system. Based on the data available, we could not assess the role that particle shape and density may play; hence, this may provide an avenue for follow-on research.

We now consider whether the absence of a velocity plateau is caused by the lack of mud (silt and clay-sized fraction) within the flow. If the bed shear stresses fall below the settling

velocity of mud (0.005 m/s) (Figure 2.6 Panel B), then this flow would not be capable of suspending mud. Conversely, if the bed shear stresses are higher than the settling velocity of mud, then it is likely that any mud within the flow would be suspended. The calculated bed shear stress of sand-rich turbidity currents falls between a minimum of 0.008 m/s (Bute Inlet) and a maximum of 0.018 m/s (Monterey Canyon). In Congo Canyon, mud-rich flows feature bed shear stresses ranging from 0.012 m/s to 0.014 m/s (Figure 2.6 Panel B).

The above analysis demonstrates that the absence of a flatten velocity in some flows is not because turbidity currents cannot carry fine-grained sediment, rather flows do not contain sufficient fine-grained sediment to sustain the flatten area (Figure 2.6 Panel B). This analysis also suggests that the duration of the flatten velocity likely relates to the amount of mud in the flow. In fact, the relative durations of the initial velocity peak and the subsequent flatten velocity, might help in providing a crude proxy for the ratio of sand to mud in a flow. As a result, flow structure may vary within individual systems (e.g. Simmons et al., 2020). As we focused on siliclastic systems, our analysis assumes a single particle density (i.e. quartz). Future studies should therefore ensure that flows are measured in different system types (e.g. carbonate-dominated canyons) to understand how widely these results hold.

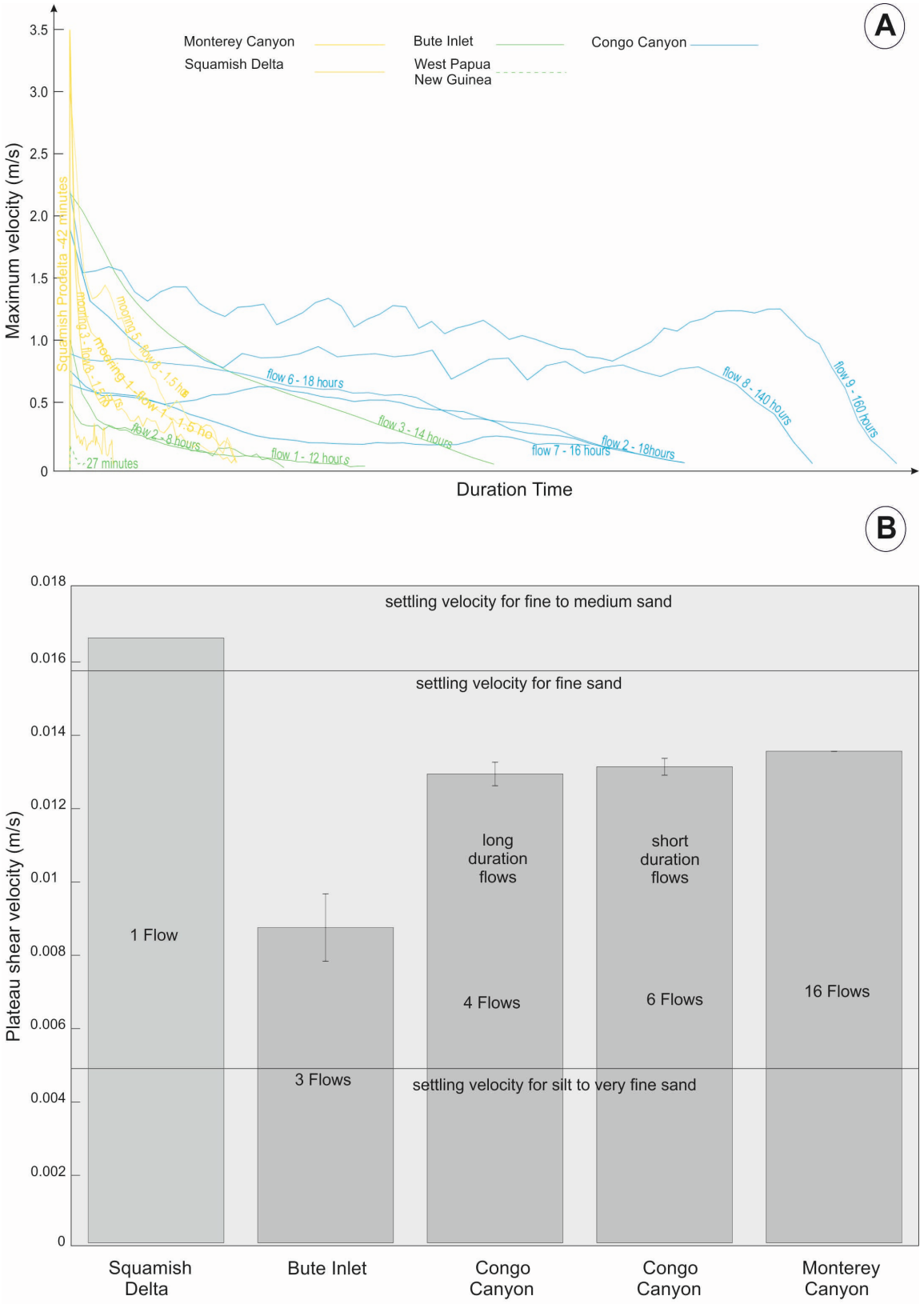

Figure 2.6: A) comparison between flow duration for some of the events analysed in this study. B) Cumulative bed shear stress of turbidity currents. In this graph, each block represents the sum of the bed shear stress estimated once each flow is more likely to deposit (plateau-like area). Vertical segments indicate the standard deviation error. For sites such as Squamish Delta, the value of the standard error

is missing because the date used herein are relative just to a single flow. Horizontal lines account for the settling velocity threshold relative to silt, fine and medium sand. Refer to the main test for the specification of the values herein considered.

2.6 Conclusions

This analysis of turbidity current structure at different sites worldwide focuses on the temporal evolution of the maximum velocity. In our analysis we mainly looked at the gradient of the system's slope and the grain size transported down stream by each event. Such parameters seem to be interconnected and equally important in determining the shape of the flow velocity. The grain size, however, seems to have the strongest control on flow behaviour; Knowing the grain size of the sediments within a specific physiographic system might help in inferring a likely flow structure. This is valuable to studies that focus on geohazards, as the initial dense, sandy portion of the flow will have a different impact to the more sustained plateau. Our findings also have implications for the transport and burial of particles such as organic carbon and pollutants (including microplastics), as they are transported according to their grain size (e.g. Galy et al., 2007; Hage et al., 2020; Pohl et al., 2020; Kane et al., 2019).

.

Data Availability

Datasets for this research are included in the following papers with the exception of the Cenderawasih Bay data which are provided as a supplementary data file (filename.csv).

Hughes Clarke, J.E., 2016. First wide-angle view of channelized turbidity currents links migrating cyclic steps to flow characteristics. Nature Communication, 7, 11896. https://doi.org/10.1038/ncomms11896

Hage, S., Cartigny, M.J., Sumner, E.J., Clare, M.A., Hughes Clarke, J.E., Talling, P.J., Lintern, D.G., Simmons, S.M., Silva Jacinto, R., Vellinga, A.J. and Allin, J.R., 2019. Direct monitoring reveals initiation of turbidity currents from extremely dilute river plumes. Geophysical Research Letters, 46. https://doi.org/10.1029/2019GL084526

Hage, S., Galy, V.V., Cartigny, M.J.B., Acikalin, S., Clare, M.A., Gröcke, D.R., Hilton, R.G., Hunt, J.E., Lintern, D.G., McGhee, C. A., Parsons, D.R., Stacey, C.D., Sumner, E.J. and Talling, 2020. Efficient preservation of young terrestrial organic carbon in sandy turbidity current deposits. Geology, 48. https://doi.org/10.1130/G47320.1

Xu, J.P., Swarzenski, P.W., Noble, M. and Li, A.C., 2010. Event-driven sediment flux in Hueneme and Mugu submarine canyons, southern California. Marine Geology, 269 (1-2), 74-88

Paull, C.K., Talling, P.J., Maier, K.L., Parsons, D., Xu, J., Caress, D.W., Gwiazda, R., Lundsten, E.M., Anderson, K., Barry, J.P., Chaffey, M., O'Reilly, T., Rosenberger, K.J., Gales,

J.A., Kieft, B., McGann, M., Simmons, S.M., McCann, M., Sumner, E.J., Clare, M.A. and Cartigny, M.J., 2018. Powerful turbidity currents driven by dense basal layers. Nature Communications, 9, 4114. https://doi.org/10.1038/s41467-018-06254-6

Khripounoff, A., Crassous, P., Bue, N.L., Dennielou, B. and Jacinto, R.S., 2012. Different types of sediment gravity flows detected in the Var submarine canyon (northwestern Mediterranean Sea). Progress in Oceanography, 106, 138-153

Simmons, S.M., Azpiroz-Zabala, M., Cartigny, M. J. B., Clare, M. A., Cooper, C., Parsons, D. R., Pope, E. L., Sumner, E. J. and Talling, P. J., 2020. Novel acoustic method provides first detailed measurements of sediment 1 concentration structure within submarine turbidity currents. Geophysical Research: Oceans, 125, e2019JC015904. https://doi.org/10.1029/2019JC015904

Azpiroz-Zabala, M., Cartigny, M.J.B., Talling, P.J., Parsons, D.R., Sumner, E.J., Clare, M.A., Simmons, S.M., Cooper, C., Pope and E.L., 2017. Newly recognized turbidity current structure can explain prolonged flushing of submarine canyons. Science Advances: 3(10), e1700200. DOI: 10.1126/sciadv.1700200

Wood, J. D., 2013. Ocean Current Measurements at the Elang-1 Location, Cenderawasih Bay, Eastern West Papua, Indonesia, July 2012 to December 2013. Ocean Data Technologies, Inc. technical report prepared for Niko Resources Ltd., Jakarta, Indonesia

Chapter 3

Autonomous Underwater Vehicles reveal a previously-hidden continuum of seafloor bedform morphometry

Vendettuoli, D., Clare, M.A., Cartigny, M.J.B., Hunt, J., Sumner, E.J., Bailey, L.

Author contributions: I led on the analysis and processing of the data, designed the study, and wrote the manuscript. M.J.B. assisted with developing the Matlab scripts for processing the bedform morphometry data. M.A.C, E.J.S, and M.J.C. provided the main editorial feedback on the manuscript draft. J.H. contributed to initial discussions on study scoping and data interpretation. L.B. assisted with initial interpretation of bedform types. All authors read and agreed on the final version of this manuscript. All the authors developed ideas, commented and approved the final version of this manuscript. This paper is planned for submission to Marine Geology. Data were provided by industry partner ENI.

Abstract

Bedforms on the seafloor are important archives to understand the behaviour of turbidity currents. Previous studies based on bathymetric surveys acquired from surface vessels found that only two main scales of bedform exists: small-scale (10s-100s of m wavelength) or large-scale sediment waves (several kms wavelength). These studies concluded that a distinction between two different flow modes exists, where small-scale bedforms are restricted to confined settings and large-scale sediment waves occur in unconfined deep water settings. By analysing an unusually extensive and high-resolution AUV bathymetric surveys collected offshore East Africa, we make consistent morphometric measurements of bedforms from water depths of 60 m to 2,800 m along two major submarine canyons, the Vamizi and Afungi Canyons. Such canyons from the proximal to the distal regions appear to be mainly confined; the Vamizi Canyon, however, opens up to a much wider splay area before reaching the deep water Querimbas Graben. First, we found that a new intermediate class of medium-scale bedforms exists within the previous data gap; thus a continuum of flow processes may exist. Second, the different scales of bedforms do not necessarily relate to water depth, as small-scale bedforms were found in two different settings: at the proximal reaches of the canyons to a water depth of 600 m; and at the distal reaches of the canyons up to a water depth of ~1,800 m. Finally, we identify an additional class of bedforms that did not exist in the previous classification. It consist of steep, stepped morphology that we identified as a knickpoint. These knickpoints occur at two scales: within the new medium-scale bedform domain, and also in much larger forms (60->70 m wave height). Finally, we observe a wider range of scatter in the wave height:wavelength ratio of large-scale scours than what previously identified. Our analysis shows that high-resolution AUV surveys provide the means to fill fundamental gaps

in our understanding of how channels are built and maintained, and to better constrain the nature of particulate transport into the deep sea.

3.1 Introduction

Recent advances in technology have provided the first direct field-scale insights into the often-powerful and fast-moving sediment-laden flows known as turbidity currents, and their seafloor interactions (e.g. Xu et al., 2011; Hughes Clarke, 2016; Normandeau et al., 2016; Azpiroz-Zabala et al., 2017; Hizzett et al., 2018; Paull et al., 2018). However, direct monitoring remains in its relative infancy, and is rare or absent in many settings Additionally, the observations are currently limited to relatively shallow water (<2 km, and mostly within a few hundreds of metres water depth; Azpiroz-Zabala et al., 2017; Clare et al., 2020 and references therein). Therefore, the records of past turbidity currents, in the form of their deposits, and the bedforms that they create on the seafloor, remain important archives for understanding the behaviour of turbidity currents (e.g. Bouma, 1964; Kuenen, 1964; Zeng et al., 1991; Piper and Normark, 2009; Hubbard et al., 2014; Postma and Cartigny, 2014; Maier et al., 2019). The dimensions, cross sectional and plan-form morphology of bedforms have previously been qualitatively and quantitatively linked to flow properties such as discharge, thickness, velocity, stratification, based on observations of field-scale turbidity currents, and analogue and numerical modeling (Hughes Clarke et al., 1990; Nakajima, 2002; Spinewine et al., 2009; Stow et al., 2009; Sequeiros, 2012; Cartigny et al., 2014; Kostic, 2014; Postma and Cartigny, 2014; Hughes Clarke, 2016; Hage et al., 2018). Understanding flow behaviour is important because it modulates the efficiency and extent of the transport of sediment, organic carbon and pollutants to the deep-sea, and dictates the nature of impacts to critical seafloor infrastructure such as telecommunication cables (Galy et al., 2007; Carter et al., 2014; Pohl et al., 2020; Zhong and Peng, 2021).

Bedforms are common across the global seafloor, particularly in submarine canyons and channels, where they form the main stratigraphic building blocks (Fox et al., 1968; Wynn and Stow, 2002; Symons et al., 2016; Covault et al., 2017). These seafloor geomorphic features can range from small-scale crescentic bedforms with wavelengths of tens to hundreds of metres, which typify many shallow water prodeltas and the heads of submarine canyons, to large-scale sediment waves with km-scale wavelengths that have been observed on many open continental slopes worldwide (Wynn and Stow, 2002; Symons et al., 2016). Previous analysis of a database of submarine bedforms from 82 sites worldwide suggested that the distribution of bedforms between these two scales is not continuous; instead observing the clustering of small-scale and large-scale bedforms either side of a statistically-significant data gap when the bedform wavelength for each of the sites was plotted against wave height (Symons et al., 2016; Figure 3.5). This data gap was interpreted by Symons et al., (2016) to represent a distinction between two main flow modes, where small-scale bedforms (<300 m wavelength and <8 m wave height) are restricted to confined settings (channels and canyons), and large-

scale sediment waves (up to 7.2 km wavelength and 220 m wave height) tend to occur in unconfined settings.

The same authors noted, however, that the data gap may also be a function of data resolution and were therefore unable to make a firm conclusion at the time. In the analysis of Symons et al., (2016), most of the bedforms were identified from multibeam echosounder surveys that were performed from a surface vessel; the resolution of which becomes poorer in greater water depths as the transponder becomes further away from the seafloor. Horizontal and vertical resolution of multibeam sonar systems is ~ 3.5–20% of water depth and ~ 0.2–0.8% of water depth respectively (Hughes Clarke, 1998; Symons et al., 2016). This resolution issue can be solved by using an Autonomous Underwater Vehicle (AUV), which can be flown a controlled height above the seafloor, thus maintaining a constant vertical and horizontal resolution (Wynn et al., 2014). As AUV surveys tend to be time-consuming and expensive, their use in scientific studies so far has largely been limited to only small portions of submarine canyon and channel systems, such as small-scale crescentic bedforms within proximal to medial reaches of confined canyons (e.g. Paull et al., 2010; Paull et al., 2011; Tubau et al., 2015) and large-scale scours at the channel lobe transition zone (Carvajal et al., 2017; Maier et al., 2020).

Offshore engineering projects require exceptionally high precision surveys to assist with the siting and design of offshore structures. As a result, extensive AUV surveys are now routinely acquired by industry, particularly for large subsea developments and linear infrastructure routes (e.g. cables, umbilicals and pipelines) and where they will interact with irregular and potentially hazardous terrain, such as submarine canyons or channels (e.g. Campbell, 2015; Nash and Roberts, 2011). In this study, we benefit from an unusually extensive and high resolution industry-acquired AUV survey offshore East Africa that spans an area of 65 x 50 km, with a horizontal resolution of 5 m x 5 m, locally with inset higher resolution (2 m x 2 m) surveys. Such dataset enables us to make consistent morphometric measurements of bedforms from water depths of 60 to 2800 m.

3.1.1 Aims

Using this extensive and high-resolution seafloor dataset, we will address the following aims. First, we aim to determine what scales of bedforms exist along 60-70 km length of two major but distinct submarine canyons and if our high-resolution survey will validate the bedform groping as identified by of Symons et al., (2016). Second, we aim to determine the nature and spatial distribution of the different bedform groups within the two submarine canyons, and how such characteristics vary relative to their specific environmental settings. Third, we explore the physical controls on the distribution of the different scales of bedform. Previous studies suggest that small-scale crescentic bedforms are most common in proximal, confined settings. Are similar small bedforms apparent in deeper water and if so, why? Are large-scale sediment waves only present in areas of reduced confinement? If intermediate forms exist, do they only occur within certain canyon morphologies? Finally, we aim to understand what may be missing from existing ship-based seafloor surveys and how future high-resolution AUV

surveys can fill outstanding knowledge gaps surrounding deep-sea sediment transport and hazard assessments.

3.2 Geological Setting

Our study area includes a series of submarine canyons that incise the continental shelf offshore Mozambique, East Africa (Figure 3.1 and Figure 3.2), which then extend beyond the study area (>2800 m water depth) into the deep-water Tanzania Channel (Maselli et al., 2020). This sector of the northern Mozambique margin is part of the Rovuma Basin whose evolution started in the Late Carboniferous to the early Jurassic with the breakup of Gondwana (Salman and Abdula, 1995). The spreading of active seafloor between Madagascar and India marked the cessation of rifting and lead to the development of the present-day East African passive continental margin (Reeves et al., 2016).

The precise age of canyon formation on the margin remains unclear, but was presumably linked to sediment supply from the Rovuma delta system, the scale of which was much larger prior to the Holocene (Fonnesu et al., 2020), Maselli et al., 2020)The Rovuma river and delta systems represent the most recent supply of terrigenous material to the continental shelf (Fonnesu et al., 2020). Core samples show that the sediments within the canyons are sandy where the dominance of the sand-sized fraction being of carbonate and biogenic material, with the remainder being siliciclastic in nature (Pers. Comm. Hunt, Figure 3.3). The continental slope features a complex morphology, the expression of which relates to a series of gravitational structures of the Palma and Macimboa thrust belts (Mahanjane and Franke, 2014). Towards the deepest water in the study area (c.2,600 m), the surface expression of a normal fault that bounds the landward extent of the Querimbas Graben (Maselli et al., 2020) creates a pronounced steepening of the continental slope (Figure 3.1).

The morphological and subsurface nature of the shelf break is indicative of a mixed carbonate-siliciclastic margin (Leeder, 1999; Chiarella et al., 2017). The shelf break exhibits a series of notches, which may represent Pleistocene palaeo-coastlines (Green, 2011) and it is crossed by several intersects associated with the head of mature submarine canyons. Since the Last Glacial Maximum (LGM) at approximately 25,000 years B.P., the present-day morphology of the Mozambique shelf break appears to be governed by sea level fluctuations (Rohling et al., 2009); however, warming at the end of the Pleistocene saw a sharp rise of the sea level that has remained relatively stable since approximately 6,000 years B.P. (Ramsay, 1995).

The typical regional gradient across the northern Mozambique continental slope ranges from less than 4° to 6° and the water reaches depth >3,000 m where the canyons reduce in gradient upon entering the Querimbas Graben, where they coalesce to create the deep-water Tanzania Channel (Maselli et al., 2020). Five large East-West trending submarine canyons (and smaller intervening gullies; Figure 3.1) provide evidence for the past downslope activity of sediment-laden flows; the canyons themselves also featuring morphologies that are indicative of additional reworking by slope failure – particularly on their flanks and at their heads (Farre et al., 1983; Maselli et al., 2020; Fuhrmann et al., 2020). The precise timing of these former

flows is also unclear and may have been more common during sea-level lowstands when canyon heads were better connected to terrestrial sediment supply but may also have been regulated by tectonic activity on the East African Rift Valley (Burger et al., 2001; Maselli et al., 2020; Fuhrmann et al., 2020).

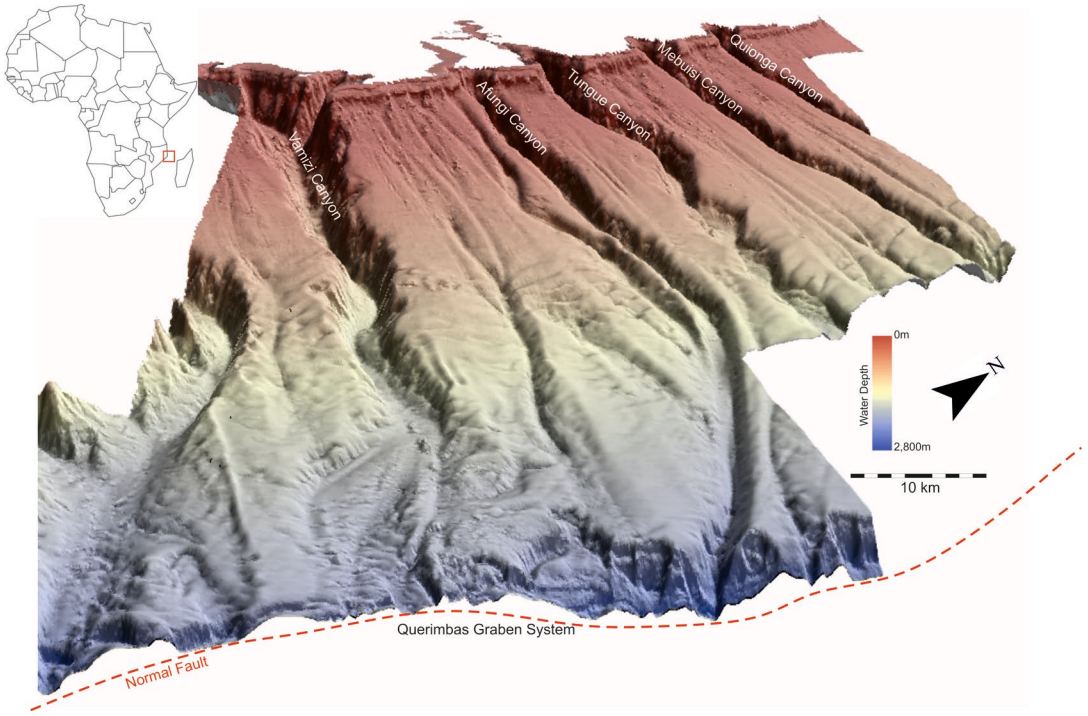

Figure 3.1: 3D image of the study area offshore the Northern Mozambique continental slope based on 5 m gridded AUV bathymetric data (vertical exaggeration 5.5x)

In this study we specifically focus on two canyons (Vamizi and Afungi canyons) (Figure 3.2) that are surveyed over 60-70 km of their length, from 60 m to 2,800 m water depth and that show a slightly different morphology. Local gradients within these canyons generally range from 1˚ to 6˚. Canyon morphology appears to be controlled by some of the regional structural features, particularly in the deepest parts of the survey area where the surface expression of the Querimbas Graben System causes a rejuvenation of the slope. The Vamizi Canyon is wider than the other canyons observed, reaching widths of between 3 and 6 km. Immediately up-dip of the Querimbas Graben System, the Vamizi Canyon is observed to broaden out, where a series of large (15 m to 60 m high, 400 to 6,000 m wide) scours are observed on the seafloor. The Afungi Canyon is less sinuous and more narrow (up to 700 m width) than the Vamizi Canyon, and rather than broadening out in deeper water, it becomes much more constricted (1 km wide) between 2,000 m and 2,500 m water depth, and then undergoes an abrupt series of steep steps where it reaches the Querimbas Graben System. These two canyons now form the basis of our study.

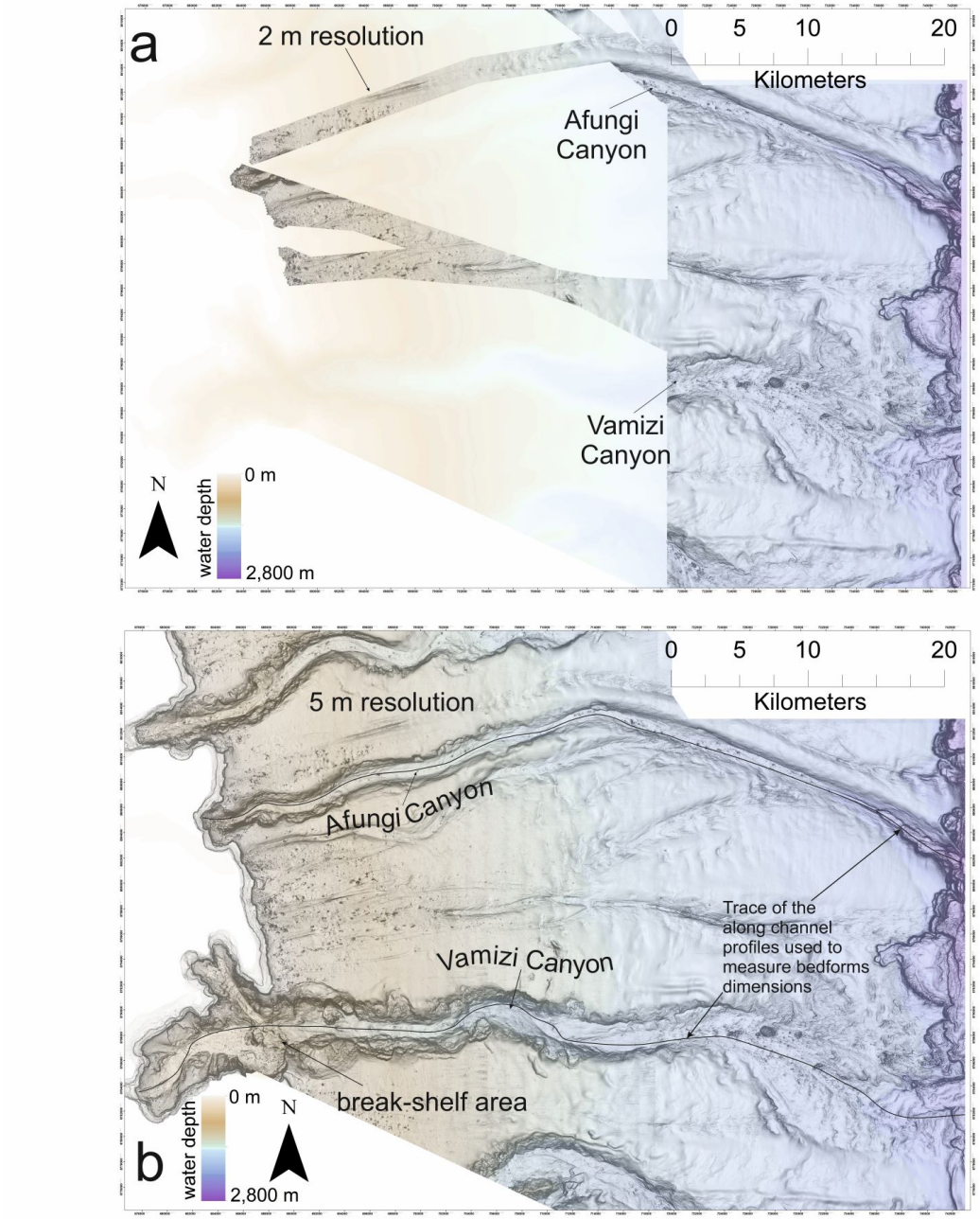

c

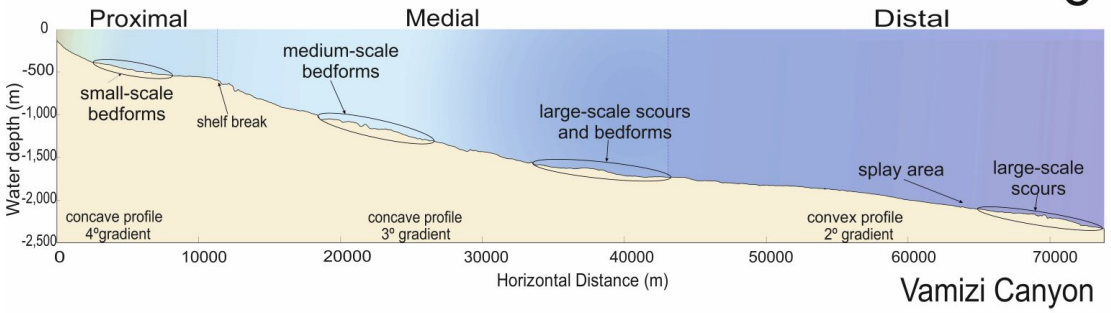

Vamizi Canyon

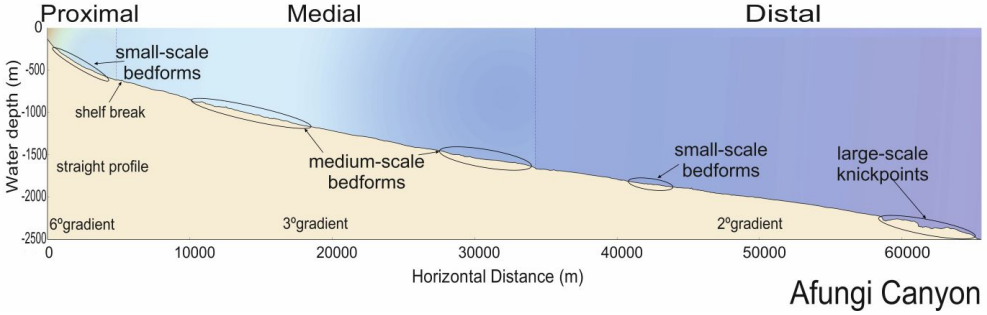

Afungi Canyon

Figure 3.2: a) 2D seafloor map of the study area surveyed using 2 m swath bathymetric data resolution. b) Same area fully covered by the 5 m data resolution. c) Simplified cartoon of the along slope bathymetric profiles of the Vamizi and Afungi canyons showing the locations of the major bedform classes found in this study.

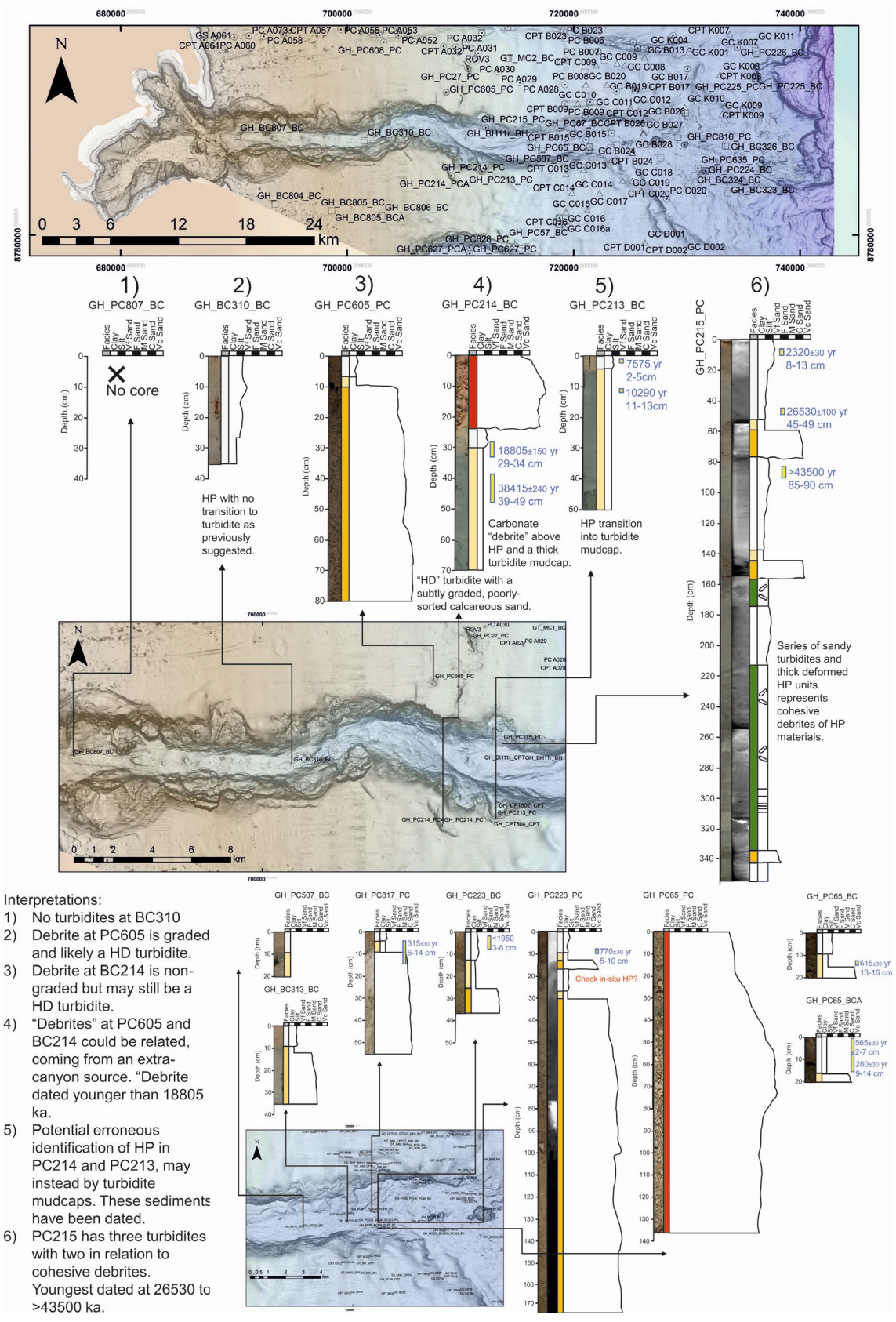

Figure 3.3: Example of the logs of seafloor cores along the Vamizi Canyon

3.3 Data and Methodology

The primary dataset analysed here is a high-resolution multibeam echo-sounder bathymetric survey that spans an area of 65 × 50 km (Figure 3.1), acquired from a Hugin 1000 AUV using a Kongsberg EM2040 sonar that provided 140^{o} coverage with a frequency range of between 200 and 400 kHz. Data across the entire area were gridded into 5 x 5 m bins. Higher resolution (2 m x 2 m) surveying was also performed to provide greater clarity in some areas (Figure 3.2).

To analyse the variability in bedforms along the two major canyons (Vamizi and Afungi canyons), we used the bedform tracking algorithm of van der Mark & Blom (2007) to quantify the morphometry of 64 specific bedforms selected on the basis of the high-resolution surveys. This algorithm analyses user-defined profiles (along the canyon thalweg or axial channel) to find the wave height and wavelength of specific bedforms selected in the profiles. We extracted this bedform information for the bedforms present within different reaches of the canyons that we define as proximal, medial and distal (as shown in Figure 3.2, Panel C)In defining such areas we mainly looked at the bathymetric contours map generated using ArcGis and the relative distance measured along the canyon. We defined the area preceding the shelf break as proximal, from 0 m to ~700 m below the sea level; up to 40 km horizontal distance and water depth of ~1,500 m was described as medial area; finally, up to 70 km along canyon and 2,500 m water depth was identified as distal area. We implemented each of the following steps in line with van der Mark & Blom (2007). For each canyon profiles, we chose a weighted moving average trend line, where the length of the moving average window is roughly 1/6 of the bedform length of interest. After detrending the profile, the start and end of the bedform of interest can be easily identified (Figure 3.4). Once the individual bedforms are identified, then bedform length is defined by the crest-to-crest distance in the unfiltered profile, and the wave height is defined as the crest and the subsequent trough in the unfiltered profile.

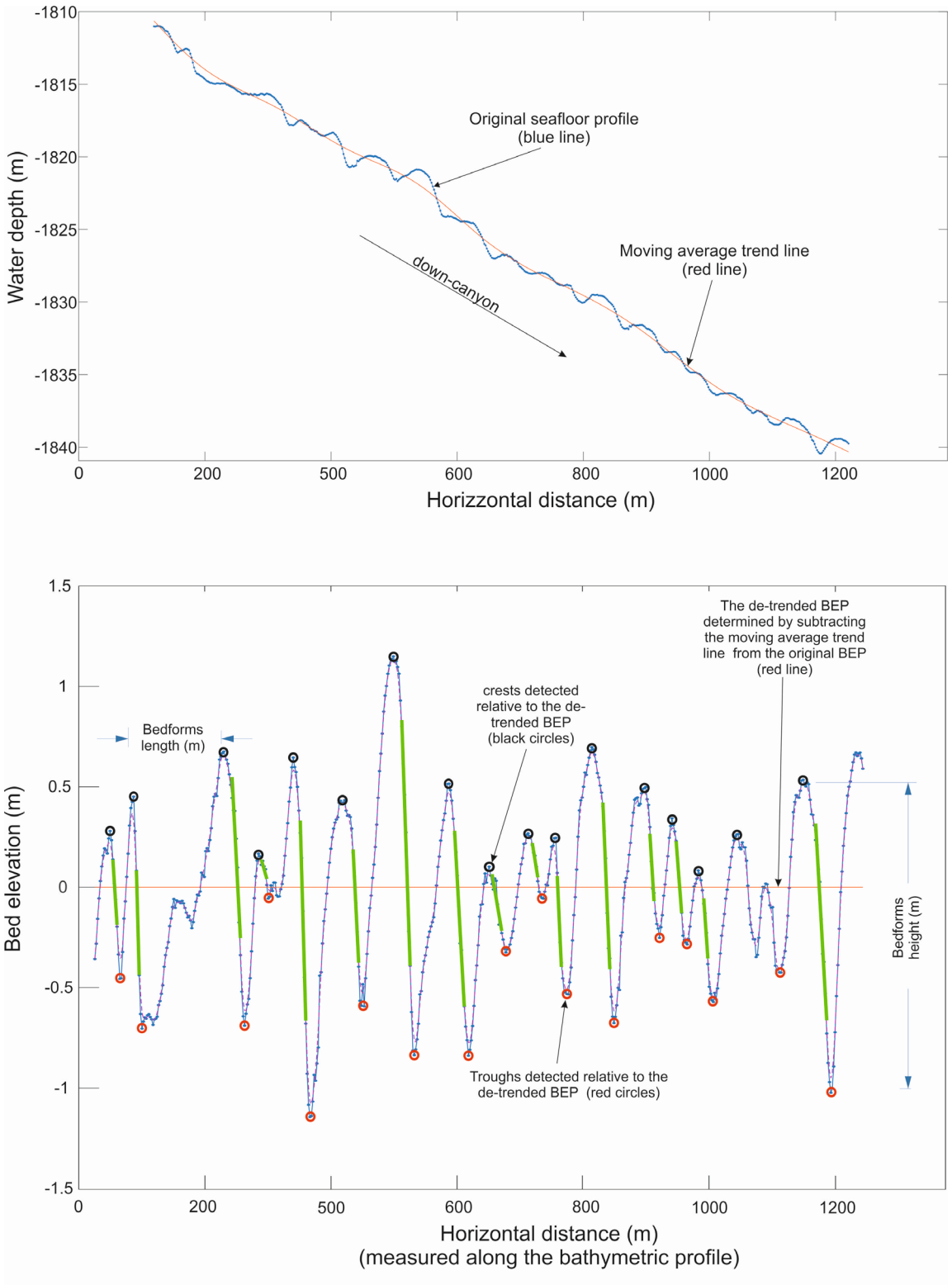

Figure 3.4: Annotated example to illustrate the methodology used to measure bedforms dimensions (BEP: bedforms elevation profile) using the Bedform Finder (der Mark and Blom, 2007). The figure displays the morphometric parameters of wavelength and wave high measured along the down-slope profile traced at the distal area of the Afungi Canyon and shown in Figure 3.13

3.4 Results

We now present the results of our analysis of the bedforms that were observed along all reaches of the Vamizi and Afungi canyons.

3.4.1 Overall observations of bedform morphometry

When plotting the measured wave heights and wavelengths of the bedforms detected along the thalweg of Afungi and Vamizi Canyons (Figure 3.5) we observe a wide variety of bedforms, with wavelengths ranging from 70 m to 8,000 m and wave heights varying from 1.5 m to 70 m. This is a similar range to that seen by Symons et al. (2016) and we also observed a very similar trend in wave height:wavelength ratio as seen by those same authors. The data indicate a very similar power-law trend to that seen by Symons et al. (2016) in wave height: wavelength, albeit with some variance from that trend (R^2 =0.41; Figure 3.5). We also observe the same scale classes of bedforms to those in Symons et al. (2016), which include: i) *small-scale bedforms* (up to 500 m wavelength and 5 m wave height); ii) *large-scale bedforms* (<10,000 m wavelength and <20 m wave height); iii) and *large-scale scours* (~10,000 m wavelength and >50 m wave height).

However, we make three observations that contrast with the study of Symons et al. (2016); First, we recognise a *medium-scale* category of bedform (up to 700 m maximum wavelength and c.10 m maximum wave height) that was absent in the study of Symons et al. (2016) and fills the data gap previously proposed. Second, we identify a type of bedform that did not exist in the classification of Symons et al. (2016) that is represented by a steep, stepped morphology, that we identify as a *knickpoint* based on morphological similarities to those identified in other studies (e.g. Mitchell et al., 2006). These knickpoints seem to occur at two scales: within the new medium-scale bedforms domain, and also much larger forms (60->70 m wave height). Third, we observe a wider range of scatter in the wave height:wavelength ratio of large-scale scours than identified by Symons et al. (2016; Figure 3.5).

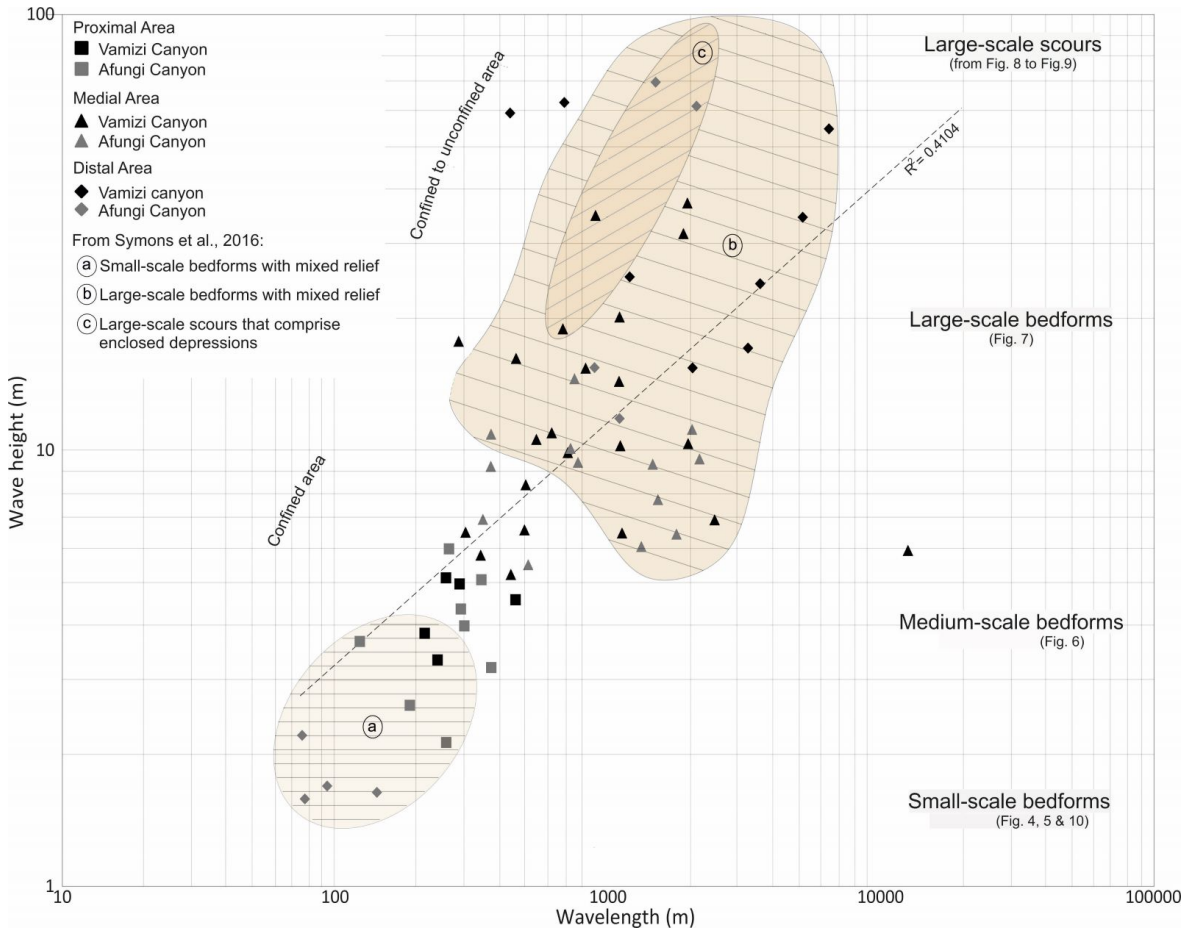

Figure 3.5: Bedforms morphometric dimensions observed in this study compared with the previous observations of Symons et al. (2016). Logarithmic plot of wavelength versus wave height for the bedforms detected along the thalweg of the Vamizi and Afungi canyons

3.4.2 Scale classes of bedforms and their spatial distribution

In this section, we discuss the different classes of bedform scale that we identify in more detail, and their locations within the Vamizi and Afungi canyons.

3.4.2.1 Small-scale bedforms

Small-scale bedforms have wavelengths ranging from 100 m to 500 m and wave heights spanning from 1.5 m to 5 m. They are asymmetric with round crests and narrow troughs and are parallel to sub-parallel to the bathymetric contours, following the canyon thalweg orientation. Such bedforms are found in two distinct locations (Figure 3.5):

[1] In the proximal to medial reaches of both the Vamizi and Afungi Canyons (up to 600 m water depth). Here, they are particularly pronounced in the head of the Vamizi Canyon, where they start with small dimensions (~100 m wavelength and ~5 m wave height). In its

proximal area, the Vamizi Canyon features a bathymetric profile gradient of 4˚, with the axial channel depth varying from 6 m to 40 m and the channel width that ranges from 30 m to 300 m. The Afungi Canyon seems to show a slightly greater gradient of 6˚, with the channel depth spanning from 2 m to 5 m and the axial channel width that varies from 100 m to 400 m (Figure 3.2, Figure 3.5, Figure 3.6 and Figure 3.7).

[2] In the distal, narrow part of the Afungi Canyon (at~1,800 m and from 2,200 m to 2,620 m). Here, small-scale bedforms are either found within a narrow (up to 300 m-wide) section of canyon (Figure 3.5 and Figure 3.11), or else superimposed on top of larger stepped bedforms (70 m–high and gradient from 3˚ to 6˚) (Figure 3.5 and Figure 3.13). The overall gradient for the distal part of the canyon is ~2˚. The depth of the shallowest reach of the canyons is 10 m and the width is 100 m. In the more distal and deeper portion of the canyon where the channel broadens to 120 m, smaller bedforms are found superimposed on top of larger bedforms (Section 3.4.2.5).

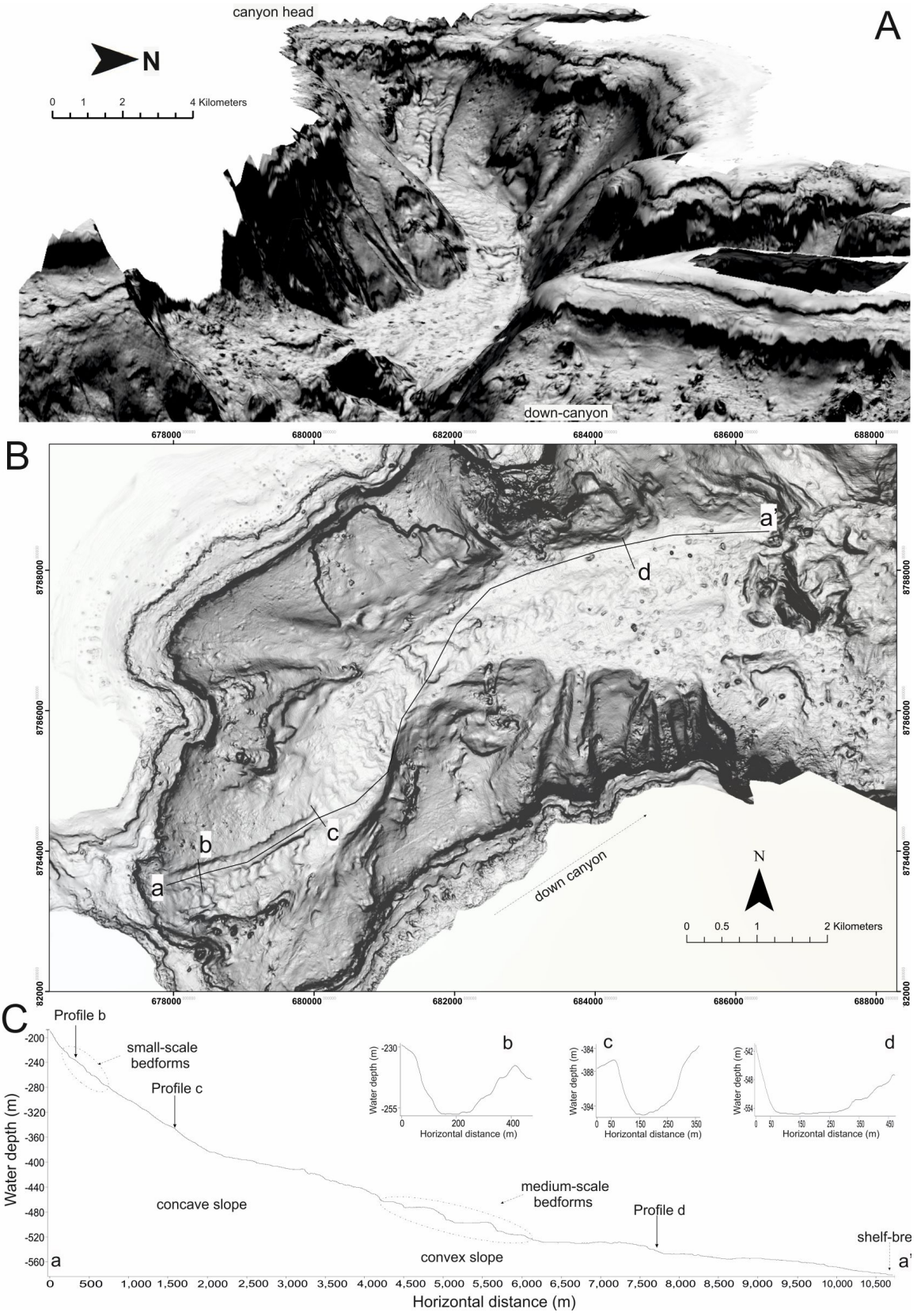

Figure 3.6: Detailed image of the Vamizi Canyon proximal area imaged using 5 m swath bathymetric data resolution. A: 3D visualization of the canyon head up to the shelf-break. B: 2D bathymetric map of the same area with visible in plan view the small-scale asymmetric bedforms. C: bathymetric profiles along and across canyon (see also Figure 3.2 and Figure 3.5)

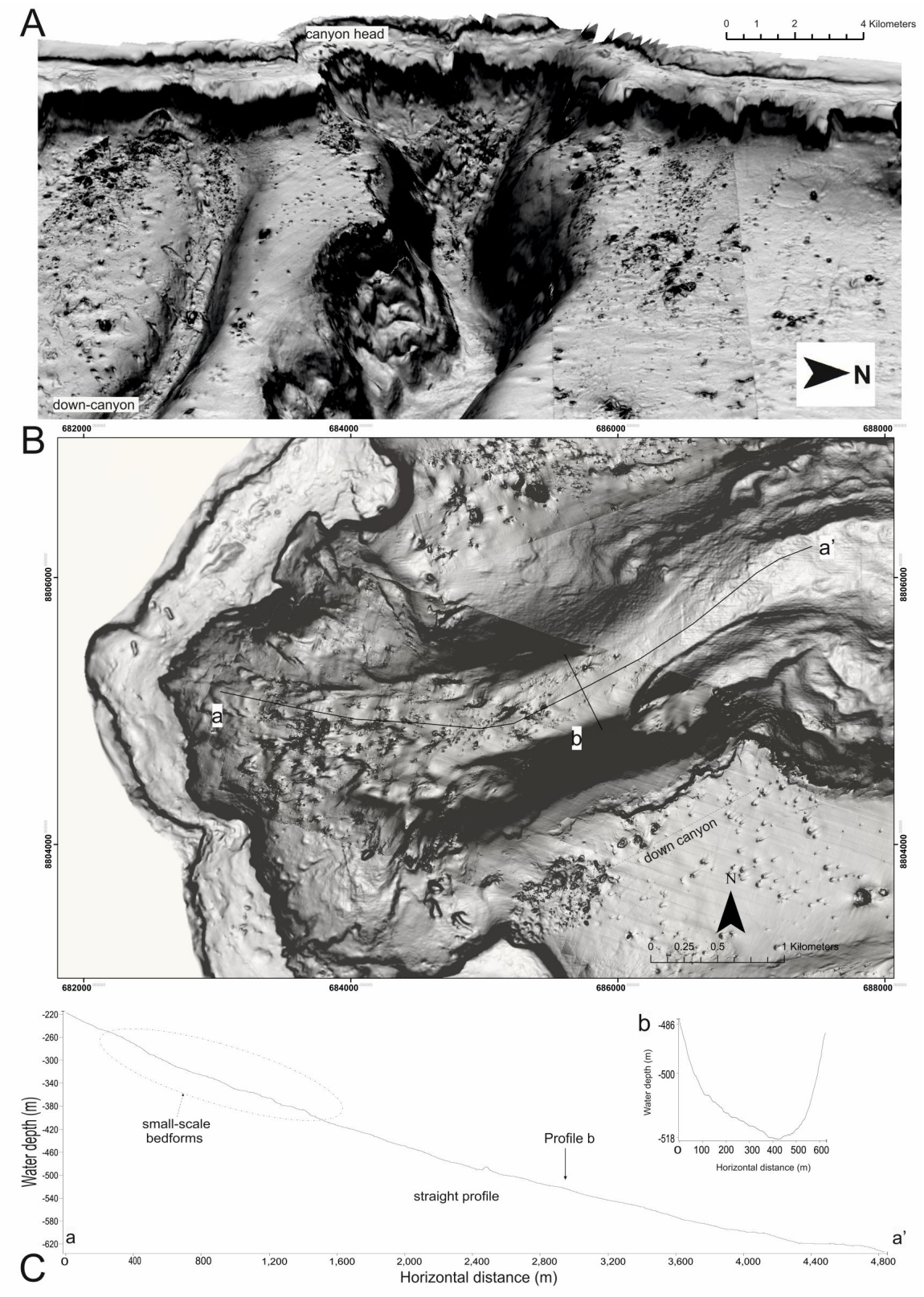

Figure 3.7: Detailed image of the Afungi Canyon proximal area realised juxtaposing 2m and 5m swath bathymetric data resolution. A: 3D visualization of the canyon head up to the shelf-break. B: 2D bathymetric map of the same area with visible in plan view the small-scale crescentic asymmetric bedforms. C: bathymetric profiles along and across canyon (see also Figure 3.2 and Figure 3.5).

3.4.2.2 Medium-scale bedforms

This scale of bedform was not previously recognised by Symons et al., 2016 (nor by the earlier study of Wynn and Stow, 2002) and forms an intermediate type between small- and large-scale bedforms. They generally feature a crescentic planform, with an upslope asymmetric cross-sectional morphology but this is not always as well defined as in the case of small-scale bedforms. Their dimensions vary from 300 m to 700 m wavelength and from 3 m to 9 m wave height and are observed from 600 m to 2,000 m water depth in the medial reaches of the Vamizi and Afungi canyons (Figure 3.5 and Figure 3.8). The Vamizi Canyon shows an average gradient of its bathymetric profile of 1˚, a channel depth ranging from 15 m to 40 m and a channel width varying from 350 m to 1,600 m. The Afungi Canyon features a similar bathymetric profile trend, a channel depth varying from 10 m to 30 m and a channel width from 400 m to 650 m.

3.4.2.3 Large-scale bedforms

Large-scale bedforms have wavelengths ranging from 700 m to <10,000 m and with wave heights between <10 m and <20 m. They show a wide range of morphologies, from straight to sinuous in planform and from symmetrical to asymmetrical in cross-section. Such sediment waves occur from ~1,200 m to ~2,000 m water depth, where the medial parts of the Vamizi and Afungi Canyons gradually transition into their distal reach. In these areas we also observe 10 m to >15 m high scours (see Figure 3.5 and Figure 3.5). The bathymetric profile of the Vamizi Canyon shows an average of 2˚ gradient with a concave to convex shape. The channels locally reach depths up to 60 m and width that spans from 500 m to >2,500 m. The Afungi Canyon shows a straight bathymetric profile also characterised by a low gradient (~1˚) and the channels locally reach depths of >50 m and widths from 70 m to >200 m.

3.4.2.4 Large-scale scours

Large- scale scours have wavelengths from 800 m to 10000 m and wave heights from 30 m to >50 m that are distinguishable from bedforms by enclosed depressions (see Figure 3.5 andFigure 3.10). They mainly occur at the distal part of the Vamizi Canyon in up to 2,500 m water depth where the canyon becomes less confined, with a splay-like morphology. Here, these large scours appear to be grouped into erosional areas bounded up- and downstream by steep-faces of 20 m to 40 m height. The overall canyon profile is 1˚ and the channel depth can reach up to >50 m and width up to >2,000 m.

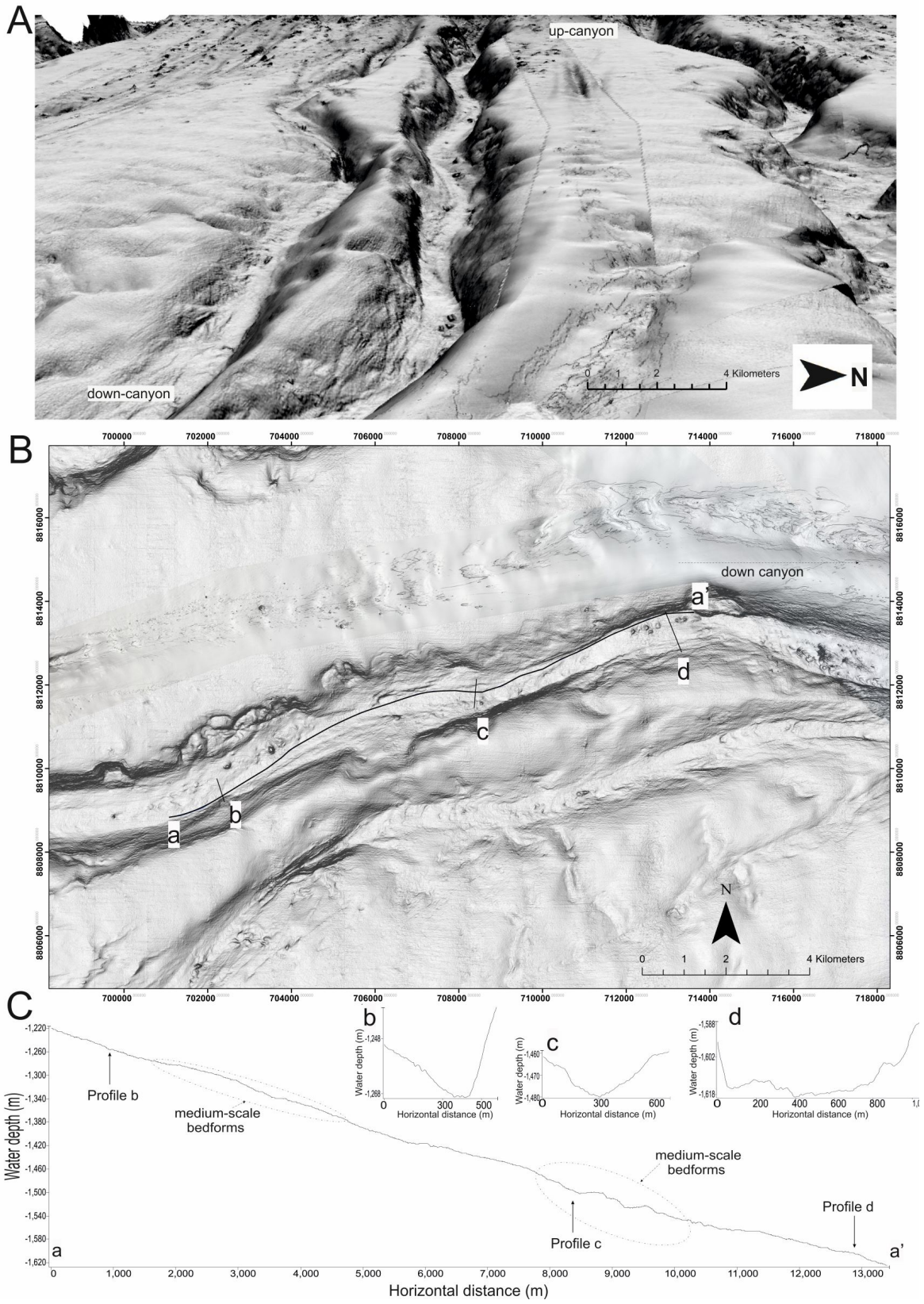

Figure 3.8: Detailed image of the Afungi Canyon medial area covered from the 5 m swath bathymetric data resolution. A: 3D visualization of the area; B: 2D bathymetric map of the area with visible in plan view the medium-scale asymmetric bedforms. C: bathymetric along and across canyon profiles (see also Figure 3.2 and Figure 3.5)

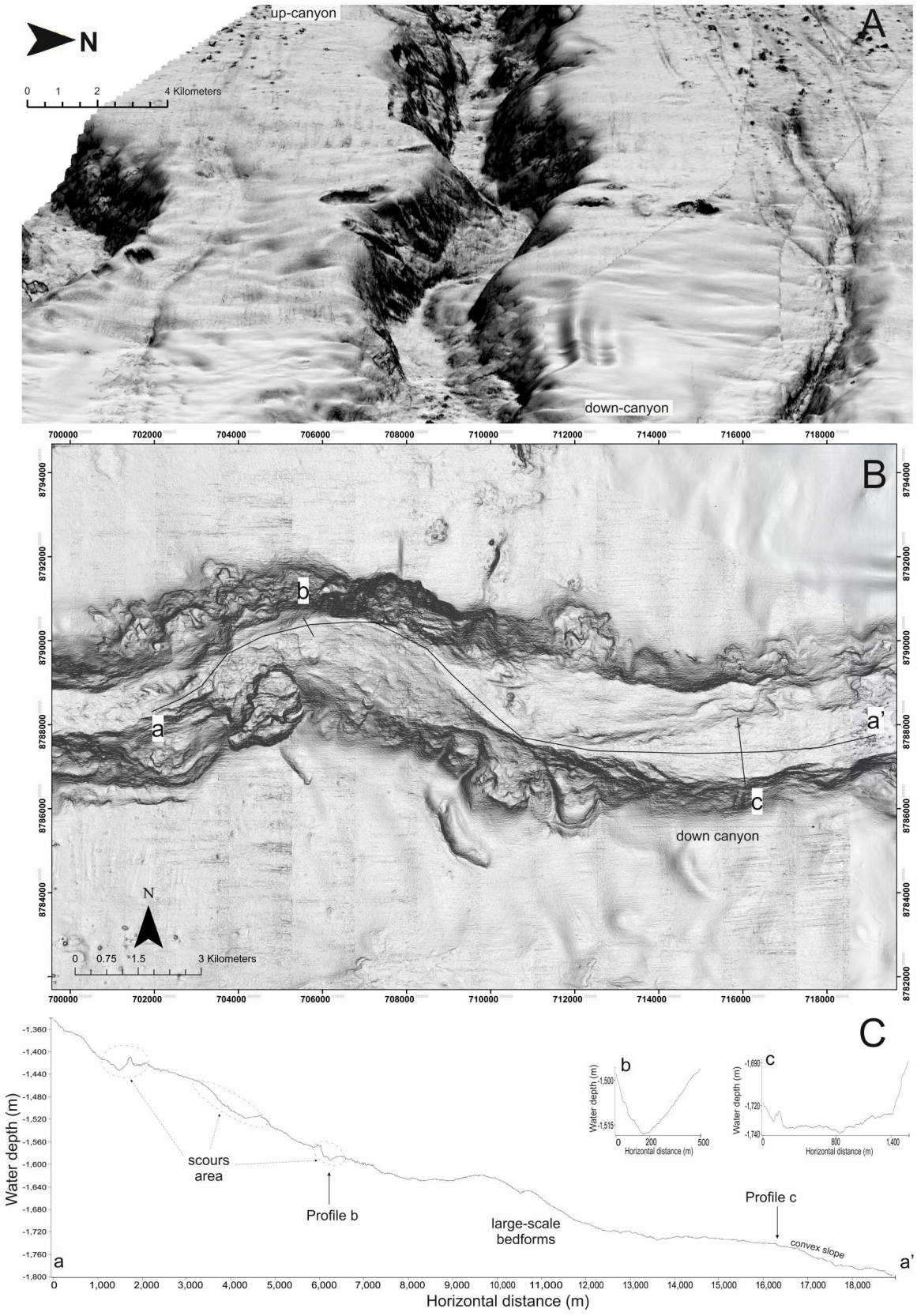

Figure 3.9: Detailed image of the Vamizi Canyon medial area realised using the 5 m swath bathymetric data resolution. A: 3D visualization of the area; B: 2D bathymetric map of the area with visible in plan view the large-scale bedforms and areas with scours. C: bathymetric profiles along and across canyon (see also Figure 3.2 and Figure 3.5).

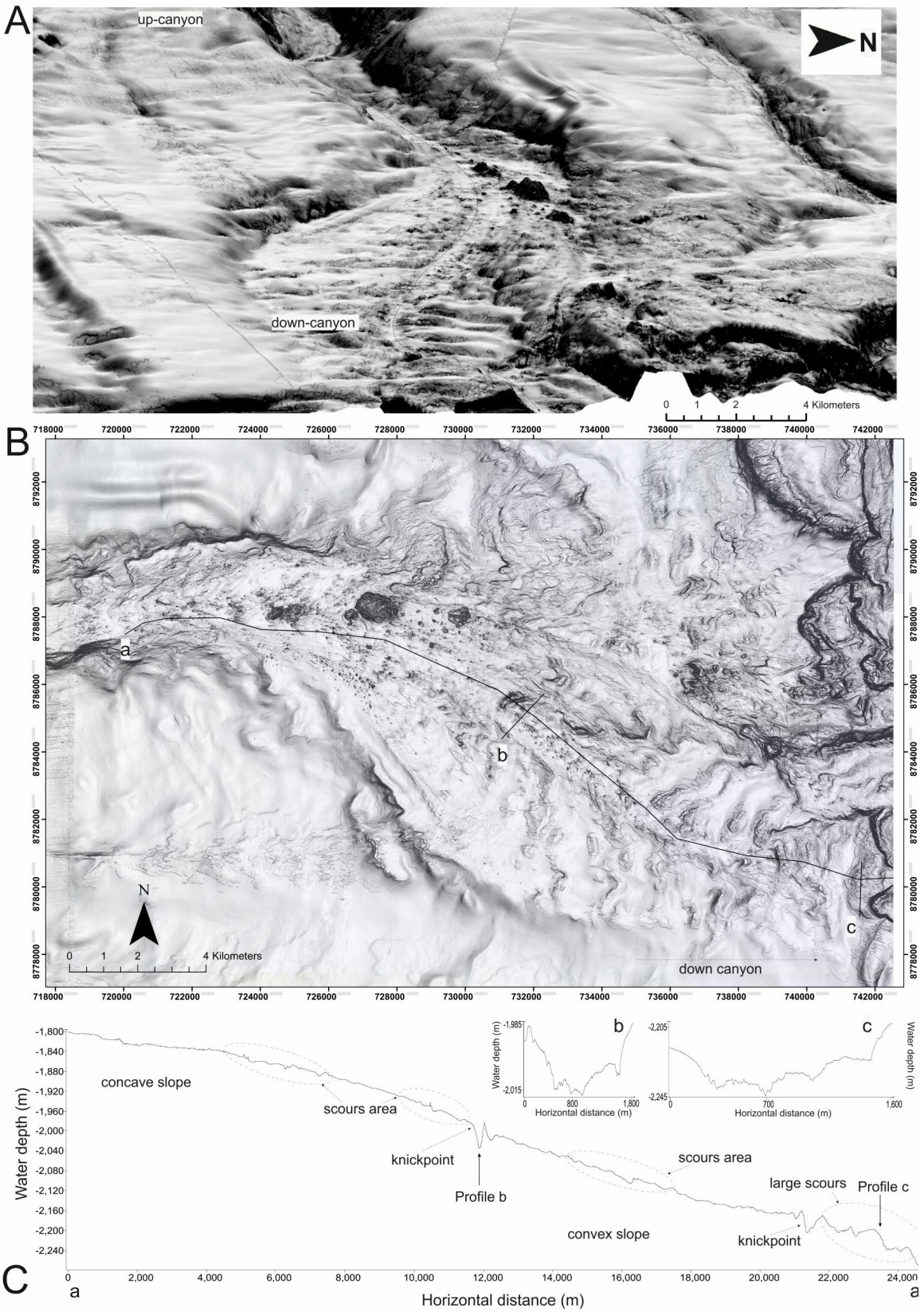

Figure 3.10: Detailed image of the Vamizi Canyon splay area fully covered by the 2 m swath bathymetric data resolution. A: 3D visualization of the area; B: 2D bathymetric map of the area with plan view of the scours. C: bathymetric along and across canyon profiles with visible knickpoints (see also Figure 3.2 and Figure 3.5)

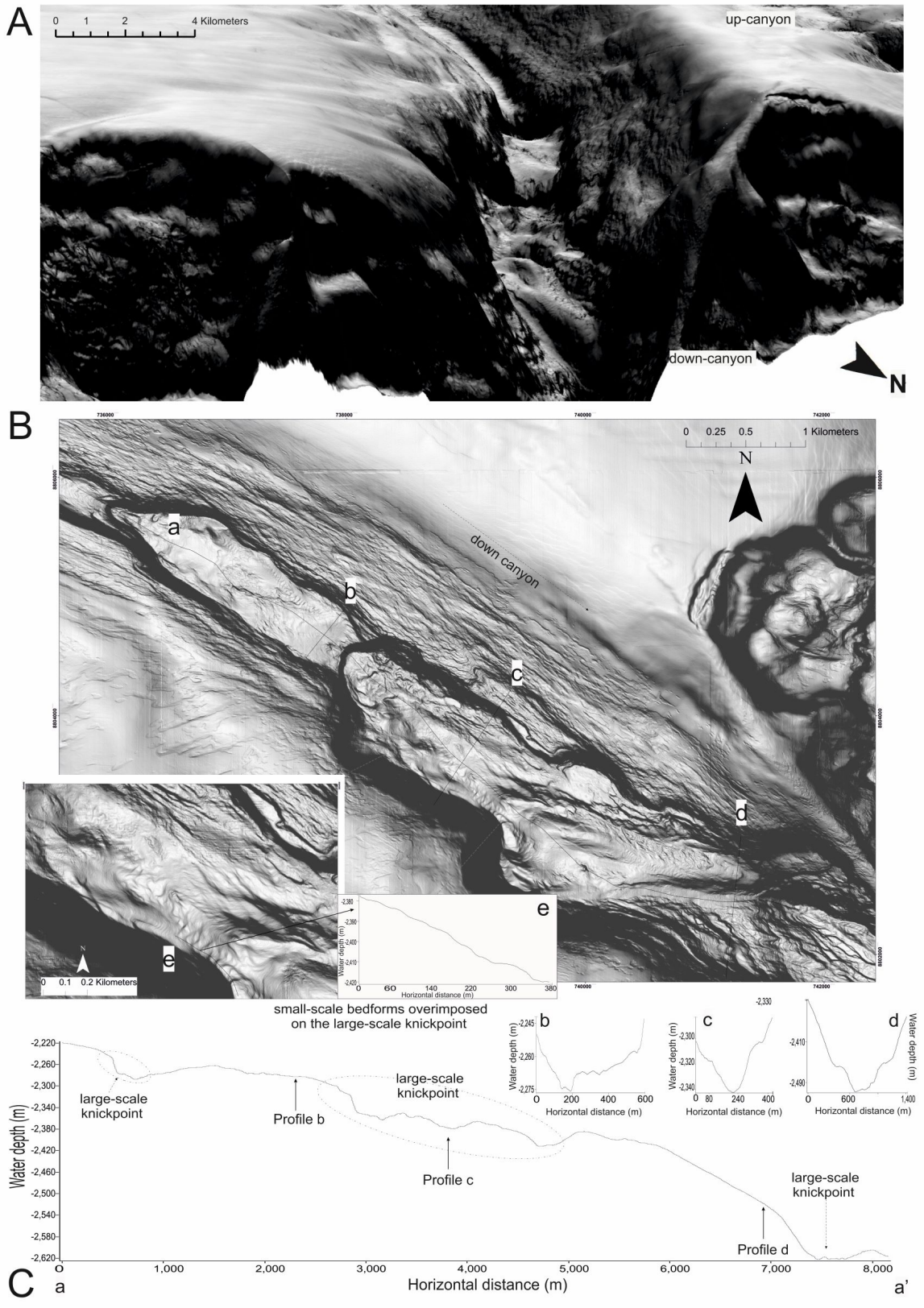

Figure 3.11: Detailed image of the Afungi Canyon distal area fully covered by the 2 m swath bathymetric data resolution. A: 3D visualization of the area; B: 2D bathymetric map of the area with visible in plan view the large-scale knickpoints with superimposed small-scale asymmetric crescentic bedforms. C: bathymetric along and across canyon profiles (see also Figure 3.2 and Figure 3.5)

3.4.2.5 Large knickpoints

Very steep and high knickpoints have wavelength varying from 2,000 m to 3,000 m and wave heights that reach values of 60 m to >70 m. They occur at the distal area of the Afungi Canyon at >2,300 m water depth and are spaced 500 m to 3 km apart, featuring a sharp crest and are often overlaid by small-scale upslope migrating crescentic bedform (see Figure 3.5 and Figure 3.11).

3.5 Discussion

3.5.1 Filling the gap in bedform scales

High resolution AUV bathymetric data have allowed us to make detailed measurements of bedform morphometry along the full length (~70 km) of two submarine canyons offshore Mozambique. While we identify similar classes of bedform scale (small-scale bedforms, large-scale bedforms and large scours), the new class of bedform that we observe (medium-scale) appears to fill in the gap in bedform dimensions of Symons et al. (2016). The exceptional resolution of the AUV bathymetry (particularly the 2 m binned data) reveals that an intermediate scale of bedform exists between the small-scale crescentic and large-scale sediment waves, which may indicate that a continuum of flow processes may exist, despite the possibility of two distinct flow modes as previously suggested (Symons et al., 2016). We also find that different scales of bedform are not necessarily dependent on water depth (Figure 3.11, Figure 3.12 and Figure 3.13). There is a very large amount of scatter when we plot wavelength and wave height against water depth, and we observe that, while small-scale bedforms are often most common in shallower water, they can also occur in deep water, such as the bedforms in the Afungi Canyon distal areas (Figure 3.11 and Figure 3.13).

3.5.2 Revisions to Symons et al. classification of bedforms

We largely find very consistent scales and types of bedform with the study of Symons et al. (2016); however, our data lead us to propose some revisions as we now discuss.

First, the medium-scale bedform appears to generally be transitional type of bedform between small-scale upstream-asymmetric crescentic bedforms and large-scale sediment waves. Medium-scale bedforms are often upstream-asymmetric in cross section and in many instances are morphologically-similar to steep-steps, known as knickpoints (e.g. Mitchell et al., 2006). The classification of Symons et al. (2016) did not include knickpoints; however, since their study was published, high resolution seafloor surveys have increasingly begun identifying these features in many submarine canyon and channels worldwide (e.g. Offshore California – Paull et al., 2010; British Columbia – Heijnen et al., 2020; Bay of Biscay -

Guiastrennec-Faugas et al., 2020). These knickpoints typically have wave heights of a few to tens of metres, and this scale of knickpoints is thought to be controlled autogenicenically (i.e. by internal channel processes; Vendettuoli et al., 2019; Guiastrennec-Faugas et al., 2020; Heijnen et al., 2020).

Second, we identify a much wider range in scales and wavelength:wave height ratio for large-scale scours than previously identified by Symons et al., 2016. Another type of much larger (up to 70 m high) knickpoints is observed within this class, which occur immediately up-dip of the large normal fault that bounds the Querimbas Graben (Figure 3.1 and 3.12). We posit that these much larger knickpoints are therefore primarily controlled by an allogenic, tectonic influence (sensu Maier et al., 2020; Whittaker and Boulton, 2012 - and references therein), rather than the autogenically-controlled medium-scale knickpoints (Heijnen et al., 2020).

Third, and as shown in Figure 3.13, we find that small-scale crescentic bedforms may occur in all water depths, at multiple parts of a canyon or channel (Figure 3.3, 3.12 and 3.13). This is evidenced by the fact that the smallest observed crescentic bedforms were found in the distal, much narrower reaches of the Afungi Canyon. Here, these bedforms were found superimposed on much larger bedforms. Such superposition can be common, but is challenging to image without sufficiently high resolution data.

3.5.3 What controls the distribution of the different bedform types?

We now relate the different scales of observed bedform to plausible controls. The small-scale bedforms we observe are equivalent to crescentic upstream-migrating bedforms that typify proximal sandy canyon systems worldwide (Paull et al., 2005; Hage et., 2018). We found that they were most concentrated in proximal settings, but can also occur where slopes are steep and/or confinement is narrow. We relate these bedforms to faster, concentrated flows that undergo a series of cyclic steps (e.g. Hughes Clarke, 2016). Their high concentration and velocity is maintained by a combination of high slope angle and constriction of the flow path (Cartigny et al., 2011; Sequeiros, 2012; Covault et al., 2017; Vellinga et al., 2018). Medium-scale bedforms occur in the medial parts of channels and we explain their occurrence either by: i) the expansion of the flows that created the small-scale crescentic bedforms, as they entrain more water and sediment, creating larger wave height and wave length bedforms (Piper and Savoye, 1993; Symons et al., 2017); or ii) from the internal generation of knickpoints that retrogress up-slope (Heijnen et al., 2020). Large-scale bedforms were only observed in distal reaches of the channels (in agreement with Symon et al., 2017), where confinement is much lower and we suggest that this relates to further expansion of flows that become more dilute (e.g. Komar, 1973; Wynn et al., 2000; McCave, 2017). Large-scale scours were only found in the distal reaches of canyons where past tectonic deformation has locally steepened the slope. The two types of scour include large-scale knickpoints, which appear to have initiated at a point coincident with a subsurface normal fault (similar to numerical modeling that showed enhanced bed shear where fault-controlled topography creates seafloor steps; Ge et al., 2017; and observations from seafloor data - Maier et al., 2019), and broader

scours, which are similar in morphology to those observed at the distal channel lobe transition zones of many submarine channel systems (e.g. Wynn et al., 2002; Macdonald et al., 2011; Hofstra et al., 2015; Carvajal et al., 2017).

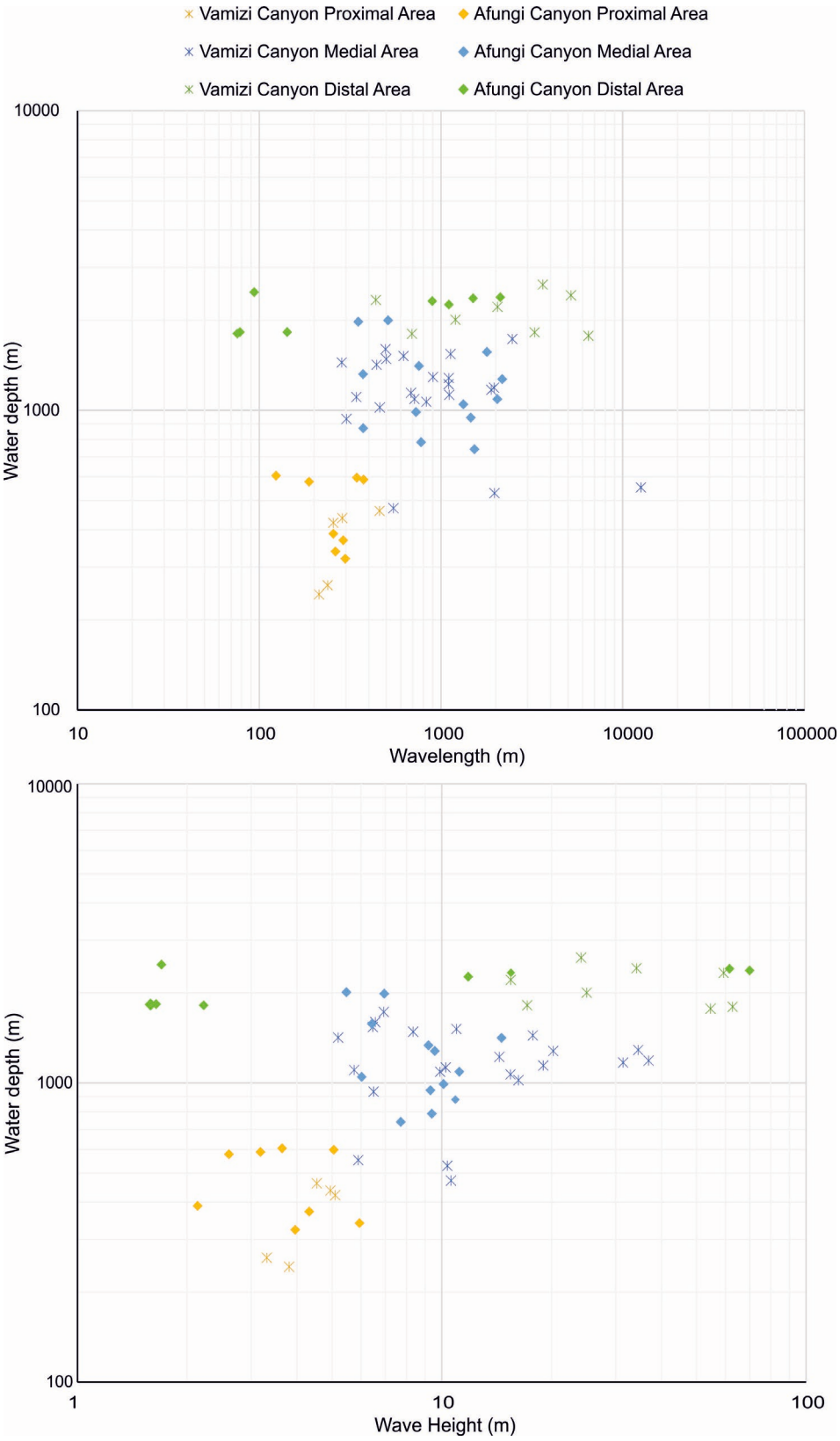

Figure 3.12: Bedform dimensions compared with water depth. Logarithmic plot of wave height (bottom panel) and wavelength (top panel) versus water depth for the bedforms analysed along the thalweg of the Vamizi and Afungi canyons.

3.5.4 Water depth-related controls on the identification of small- and medium-scale bedforms

In order to compare what may realistically be resolved from ship-based surveys compared with our higher resolution AUV data, we re-gridded our high resolution bathymetry more coarsely (up to 50 m x 50 m grid size). This coarsest gridding is equivalent to the spatial resolution of a ship-mounted multibeam sonar system in 2,500 m water depth with a one degree beam (Mayer, 2006). When the 2 m-grid size bathymetry is re-gridded to 5 m, the planform morphology of the small-scale crescentic bedforms is largely lost. While, cross sections at this resolution allow for the identification of peaks and troughs and render a general upslope-asymmetric morphology, their initial identification may be hindered. Re-gridding at coarser scales degrades the data further still, such that any evidence of these bedforms is lost completely (Figure 3.13). The recognition of small to medium-scale bedforms will therefore be limited in deep water without the use of AUV-acquired bathymetry. Other AUV surveys that covered small sections of canyons or channels have also identified that small-scale bedforms may be typical of many reaches of active confined submarine systems (e.g. Paull et. al., 2010; Carvajal et al., 2017) and they are thus not limited to proximal reaches alone. We suggest that this small scale bedform may be far more pervasive than previously thought and that there is a continuum of flow behaviour, between flows that create small- and medium-scale bedforms. As bedforms provide valuable information on the nature of the flows that have occurred within a channel, we suggest that more high resolution seafloor surveys provide an exciting tool to further our understanding of the local to global variations and trends in turbidity current behaviour.

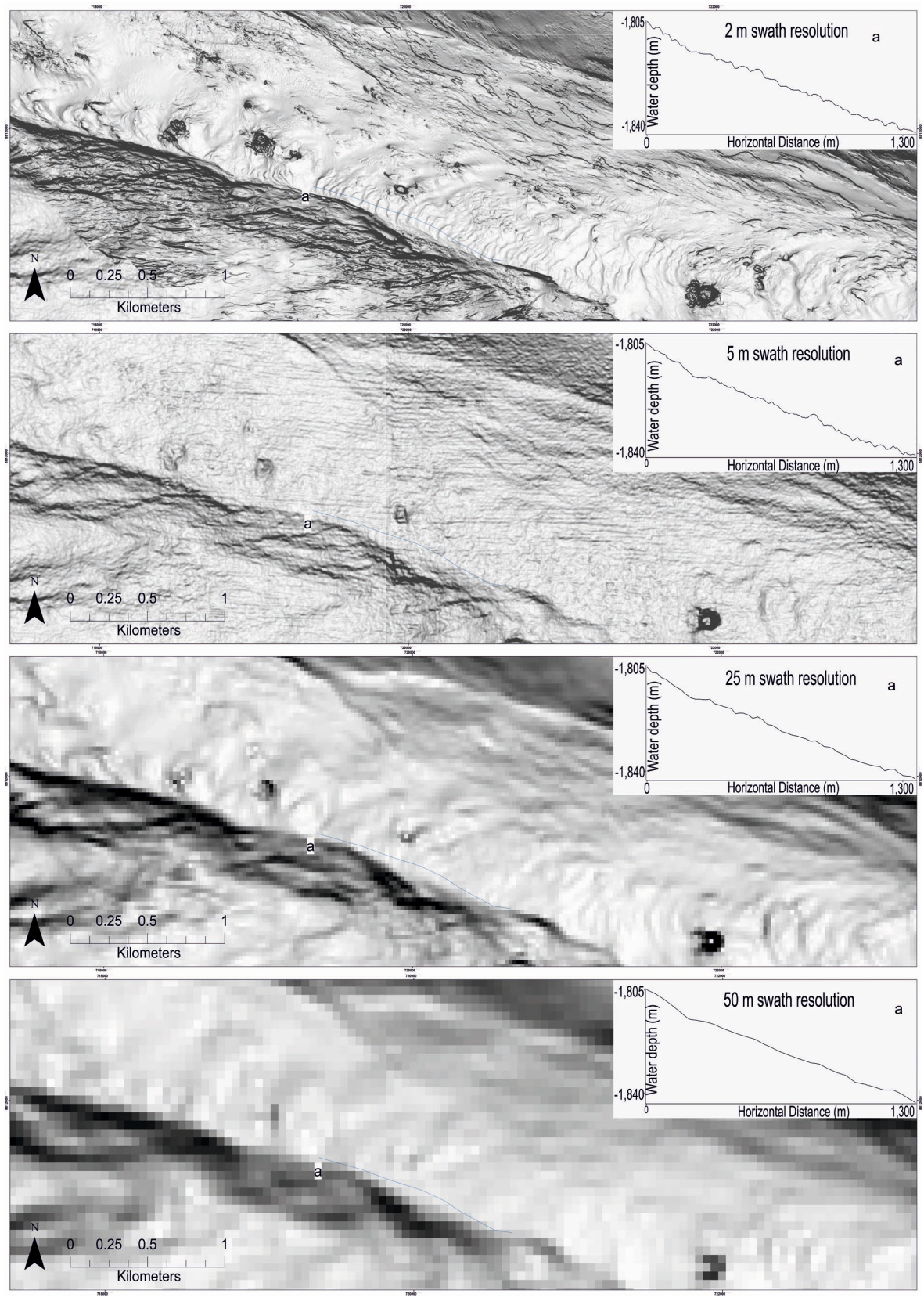

Figure 3.13: Comparison of different data resolution covering a portion of the distal area of the Afungi Canyon where small-scale bedforms are visible (Figure 3.2,Figure 3.5and Figure 3.6). The black line indicates the downslope profile shown in the insert (a). From the top to the bottom the figures displays the different swath bathymetric data of 2 m, 5 m, 25 m and 50 m resolution

3.6 Conclusions

Over the past few years there have been remarkable changes in the ability to map and visualise the seafloor thanks to the employment of autonomous underwater vehicles (AUV) that do not suffer from water-depth related issues. By analysing an unusually high resolution and extensive AUV bathymetric dataset, we identify a previously-unrecognised continuum between small, crescentic bedforms and large-scale sediment waves. We identify a class of medium-scale bedforms that was omitted from a previous global database. These medium-scale bedforms relate to a bedform that is either transitional between the small crescentic bedforms and large-scale sediment waves or is either a steep stepped-form, known as a knickpoints and that is increasingly observed in many other canyons and channels worldwide. Bedform dimensions can vary independently of water depth, but the identification of the smallest scale bedforms is hampered in increasing water depths. High resolution AUV surveys provide the means to fill fundamental gaps in our understanding of how channels are built and maintained, and to better constrain the nature of particulate transport into the deep sea.

Chapter 4

*Evolution of stratigraphy within submarine channels based on timelapse surveys

This chapter forms a peer-reviewed paper published in *Earth and Planetary Science Letters*: **D. Vendettuoli,** M.A. Clare, J.E. Hughes Clarke, A. Vellinga, J. Hizzet, S. Hage, M.J.B. Cartigny, P.J. Talling, D. Waltham, S.M. Hubbard, C. Stacey, D.G. Linterng. Daily bathymetric surveys document how stratigraphy is built and its extreme incompleteness in submarine channels. Earth and Planetary Science Letters, Volume 515, 2019, 231-247.

*This paper was published in 2019, ahead of the studies focused on flow behaviour (i.e. Chapter 2), and the morphometric analysis of AUV bathymetric data (Chapter 3). Therefore, results from such chapters are not referenced herein.

**The dataset used for this chapter was also presented for the first time in 2016 in the format of master thesis at the Royal Holloway University of London, Egham

I also analysed a subset of the generated stratigraphic data presented in this chapter, which contributed to subsequent peer-reviewed papers published in *Geology* and *Sedimentology:*

Hage, S., Cartigny, M.J., Clare, M.A., Sumner, E.J., **Vendettuoli, D.,** Clarke, J.E.H., Hubbard, S.M., Talling, P.J., Lintern, D.G., Stacey, C.D. and Englert, R.G., 2018. How to recognise crescentic bedforms formed by supercritical turbidity currents in the geologic record: Insights from active submarine channels. *Geology*, 46(6), pp.563-566.

Englert, R.G., Hubbard, S.M., Cartigny, M.J., Clare, M.A., Coutts, D.S., Hage, S., Hughes Clarke, J., Jobe, Z., Lintern, D.G., Stacey, C. and **Vendettuoli, D.,** 2020. Quantifying the three-dimensional stratigraphic expression of cyclic steps by integrating seafloor and deep-water outcrop observations. *Sedimentology*.

Author contributions: I led on the analysis and processing of the data derived from the mapped bathymetric surfaces, designed the study, and wrote the manuscript. J.E.H acquired and processed the raw bathymetry data. M.C. assisted with processing of data in ArcGIS. S.H. and C.S. provided sediment core logs. I developed the Matlab-based stratigraphy-building algorithm with support from A.V., following an earlier excel-based version developed with D.W. M.A.C., P.J.T. and S.M.H. provided editorial comments on the manuscript. All authors contributed with ideas and suggestions, read and agreed on the final version of this manuscript.

Abstract

Turbidity currents are powerful flows of sediment that pose a hazard to critical seafloor infrastructure and transport globally important amounts of sediment to the deep sea. Due to challenges of direct monitoring, we typically rely on their deposits to reconstruct past turbidity currents. Understanding these flows is complicated because successive flows can rework or erase previous deposits. Hence, depositional environments dominated by turbidity currents, such as submarine channels, only partially record their deposits. But precisely how incomplete these deposits are, is unclear. Here we use the most extensive repeat bathymetric mapping yet of any turbidity current system, to reveal the stratigraphic evolution of three submarine channels. We re-analyze 93 daily repeat surveys performed over four months at the Squamish submarine delta, British Columbia in 2011, during which time >100 turbidity currents were monitored. Turbidity currents deposit and rework sediments into upstream-migrating bedforms, ensuring low rates of preservation (median 11%), even on the terminal lobes. Large delta-lip collapses (up to 150,000 m^3) are relatively well preserved, however, due to their rapidly emplaced volumes, which shield underlying channel deposits from erosion over the surveyed timescale. The biggest gaps in the depositional record relate to infrequent powerful flows that cause significant erosion, particularly at the channel-lobe transition zone where no deposits during our monitoring period are preserved. Our analysis of repeat surveys demonstrates how incomplete the stratigraphy of submarine channels can be, even over just 4 months, and provides a new approach to better understand how the stratigraphic record is built and preserved in a wider range of marine settings

4.1 Introduction

It is important to understand how offshore sedimentary systems evolve, and the resultant stratigraphic architecture. For example, predicting this stratigraphic architecture is important for recovering oil and gas reserves, or when attempting to reconstruct past records of geohazards, such as submarine landslides or powerful gravity driven sediment flows known as turbidity currents (Clark and Pickering, 1996; Carter et al., 2014). Stratigraphic architecture observed in seismic profiles, sediment cores and outcrops is typically used to reconstruct sedimentary system evolution; however, from these data we cannot tell what may have been deposited but not preserved (Hubbard et al., 2014; Durkin et al., 2018). Thus, we often rely upon forward numerical models to understand how architecture is built (Sylvester et al., 2011; Jobe et al., 2017). In subaerial environments, repeat satellite or aerial photogrammetry surveys enable monitoring of river and delta evolution, and thus calibration of these models (Moody and Meade, 2014; Schwenk et al., 2017). Such aerial techniques cannot image seaward of the shallow coastal zone, however. Therefore, laboratory experiments are used to understand how architecture is built and preserved in deep-sea sedimentary systems (e.g. Paola et al., 2009). These experiments are subject to scaling issues; hence, there is a pressing need for field-scale observations to understand the accuracy of such models and interpret geological archives

(Talling et al., 2015).

4.1.1 Using repeat seafloor surveys to observe stratigraphic evolution of marine systems

Recent technological advances have enabled accurate bathymetric surveys to be collected repeatedly, to produce time-lapse data. These time-lapse surveys can provide a major advance in understanding of the rate and nature of seafloor change in different settings. Previous examples of marine time-lapse surveys include studies of estuaries (Mastbergen et al., 2016), submarine deltas (Hill et al., 2008; Casalbore et al., 2011; Biscara et al., 2012; Clare et al., 2017; Lintern et al., 2016), continental slopes (Kelner et al., 2016), deep-sea submarine canyons (Smith et al., 2007; Xu et al., 2008; Paull et al., 2018; Mountjoy et al., 2018), submarine channels in fjords (Conway et al., 2012; Normandeau et al., 2014; Gales et al., 2019), and lakes (Corella et al., 2016; Silva et al., 2018). These time-lapse datasets cover seven or fewer repeat surveys, over timescales of months to decades (Table 1.1), which is much less frequent than the rate at which sediment transport events occur. As a result, it has been challenging to document stratigraphic evolution in detail.

Here we analyze the most detailed time-lapse mapping yet of any marine system. This data set comprises 93 bathymetric surveys along the three submarine channels of the Squamish Delta, British Columbia. These surveys were collected over successive weekdays in the spring and summer of 2011 (Hughes Clarke et al., 2012). Based on changes in seafloor elevation, and direct flow measurements using an acoustic Doppler current profiler, over 100 turbidity currents were recorded in the highly-active proximal channels. However, less than half of these events reached the lobes at the channel mouths (Hughes Clarke et al., 2012; Hizzett et al., 2018; Stacey et al., 2018). We use this unique dataset of closely-spaced repeated surveys to document directly, for the first time, how the stratigraphy of submarine channels is built and preserved at field- scale.

While these data are unusually detailed, we recognise some important caveats in our method and data set. First, the study timescale covers only four months. Hence, we probably do not capture rare but powerful sediment transport events that may decimate the stratigraphic record and cause major topographic modifications (e.g. Strauss and Sadler, 1989; Durkin et al., 2018). Second, repeat surveys should be acquired at a frequency appropriate to the rate of the process being monitored. Hughes Clarke (2016) documented that up to seven turbidity currents may occur within one day. Thus, it is likely that the daily survey repeats may miss some events. Despite these caveats, we know of no other data set that is so detailed (covering the full extent of three channels, with such repetition). We use this exceptionally detailed series of time-lapse bathymetric surveys to understand: (1) how stratigraphy from submarine channels deposits is generated, and (2) the extreme incompleteness of the depositional record, even over a period of just 4 months.

4.1.2 Why study the stratigraphic evolution of submarine channel deposits?

Turbidity currents transport sediment from shallow to deep water via submarine channels. As well as carrying globally important volumes of sediment, these flows transport organic carbon, oxygenated waters, nutrients and contaminants that accumulate within submarine channels and downslope at their terminal lobes or submarine fans (Galy et al., 2007; Kao et al., 2010; Gwiazda et al., 2015; Hughes et al., 2015). The often-powerful nature of turbidity currents poses a significant hazard to critical seafloor infrastructure (Carter et al., 2014), which also makes direct monitoring challenging (Inman et al., 1976; Clare et al., 2017). There is a paucity of direct measurements of turbidity currents (Talling et al., 2015), so one typically has to make inferences of past flows based upon the deposits ('turbidites') that are left behind (Hubbard et al., 2014; Jobe et al., 2017). Stratigraphic analysis of turbidites from submarine channels increasingly forms the basis for a wide range of paleo-environment interpretations, including geohazard assessment (Cattaneo et al., 2012), climatic reconstructions (Nakajima and Itaki, 2007), extending historical earthquake catalogues (Bernhardt et al., 2015), and to inform forward stratigraphic modeling for hydrocarbon exploitation (Jobe et al., 2018). Given this importance, it is thus crucial to understand the architecture and completeness of the depositional record for submarine channels. Our study shows how time-lapse bathymetric surveys, allied to sediment cores and monitoring data, can make significant advances in the genesis of deposit architecture.

4.1.3 Why does stratigraphic completeness matter?

Stratigraphic completeness matters because we need to understand how well deposits can be used to reconstruct sediment transport fluxes, records of geohazards, and to understand the accuracy of numerical models. Stratigraphic completeness is defined here as the proportion of accumulated deposit thickness preserved over a given time period (Sadler, 1981; Strauss and Sadler, 1989). As time increases, the likelihood for preservation of a sedimentary package decreases (Strauss and Sadler, 1989; Figure 4.1), due to short-term autogenic phases of reworking or erosion that follow or intervene phases of deposition, and/or longer-term allogenic factors such as regional subsidence or sea level fluctuations (Barrell, 1917; Paola et al., 2018). Detailed studies of stratigraphic completeness have been performed in fluvial (Reesink et al., 2015; Durkin et al., 2018) and delta-shoreline environments (Straub and Esposito, 2013), but to date no study has attempted to quantify stratigraphic completeness using repeat bathymetric surveys for turbidite systems. Thus, our novel study fills an important knowledge gap and demonstrates the potential for future studies of this type, across a broader range of offshore sedimentary systems.

4.1.4 Aims

Our overarching objective is to show how very frequent time-lapse bathymetric surveys can show (a) how stratigraphic architecture is built, and (b) quantify the incompleteness of that record. We do this over four months for an offshore delta with submarine channels. To address this larger objective, we tackle four specific aims.

In this study, we analyse the most detailed time-lapse bathymetric surveys yet of any marine system, including turbidite or deltaic systems (Table 1.1). We combine this with some of the most detailed direct flow monitoring yet conducted (Hughes Clarke, 2016; Hage et al., 2018), and a series of sediment cores (<10 m penetration; Hage et al., 2018; Stacey et al., 2018). First, we show how the stratigraphic architecture of three submarine channels at Squamish Delta is built. We explore how this architecture changes from proximal to distal locations within the channels, and identify how individual stratigraphic elements (i.e. crescentic bedforms, landslide and lobe deposits) are formed and evolve. Second, we determine the stratigraphic completeness of deposits in those three channels following >100 turbidity currents over four months. The results are key for interpreting depositional sequences, or informing where sediment cores should be taken to reconstruct flow frequencies and delta history. Third, we seek to understand how stratigraphic completeness of three submarine channel deposits varies over the surveyed period, exploring whether occasional large events control the preservation potential of deposits. Finally, we explore how our detailed observations of stratigraphic evolution at an active submarine delta may relate to other deeper-water submarine channel systems.

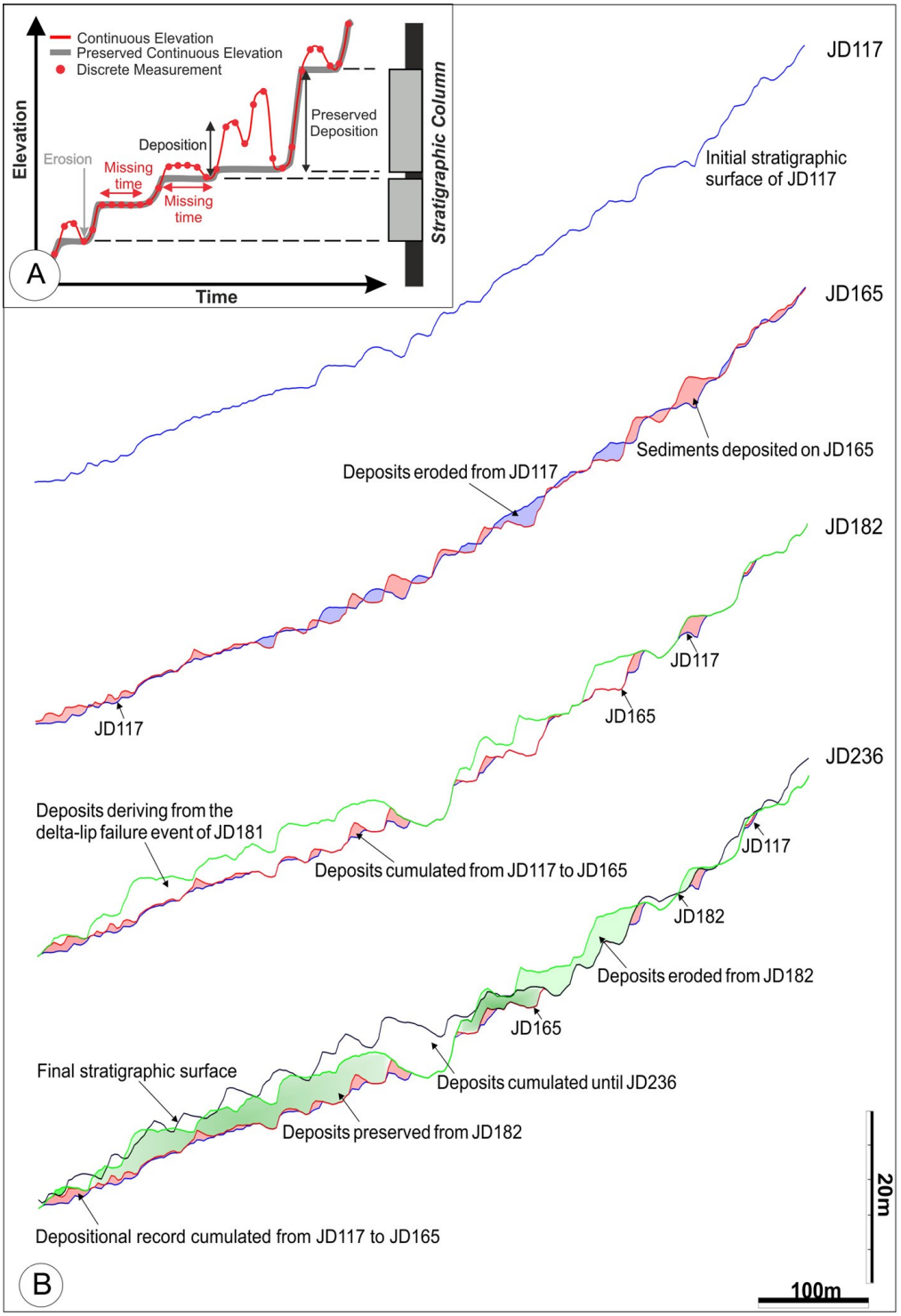

Figure 4.1: (A) Schematic diagram illustrating the construction of a stratigraphic column from elevation increments and parameters controlling stratigraphic completeness. Preserved time in stratigraphy is housed in deposits constructed during positive elevation changes that are not later eroded. Gaps in the record occur as a result of stasis on the geomorphic surface and erosion (from Straub and Esposito, 2013). (B) Schematic representation of the algorithm developed to identify the stratigraphic architecture of submarine channel deposits herein studied. JD117 and JD236 are the along channel profiles traced for the first and last bathymetric surveys realized over 4-months period (refer to paragraph 4.3.2 of the main text). Vertical exaggeration: 8x

4.2 Background: study area and data

The Squamish River carries more than 10^6 m^3 of sediment to its delta annually, where much of that sediment is transported down the submarine prodelta slope by turbidity currents (Hughes Clarke, 2016). Direct monitoring has revealed that >100 turbidity currents may occur during the spring and summer freshet each year, when seasonal meltwater increases the river discharge from ~100 m^3/s in the winter to >500 m^3/s, with peaks of up to 1000 m^3/s (Hughes Clarke et al., 2012). This high frequency turbidity current activity has formed three submarine channels ("northern", "central" and "southern"; Hughes Clarke et al., 2012; Figure 4.2 Panels A and D). The channels initiate at or very close to the delta-lip, which is partially sub-aerially exposed at low tides. At a distance of ~2 km from the delta-lip, these channels widen and flows become unconfined in water depths of ~150 m (the effective base of the slope; Figure 4.2). Recent monitoring has shown that more than two thirds of turbidity currents in these channels are triggered by the settling of sediment from a dilute surface river plume (Hizzett et al., 2018). The other flows are triggered by localised delta-lip collapses (up to 150,000 m^3), which are inferred to result from transient pore pressure changes due to rapid sedimentation and/or tidal fluctuations (Clare et al., 2016).

Detailed multibeam bathymetric surveys were performed on 93 consecutive week days from 17th April 2011 to 24th August 2011, covering an area from the delta top to a distance of ~3,500 m offshore (Hughes Clarke et al., 2012; Figure 4.2 Panel D). The vertical resolution of these surveys is ~0.1 m, thus it is possible to resolve relatively small changes in seafloor relief between successive surveyed days (Hizzett et al., 2018). These surveys capture the evolution of three highly active submarine channels at an exceptional level of spatial and temporal detail over four months.

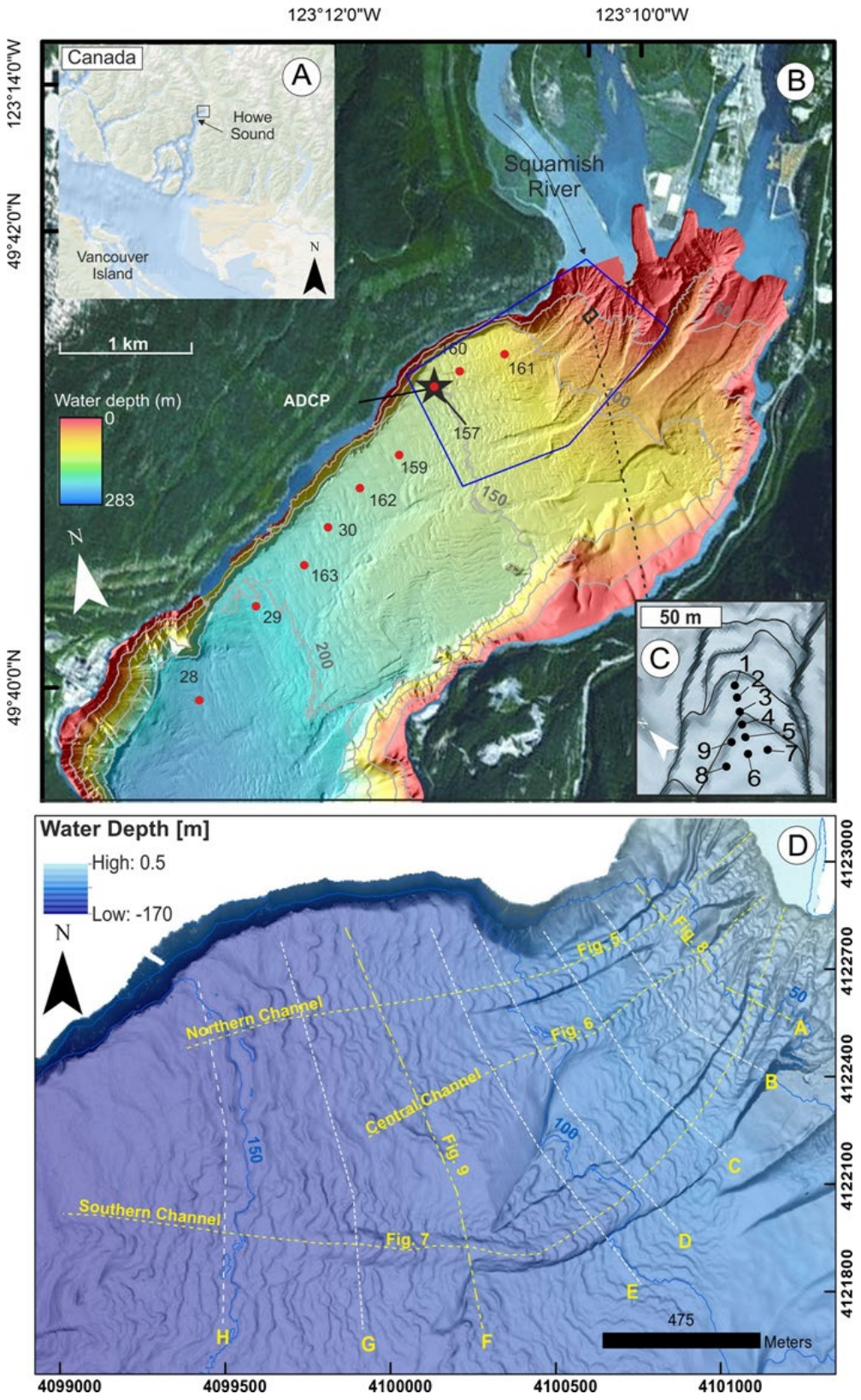

Figure 4.2: (A) Location of Squamish Delta in Howe Sound, British Columbia. (B) Location of available sediment cores (red filled circles) from Stacey et al. (2018), ADCP to measure turbidity currents (black star) from Hughes Clarke et al. (2012) and Hughes Clarke (2016), and location of the survey area (blue polygon). (C) Sediment cores from the proximal part of the Central Channel from Hage et al. (2018). (D) In blue extent of area surveyed in 2012 (the focus of this study) annotated with down-channel (northern, central and southern) and cross-channel (A–H) profiles. Selected profiles are shown as

figures in this paper (for parts of the down-channel profiles, and cross-channel profiles A and F). All across-channels profiles are available as figures in the supplementary material. Animations are also available for all of the profiles as online videos. (For interpretation of the colors in the figure(s), the reader is referred to the web version of this article.)

4.3 Methodology

To quantify stratigraphic completeness at the Squamish Prodelta, we generated maps and profiles from the multibeam bathymetric surveys performed on 93 successive weekdays in 2011. Each daily survey is referred to by the Julian Day (JD) on which it was performed.

4.3.1 Daily difference maps

We quantified how the seafloor elevation changed by generating daily difference maps between pairs of successive surveys (e.g. JD118 minus JD117, JD119 minus JD118) using the same approach as Hizzett et al. (2018). Previous work has shown that the seafloor elevation only changed when a turbidity current or delta-lip failure occurred (Hughes Clarke et al., 2012; Hizzett et al., 2018). In these daily difference maps, negative values represent loss (erosion) and positive values represent sediment accumulation (aggradation). Seafloor changes were detected at the pixel scale, which has a horizontal resolution of 2 m x 2 m and vertical resolution of approximately 0.1 m (Hughes Clarke et al., 2012; Hizzett et al., 2018). An illustration of how the seafloor level changed with time within the channel axes is presented in the supplementary material, Figure S1.

4.3.2 Reconstruction of stratigraphic architecture

We calculated the evolution of stratigraphic architecture along eight cross-channel (i.e. along-strike) and three down-channel (i.e. axis-parallel) profiles (Figure 4.2 Panel D). To do this, we developed an algorithm to build the stratigraphy for each surveyed day along each of those profiles. We extracted the bathymetric elevation along each of those profiles for each successive daily survey. Where a point along a profile is higher than it was in the preceding survey (i.e. aggradation occurred), a stratigraphic horizon was created. However, when a point along a profile was lower than it was in the preceding survey (i.e. erosion occurred), the stratigraphy at that point was removed. Each iteration of the algorithm draws all the stratigraphic surfaces traced from the first bathymetric survey until the day that is being processed, accounting for effects of both aggradation and erosion (Figure 4.1 Panel B).

Three down-channel (Figure 4.5-Figure 4.7) and two across-channel profiles (Figure 4.8 and Figure 4.9) are presented; however, the remaining six along-strike profiles are presented in the supplementary material (Figure S2-7), as well as accompanying time-lapse movies that visualise the stratigraphic evolution (Movies S1-18).

4.3.3 Total difference map

The total difference map (Figure 4.3A) shows the net thickness of sediments accumulated or eroded over the total surveyed timescale (i.e. JD236 minus JD117). As with the daily difference maps, positive values show where the elevation of the final bathymetric area is higher than the elevation at the start of the survey and indicates net sediment accumulation over the surveyed period. Negative values occur in areas where the final seafloor elevation was lower than at the start.

4.3.4 Cumulative aggradation map

Turbidity currents deposit, as well as rework sediments emplaced by previous flows; hence, the seafloor may either aggrade or erode at different locations. To create the cumulative aggradation map (Figure 4.3 Panel B), first, we generated the daily difference bathymetric maps. Second, we removed the effect of erosion from each of these daily difference maps by excluding any negative values. In doing so, we only account for the thickness of sediment that would have been deposited at each pixel, had erosion not occurred in the same time period. These positive-value-only difference maps were summed in order to generate the cumulative aggradation map.

Confidence in the multibeam data is lower at the edges of the surveyed areas, where there is no overlap between adjacent swath lines. As a result, the cumulative aggradation map shows artificially higher values at the outer fringes of the survey data. These areas are well outside of the channels, however, and therefore do not affect our analysis.

4.3.5 Stratigraphic completeness map

The stratigraphic completeness map (Figure 4.3 Panel C) records the ratio between the actual deposit thickness determined over the surveyed period (i.e. the cumulative elevation difference as shown in Figure 4.3 Panel A) and the total thickness of sediments accumulated over the same time (i.e. the cumulative aggradation of sediments shown in Figure 4.3 Panel B). A value of 1 means that 100% of the sediment deposited at a pixel scale was recorded at the end of the surveyed period. A zero value means that none of the deposited sediment was preserved. The vertical resolution of the multibeam data means that small elevation changes may not be accurately recorded, which can affect our calculations. We determined error ranges following the approach outlined in Hizzett et al. (2018). They determined that during ten days that lacked any turbidity current activity (i.e. when the seafloor was stationary), the distribution of difference map offset values is normally distributed with a mean offset of 4 cm and a standard deviation of 23 cm. In order to model the potential propagated error in our calculations, we added a random value within the range +/-4 cm to each pixel of each daily

difference map, and each cumulative daily aggradation map. We then recalculated the stratigraphic completeness map from that series of modified maps, and repeat the process a further 99 times. This allows us to understand how confidently we can measure stratigraphic completeness. Based on these calculations, the range in this propagated error for stratigraphic completeness was found to be normally distributed, with a mean of 0.05% and standard deviation of 3%.

4.4 Results

First, we show how stratigraphy is built by submarine flows using 93 time-lapse surveys. We include a brief summary of lithofacies from sediment cores and information from direct monitoring to understand flow types and behaviour (Figure 4.10). We then document how the stratigraphic completeness of the channels and delta front sequences evolves through time.

4.4.1 How does the stratigraphic architecture evolve and what elements are involved?

Through the analysis of the daily difference maps and the animations of stratigraphic evolution along 11 profiles (annotated on Figure 4.2 Panel D, and presented as supplementary movies S1-S18), we identify five distinct stratigraphic elements that make up the stratigraphic architecture developed over the surveyed period. We now discuss these elements in turn.

4.4.1.1 Crescentic bedforms

The most common differences observed from repeat surveys were up-slope migrating bedforms with a crescentic planform (Figure 4.2; Hughes Clarke, 2016; Hage et al., 2018). These bedforms are up to 7 m high with a wavelength of tens of metres (i.e. of equivalent scale to the small-scale bedforms of Symons et al., 2016), and occur along the axial length of all three of the submarine channels and also on the terminal lobes (Figure 4.2 Panel D). Thalweg-parallel profiles clearly image erosion on the steep lee sides and deposition on lower angle stoss-sides, which explains their upstream migration (Figure 4.6). The upstream migration of bedforms results in the partial, and sometimes entire, reworking of deposits emplaced by previous flows, as an individual bedform trough can migrate a full wavelength in as short a period as two days. This reworking creates a complex final stratigraphy along the channel axis, with a combination of truncated low angle-backsets, bedform remnants and foresets (Figure 4.5-Figure 4.7). The crescentic bedforms in the channel axes comprise massive sands that infill complex scours (Hage et al., 2018). The sand is largely ungraded to poorly graded and structureless. Bed thicknesses vary from 1 to 2 m and contacts between layers are sharp and erosive (Figure 4.10; Hage et al., 2018). Monitoring using multibeam sonars and acoustic Doppler current profilers show that these bedforms are created by

supercritical turbidity currents (1-3 m/s) that undergo repeated hydraulic jumps (Hughes Clarke, 2016; Hage et al., 2018). Flow acceleration on the lee-sides generally causes erosion, whereas deceleration on the stoss-side promotes deposition (Hughes Clarke, 2016; Hage et al., 2018).

4.4.1.2 Delta-lip collapse deposits

Five large (up to 150,000 m^3) delta-lip collapses occurred during the surveyed period (Hughes Clarke et al., 2012). The bulk of the run-out from these slope failures is generally limited to the upper and middle sections of the submarine channels, where a considerable thickness of sediment is emplaced en-masse (Figure 4.5). The largest delta-lip collapse occurred at the head of the northern channel a few hours after a peak in river discharge (JD180-182), and dramatically changed the channel morphology by plugging its upper reach with ~5 m of sediments (Figure 4.3 Panel A and Figure 4.5) (Hughes Clarke et al., 2012). This event effectively filled the proximal part of the channel and triggered a partial avulsion; forming a small splay to the south (Figure 4.3 Panel A). Within a few days, however, the northern channel adopted a new axis, offset by ~50 m to the south of the original, incising into the delta-lip collapse deposits (Figure 4.8). The thalweg-parallel profile in the upper part of the northern channel also reveals that the delta-lip collapse locally 'smoothed out' the stepped seafloor texture formed by the upstream-migration of bedforms by emplacing a sediment drape (~5 m) (Figure 4.5– middle panel). In the days following this event, upstream-migrating bedforms were more elongate and less regular, but ultimately resumed their original morphology and dimensions within a few tens of days (Figure 4.5- lower panel; Movie S1-3 of supplementary material). While not cored here, their deposits likely comprise coarse delta-derived massive or convoluted sand with an erosional base, based on granular slope failures in delta and estuarine settings (van den Berg et al., 2017).

4.4.1.3 Steep-faced channel-lobe-transition scour zones

Two major erosional events, which created scour zones, are clearly observed along the profile that orthogonally transects the southern channel at its transition from the channel to the terminal lobe (Figure 4.9). The first occurred on JD180, when the channel base level dropped by ~5 m. In the following days, 2 m of progressive sediment infill occurred, until JD203 when the axis of the channel vertically incises a further ~4 m. These two short-lived but significant incisional events ensure that the channel-lobe transition zone of the southern channel is an area of net erosion. Thalweg-parallel profiles reveal that these abrupt and steep-faced erosional features migrated upstream ~50-100 m in one day (Figure 4.7– bottom panel). No cores have been acquired in these features to date.

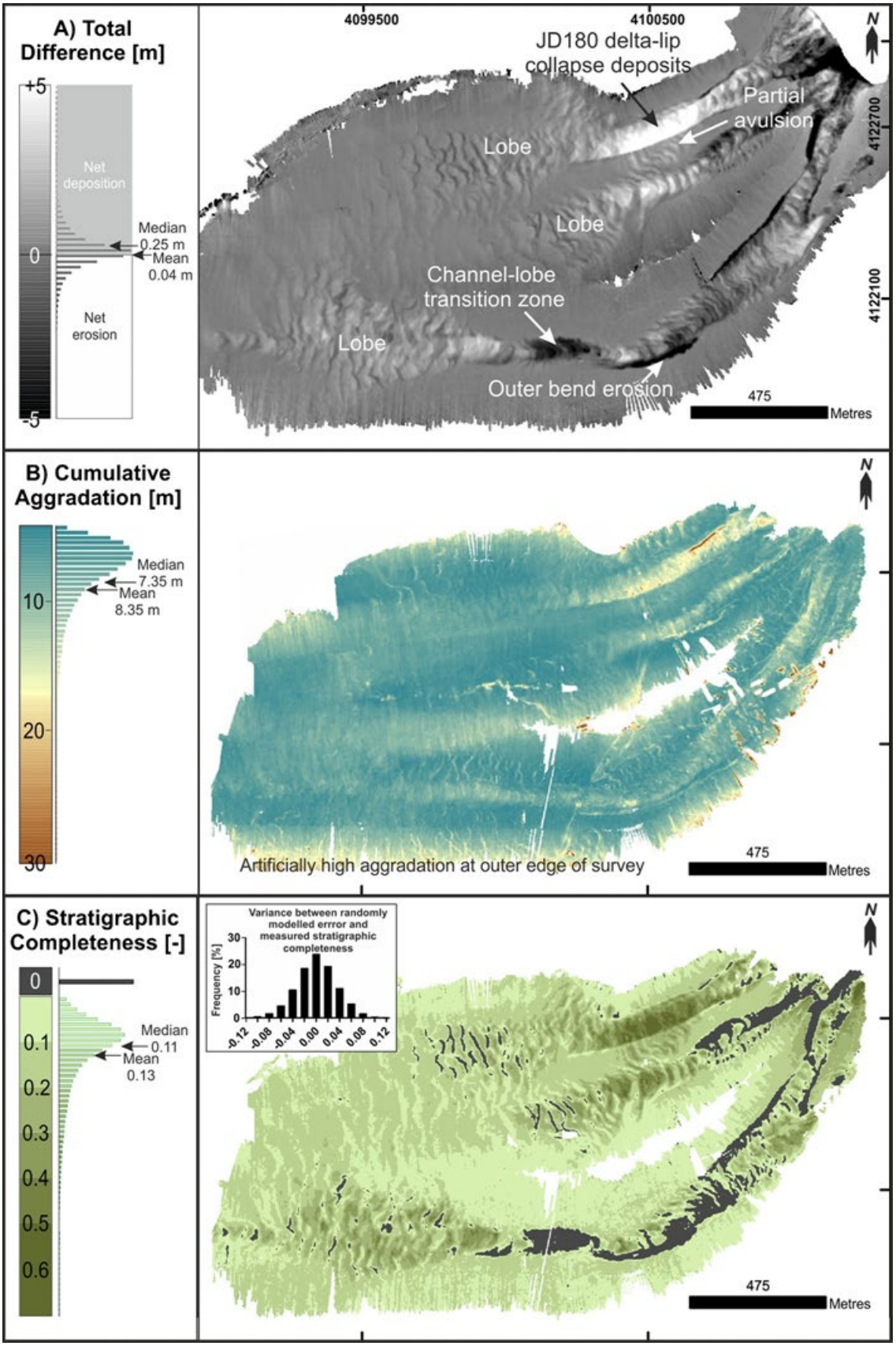

Figure 4.3: (A) The Cumulative Elevation Difference Map accounts for the total thickness of sediments at each pixel location at the Squamish prodelta area. Herein, areas with positive values feature deposition, while negative values are related to areas affected by erosion. The Cumulative Aggradation Map (B) shows the aggradation of sediments at each pixel location along the surveyed area. This map

does not display the effect of erosion; negative values have, thus, been removed. Artificial over estimation of aggradation is observed at the edges of the surveyed area as a result of non-overlapping swaths of multibeam data. (C) The Stratigraphic Completeness Map shows how complete is the stratigraphic record left behind by multiple turbidity current events. Inset histogram shows the range of error (the bathymetric survey was only realized during weekly day and some days are thus missing, as shown by the white areas of B and C).

4.4.1.4 Channel margins

In addition to the abrupt lateral offset of channel axes in response to delta-lip collapses (Figure 4.5), we also observe lateral migration that does not appear to respond to the emplacement of an obstacle. Two pronounced episodes of lateral axis shifting affected the southern channel during the surveyed period. The first migration occurred between JD158 and JD175 when the channel axis shifted ~3 m southwards. The second occurred between JD188 and JD189 when the channel axis shifted ~3 m northwards. It remains in this position until the end of the survey (Figure 4.8). Accretion packages formed on the inner side of the channel composed of multiple 0.1-1.5 m-thick beds are dominated by a mixture of coarse- and fine-grained sand at their base with finer grained, less amalgamated beds towards the top (Figure 4.10; Hage et al., 2018).

4.4.1.5 Draped interfluves

Across-slope profiles reveal a steady but low rate of aggradation on the interfluves (Figure 4.8-Figure 4.9; see supplementary movies S11-S18). Proximal areas feature ~1.5 m of aggradation over the survey period, whereas in distal areas up to 5 m aggradation occurs (Figure 4.8-Figure 4.9). Deposits comprise thick silty mud beds interbedded with very thin layers of sand (Figure 4.10). Plane-parallel to wavy and sub-parallel laminations are often present, ranging from 1 mm to 1 cm (Hage et al., 2018). The level of daily aggradation on the interfluves is often at, or very close to, the vertical resolution of the multibeam (i.e. <0.1-0.2 m), hence confident identification of internal architecture is not always possible. For this reason, it is also likely that the algorithm we use to build the stratigraphy may overestimate the amount of erosion in these areas of low aggradation outside of the submarine channels and lobes. Thus, we primarily focus our attention on understanding the stratigraphic completeness within and immediately adjacent to the channels and lobes, rather than the interfluves.

4.4.2 What is the stratigraphic completeness, and how does that vary spatially?

Over the 4-months study period, the median stratigraphic completeness of the area including the three submarine channels is 11% (mean of 13%; Figure 4.3). However, there is a large degree of spatial variability, related to the various stratigraphic elements (Figure 4.3-Figure

4.4). The three submarine channels also show slightly different patterns of stratigraphic completeness. The extent of areas featuring no preservation of deposits accounts for 4.4% of the total surveyed area (2.6 x 106 m^2).

Northern Channel: The northern channel features the highest stratigraphic completeness proximally, ranging from 35% to 60% (Figure 4.3 Panel C). These relatively high values are coincident with the run-out extent of major delta-lip failures, which appear to be better preserved compared to the 'background' deposition from repeated turbidity currents. While post-emplacement reworking occurred, much of the delta lip-collapse deposits remain at the end of the survey period.

Central Channel: Since there was no delta-lip failure within the central channel, the overall stratigraphic completeness recorded is much lower than the northern channel. The highest value within the channel is in its medial to distal segments (20-50%; Figure 4.3C), while much of its proximal reach was completely eroded (i.e. 0%; Figure 4.3 Panel C).

Southern Channel: In the southern channel, the stratigraphic completeness varies between 0% and ~25%. However, at the lobes it reaches values of 40%, and can be as low as zero due to localised erosion on the lee-side of upstream-migrating bedforms (Figure 4.7– bottom panel). In particular, the areas of greatest erosion occur at an outer channel bend and the channel-lobe transition zone, which both yield no stratigraphic record. In these areas, the channel base level was lower at the end of the surveyed period than at the start (Figure 4.3Panel C).

4.4.3 How does stratigraphic completeness vary through time?

The evolution of stratigraphic completeness is demonstrated through time, by presenting an averaged (mean) value for 500 m-long sequential sections along the thalweg-parallel profiles (Figure 4.4). Following the first pair of daily surveys, stratigraphic completeness quickly drops and assumes values that closely straddle the survey-wide median of 11%, primarily due to the repeated deposition and reworking during upstream-migration of crescentic bedforms. This apparent equilibrium is disrupted on JD181, however; one day after the first significant river flood peak of the freshet (~900 m^3/s on JD180). In the northern channel, a rapid increase in stratigraphic completeness is documented in the upper 1000 m along its course (up to two times greater in the upper 500 m), which corresponds to the emplacement of the largest delta-lip collapse deposit (150,000 m^3) observed in the surveyed period. The central channel shows an increase in stratigraphic completeness between 500 and 1000 m along its course, due to mostly depositional events occurring between JD155 and JD182. At the same time in the southern channel, there is a sudden drop in completeness (mean of 0% between 900 and 1000 m and between 2000 and ~ 2300 m down-channel) when channel-filling deposits are flushed

down-channel. This decrease in stratigraphic completeness is coincident with the most pronounced period of channel axis incision (Figure 4.9). After that point, the stratigraphic completeness appears to more-or-less plateau and reaches a steady state (Figure 4.4).

4.5 Discussion

While the proximal channelized part of the fjord-delta (the focus of our study) features ~100 turbidity currents per year, much larger, but rarer, events are known from sediment cores in the distal parts of the fjord (Stacey et al., 2018) (Figure 4.10). Flows that run ~10-15 km further downslope, to the distal fjord basin, have a recurrence of ~100 years and are not included in our analysis. We must therefore recognise that our study is limited to observing the relatively short-term stratigraphic evolution of the proximal channels and lobes, and the stratigraphy over longer timescales is likely to be even less complete than our data indicate.

4.5.1 Up-stream migrating bedforms ensure low stratigraphic completeness within submarine channels

The most common sediment transport process at Squamish submarine delta is by Froude-supercritical turbidity currents, which create upstream-migrating bedforms. These flows account for the lee-side erosion and stoss-side deposition observed in the time-lapse stratigraphic evolution animations (Movies S1-S10), and have been directly monitored by Hughes Clarke (2016). Sequential trains of these upstream-migrating bedforms, interpreted to be formed by a cyclic step instability in the turbidity current, are the dominant feature in many proximal, sandy submarine channels on steep slopes worldwide (Kostic et al., 2010; Symons et al., 2016; Casalbore et al., 2016; Covault et al., 2017; Hage et al., 2018). Upstream-migrating bedforms occur along all reaches of the submarine channels at Squamish, from their mouths to the terminal lobe. By analyzing a small section (over five bedform wavelengths) of the proximal part of the central channel, Hage et al. (2018) showed how deposits of these bedforms may initially be preserved as low-angle back-stepping beds, but that progressive reworking by successive flows may only preserve remnants of the basal scour-fill (Lang et al., 2017; Ono and Bjorkland, 2017). Low-angle backsets appear to be preserved locally along the three channel axes, from proximal to distal. (Figure 4.5-Figure 4.7). A further trace of this intense reworking it is also represented by erosional surfaces visible as possible foresets along the channel lobe transition zone of the southern channel (Figure 4.7).

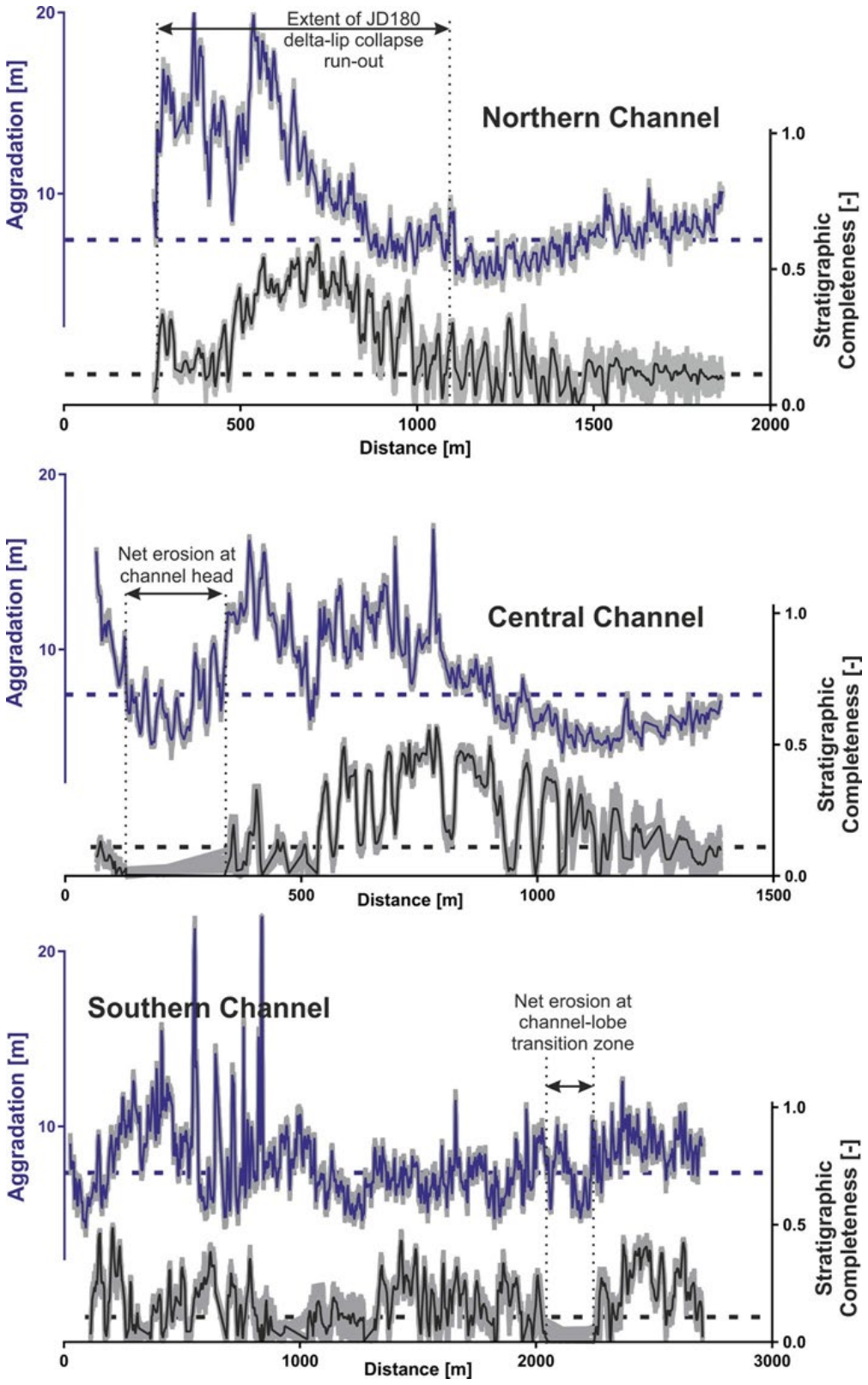

Figure 4.4: Error estimation. Thalweg-parallel plots of aggradation and stratigraphic completeness for the three submarine channels. Aggradation is shown in blue, stratigraphic completeness in black, and gray lines represent the error ranges based on random additions of 5 cm to the seafloor elevation for each survey over 100 runs. Median values for stratigraphic completeness and cumulative aggradation across the surveyed area are shown as dashed lines.

The progressive reworking of previously deposited sediments by successive flows explains the relatively low stratigraphic completeness (Figure 4.5-Figure 4.8) of all the three channels axes. Only ~10% of deposit thickness (typically the lowermost scour-fill) is preserved on average due to subsequent reworking. In cases where bedforms migrate upstream faster than the aggradation rate, deposits are entirely obliterated from the stratigraphic record. This is particularly pronounced in the upper reaches of the southern channel that seems to be deepening its course. Stratigraphic completeness is generally much higher at the terminal lobes of all three channels, where flows expand and decelerate (and hence the potential for erosion is lower; Kostic and Parker, 2006). Despite lobe deposits are relatively well preserved, the maximum observed lobe stratigraphic completeness is still only 40%. Therefore, the often-held assumption that lobes provide a near-complete stratigraphic record of long run-out flows may not always hold (Jobe et al., 2018).

4.5.2 Landslide deposits that modify channel morphology are disproportionately well preserved, but may still be extensively reworked over longer timescales

The highest stratigraphic completeness within the channels corresponds to areas with the highest aggradation. In the most extreme case, the high aggradation within channels relates to en-masse emplacement of 150,000 m^3 of sediments following a delta-lip collapse event on JD180 at the head of the northern channel (and not a cyclic step process) (Figure 4.5). This sudden deposition of sediment fundamentally changed channel morphodynamics by 'smoothing out' the relief of crescentic bedforms and effectively plugging the channel, and triggering a partial avulsion (Figure 4.3 Panel A). Similar observations of subaqueous landslides modifying channel morphology and turbidity currents pathways have been made in deep-sea (Armitage et al., 2009; Brooks et al., 2017) and lacustrine settings (Corella et al., 2016). The stratigraphic completeness in the proximal part of the northern channel is anomalously high compared with the other channels. This high completeness corresponds to the run-out extent of the JD180 delta-lip failure; hence, it appears that slope failures, for which the majority of their volume is not transformed into a turbidity current (i.e. a landslide), are preserved in the depositional record (at least over the surveyed timescale). However, at least 64% of the landslide mass was subsequently reworked by repeated turbidity currents, which ultimately incised a new channel axis into its deposits (Figure 4.8). This is similar to observations from other repeat surveys, such as in Monterey Canyon, California, where 80% of an emplaced landslide volume was removed by turbidity currents over less than two years (Smith et al., 2007). Biscara et al. (2012) suggested that the entirety of a landslide deposit may be reworked by frequent turbidity currents, based on repeat surveys at the Ogooué Delta, Gabon. Reconstruction of landslide frequency and volume in submarine channels may therefore be challenging when analyzing outcrops, seismic data and sediment cores and significant post- emplacement reworking has occurred.

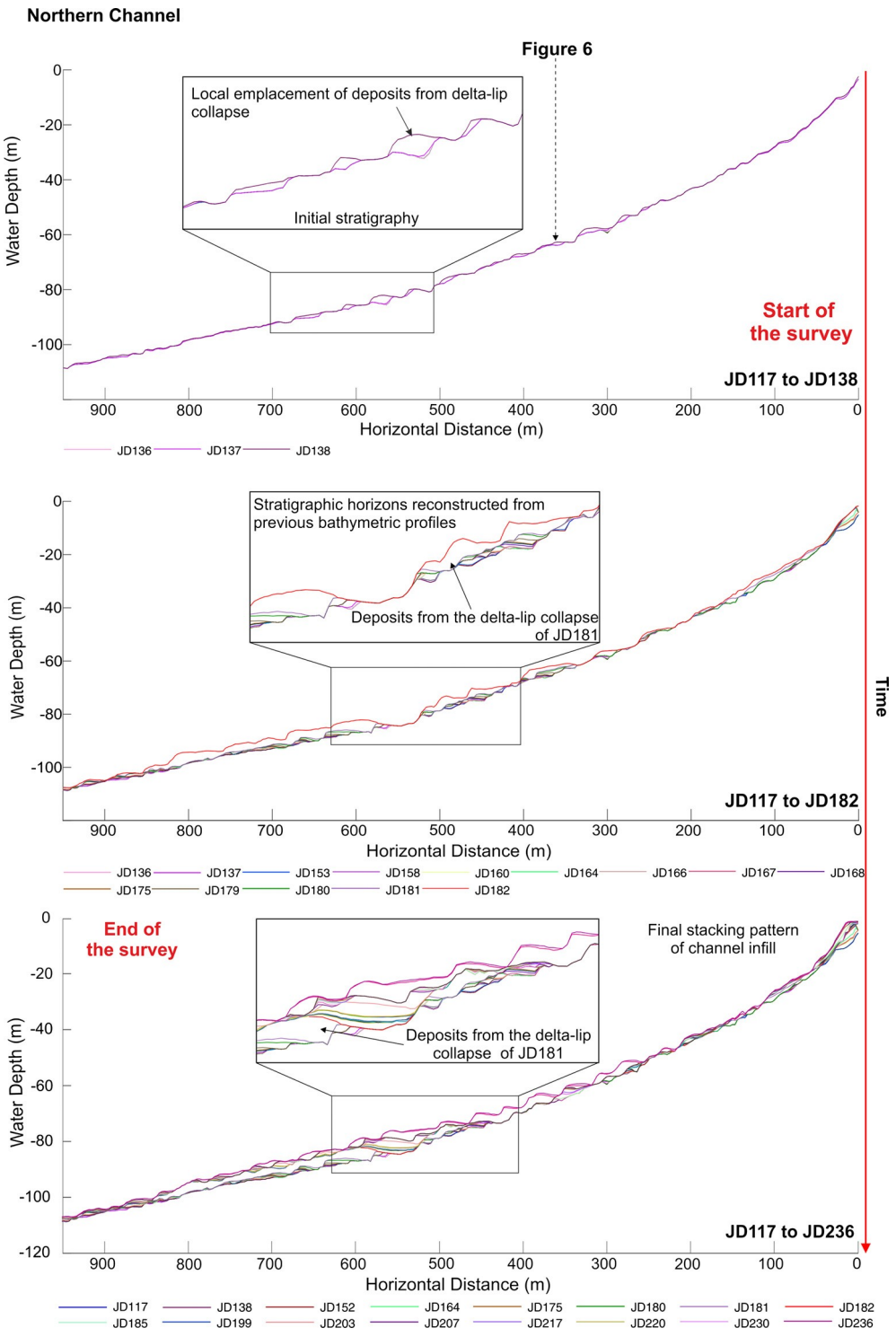

Figure 4.5: Down channel profiles of the proximal to medial area of the northern channel generated from the start JD117 (upper panel) to the end of the survey JD236 (bottom panel). The upper panel shows the seafloor at the start of the survey until JD138. The central panel displays the stacking pattern of channel deposits from JD117 to JD182. This includes the major delta-lip failure event occurring between JD181 and JD182 in response to a pick in the river discharge. The bottom panel shows the final stratigraphic architecture of those deposits resulting from >100 turbidity currents events that occurred during 4 months' survey period. Geomorphic surfaces are here represented with single lines color-coded by Julian Day (refer to Figure 4.2D for the location of the profile and see animated video Movie S1 to Movie S3 in the supplementary material) (vertical exaggeration: 7x).

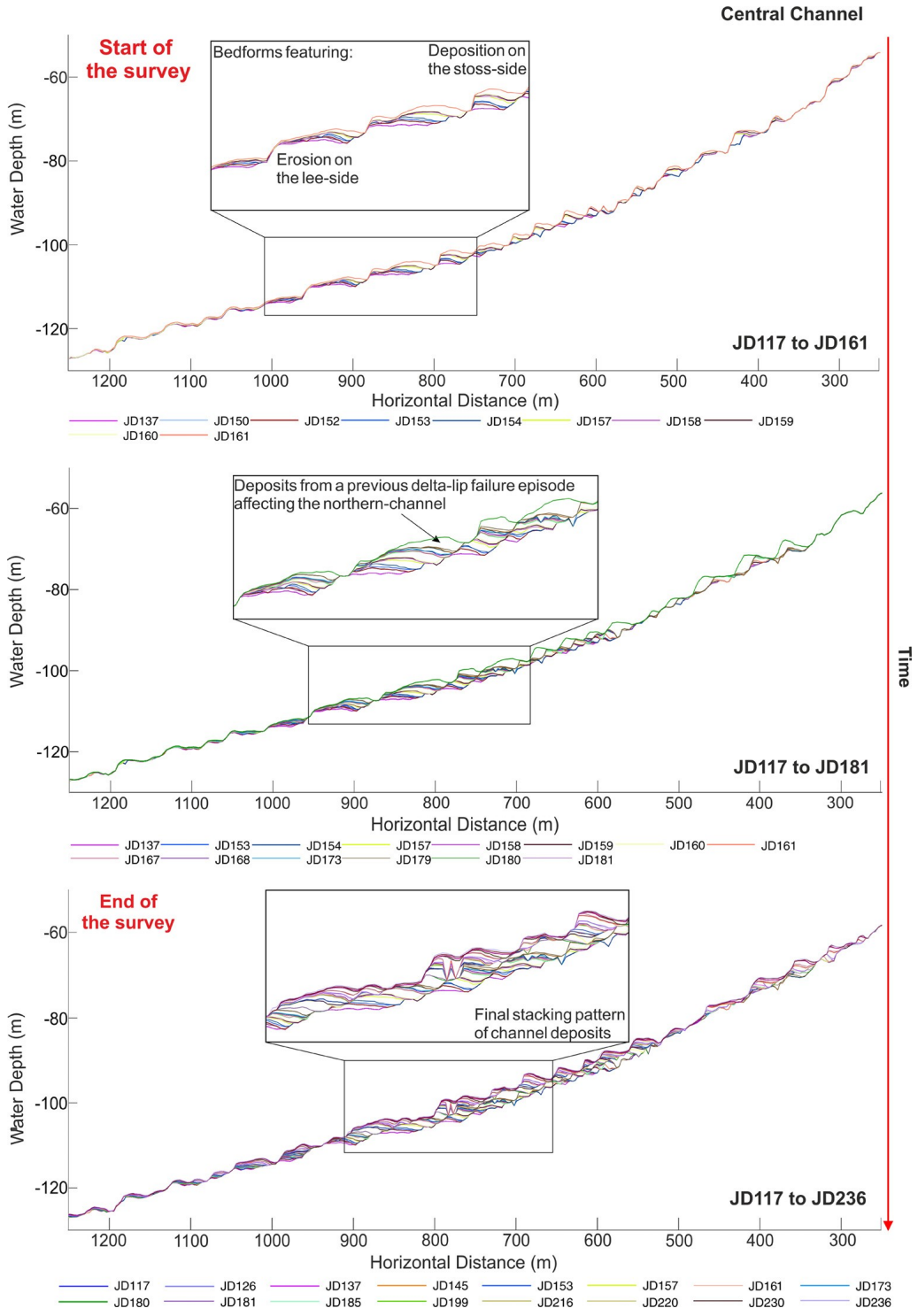

Figure 4.6: Along channel profiles of the medial to distal area of the central channel. The upper panel displays the stacking pattern of the submarine channel deposits as consequence of turbidity currents happening between JD117 (start of the survey) and JD161. At the slope breaks upstream migrating bedforms act to both emplace and erode/rework deposits. In the central panel upslope crescentic bedforms feature erosion on the lee-side and deposition on the stoss-side. The bottom panel displays the final stratigraphic architecture of those deposits at the end of the survey JD236. Due to the upper-slope migrating bedforms this area represents the zone of the most intense reworking of sediments. (JD = Julian day, see Figure 4.2D for the location of the profile) (vertical exaggeration: 5x).

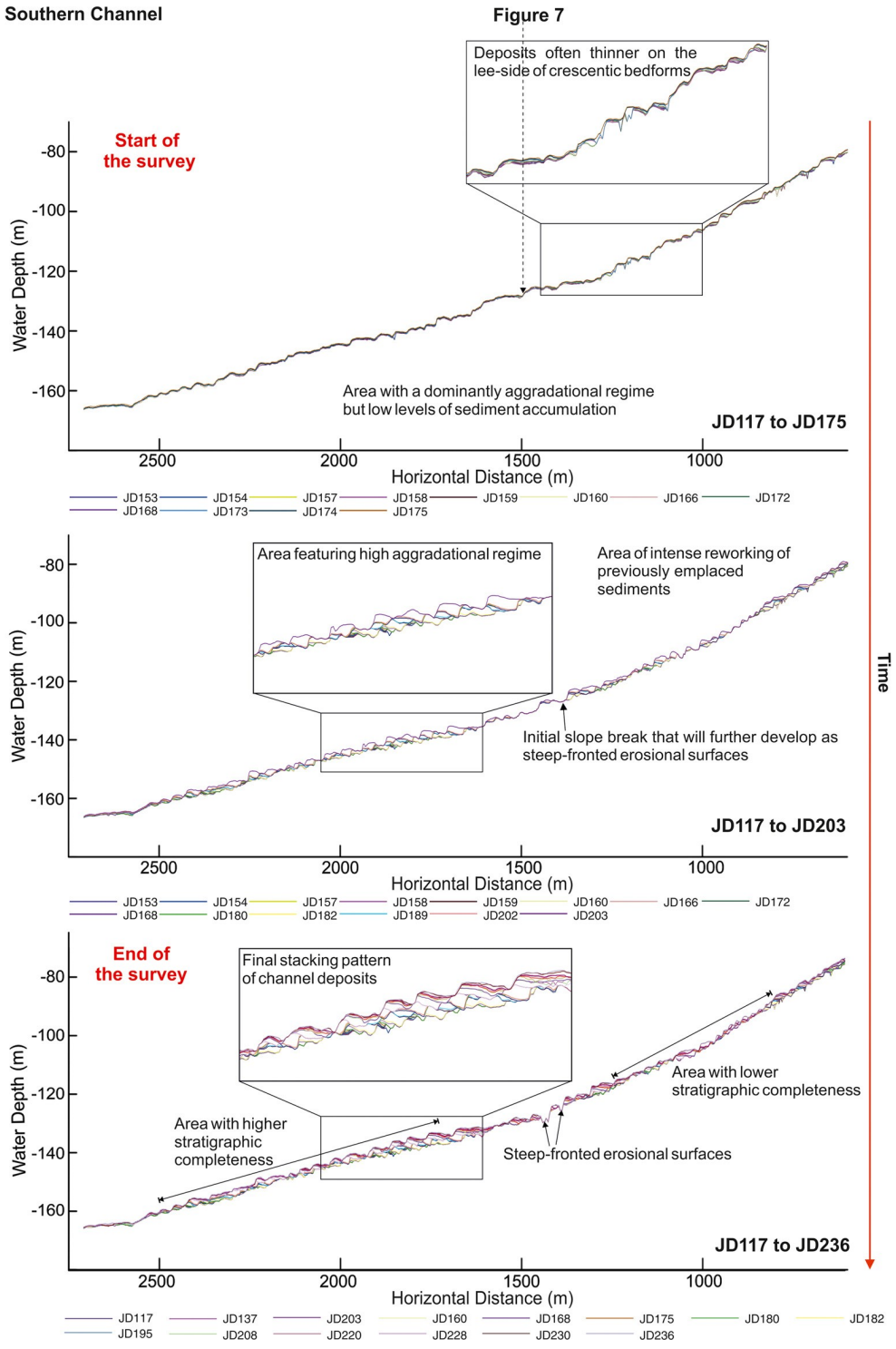

Figure 4.7: Along channel profiles at the channel lobe transition zone of the southern channel (see Figure 4.2D for their location). The upper panel shows the stratigraphic architecture of submarine channel deposits from the start of the survey JD117 until JD175. The central panel shows the evolution of those bedforms to much more defined features with foreset on the lee-side and more gentle backsets on the stoss-side. The bottom panel displays the final patterns of deposition and erosion of those deposits; herein, sediments are often thinner on the lee-side of crescentic bedforms rather than eroded (vertical exaggeration: 8x).

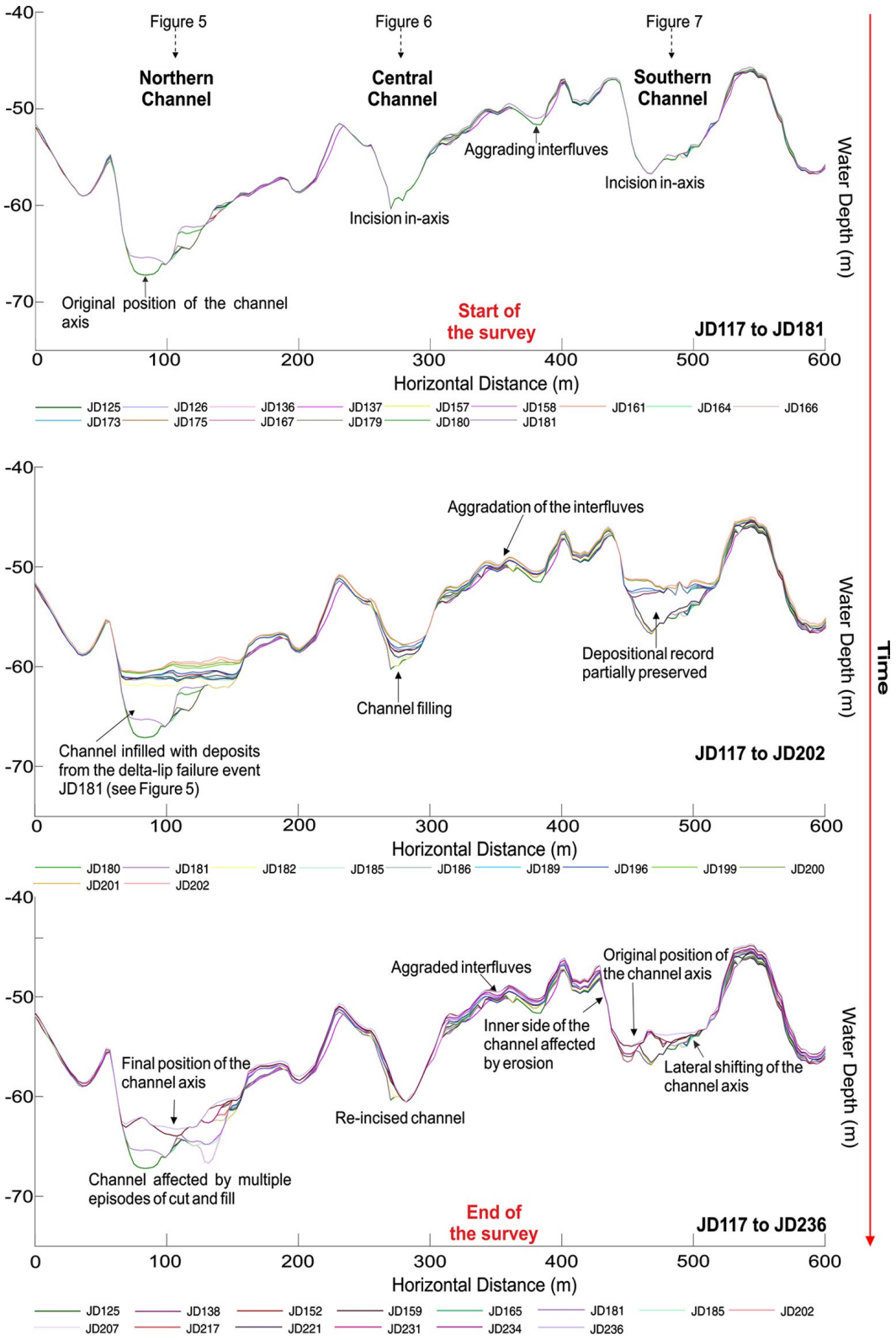

Figure 4.8: Cross-channel profiles of the proximal sector of Squamish prodelta (see Figure 4.2D, Line A). In this section, the northern and southern channels feature a later migration of their axis, and complex off-axis accumulations. The preservation of depositional records is commonly higher on the interfluves (refer to Figure 4.3C) (vertical exaggeration: 14x).

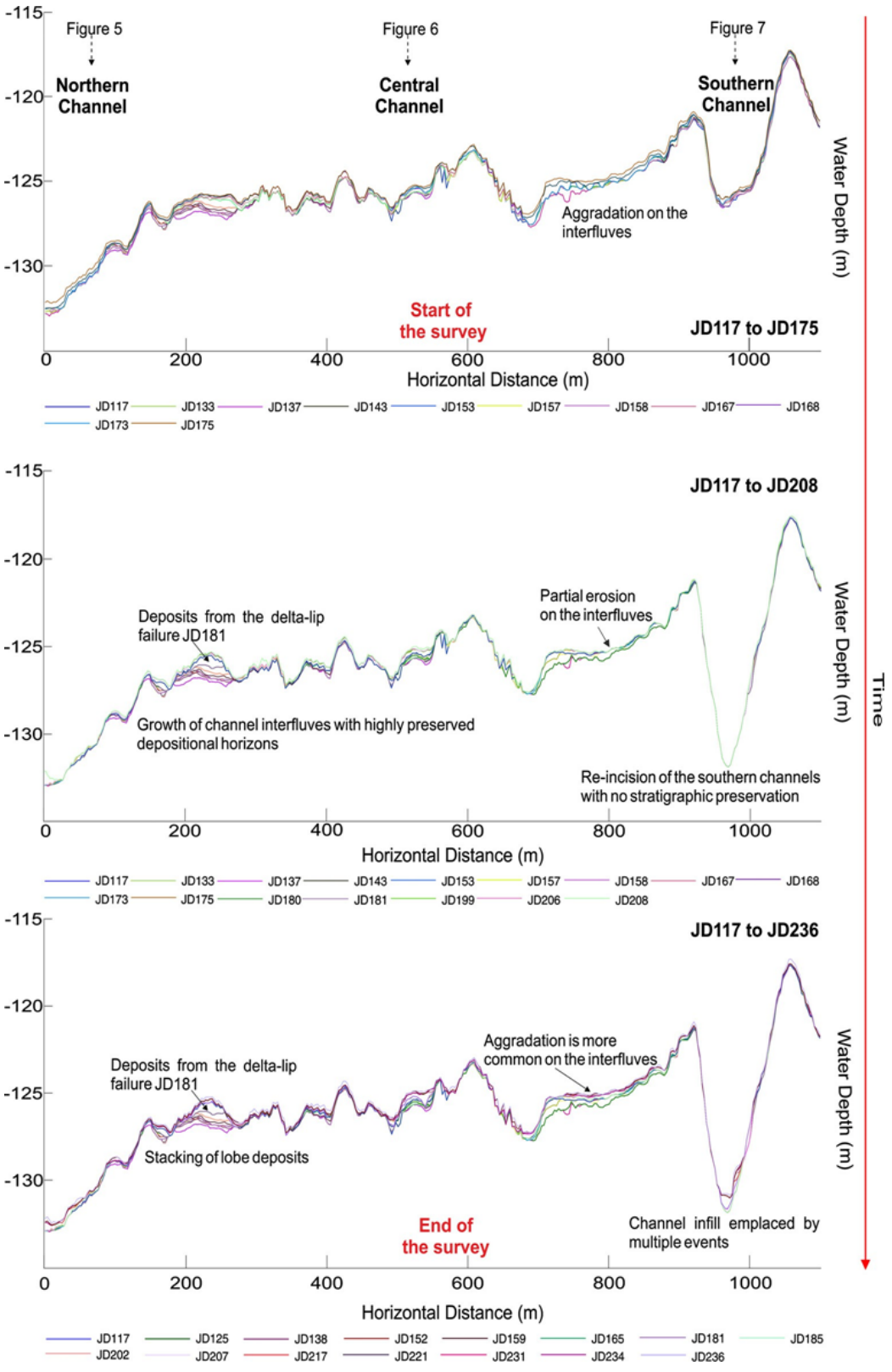

Figure 4.9: Cross-profiles of the distal area (see Figure 4.2D, Line F). Temporal evolution of the distal sector of the prodelta area. Preservation of the depositional records mainly affects the interfluves and aggrading levees. The southern channel features multiple episodes of channel filling and cut off the stratigraphic records (refer to the main test) (vertical exaggeration: 21x).

4.5.3 The most incomplete records result from short-lived and infrequent erosive events

Two short-lived erosional events were responsible for not only the removal of deposits accumulated at the channel-lobe transition of the southern channel during 2011, but also incision into deposits from previous years (Figure 4.9). Up to 5 m of vertical erosion occurred, with 200 m of retrogression, which is clearly shown by a sudden drop in the averaged stratigraphic completeness in the southern channel (between 1,001 and 1,500 m down-channel of Figure 4.4) on JD181 (Figure 4.3). At several time-steps, these features resemble steep-fronted erosional steps in rivers known as knickpoints that may be triggered by changes in the base level (Crosby and Whipple, 2006; Gales et al., 2018) (video S9 and S10). These scours may form in a similar manner, as progradation of the lobe could have a similar effect to the base level change in a river. If the southern channel extends seaward, for instance, then the present day channel lobe-transition zone may become a site of backfilling, or back stepping and deposition, while the focus of erosion will advance down-slope (Hamilton et al., 2013).

4.5.3.1 Why is stratigraphic completeness so low at the channel-lobe transition?

Stratigraphic completeness at this channel-lobe transition is zero, and may be explained by the strengthening of the erosional capacity that the most powerful flows have at the exit of channel confinement (Kostic and Parker, 2006; Covault et al., 2017; Dorrell et al., 2016). Mega-scours have been observed at similar transitional points at several sites in the deep sea (Wynn et al., 2002); hence such areas should be expected to have very low stratigraphic completeness (Mutti and Normark, 1987; Macdonald et al., 2011). These two major incisional events were also coincident with flushing of much of the previously accumulated sediment from the upper reaches of the southern channel, and the lateral erosion at the outer channel bend. Such channel-incising events represent ~2% of the total number of events occurring during the surveyed period, compared to ~98% that fill the channel, but appear to be strong controls on stratigraphic completeness. These events have the potential to remove significant thicknesses of sediment, and thus erase several years of sediment accumulation in locations such as the channel lobe transition zone (Conway et al., 2012). The location of the channel lobe transition zone may change over time as the channel evolves through developing slope breaks that can migrate up or down-stream and will consequently influence successive flows (Figure 4.9). Such events are perhaps more important for sculpting the geometry of channels and dictating what will ultimately be preserved over geologic timescales, than the more frequent flows that form upstream-migrating bedforms.

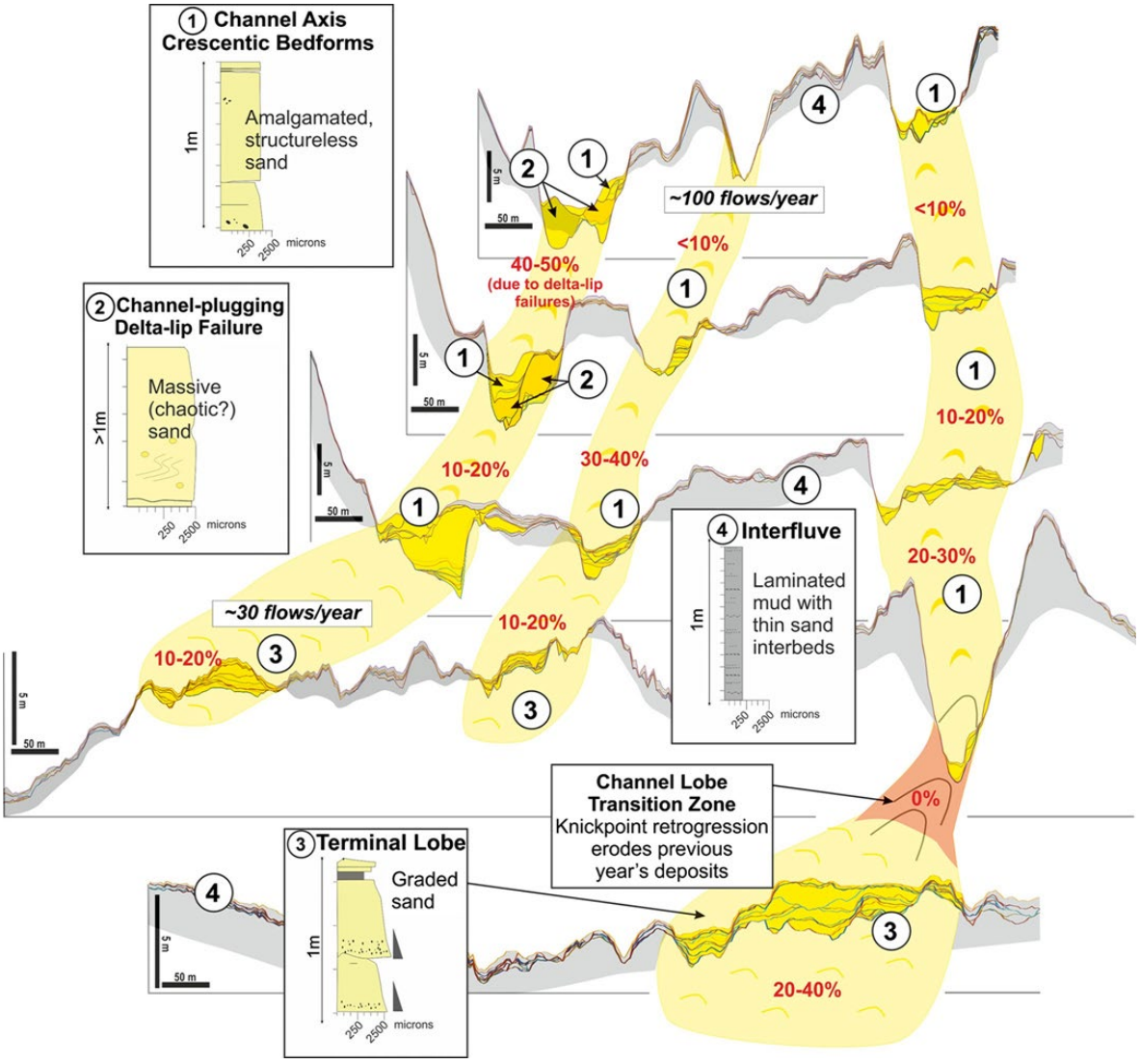

Figure 4.10: Correlation of submarine channel deposits with their resultant stratigraphic architecture across the surveyed area. Black numbers recall the depositional facies of the sediments cores used to reconstruct this section. Red numbers refer to the completeness of the stratigraphic records from the proximal to the distal area. Flow frequency is also estimated from higher at the channels head to lower at the channels mouth (vertical exaggeration 10x).

4.5.3.2 Do the powerful erosive events relate to an exceptional trigger?

It has been suggested that powerful triggers are required for channel-incising events, such as major earthquakes, extreme river floods or sea level change (Canals et al., 2006; Piper and Normark, 2009). The timing of the first channel-incising event is closely associated with the first major river flood discharge peak of the year, hence a sudden seaward flushing of delta-top sediments may be responsible (Clare et al., 2016); however, the specific cause for the second is unclear. It is plausible that once sufficient sediment had accumulated within the upper reaches of the channel, a 'normal' turbidity current was able to bulk up through entrainment of freshly deposited sediment, and 'ignite', without needing an exceptional trigger (Pantin, 1979; Parker, 1982; Hizzett et al., 2018).

4.5.4 How do our findings relate to other systems worldwide?

It is important to understand the wider implications of our results at Squamish Delta for interpreting submarine channel deposit geometries and completeness more generally. Currently, there are no comparably detailed time-lapse bathymetric datasets available, however. This makes it impossible to make direct comparisons to similar data from other sites. We thus first discuss whether the morphological features seen at Squamish Delta (e.g. crescentic bedforms) are found in other proximal sandy submarine or sub-lacustrine channels. If they are, then results from Squamish Delta can form part of more general models. We then discuss morphologies of muddier submarine channel systems.

4.5.4.1 Implications for other sandy submarine channels

Similar scale upstream-migrating bedforms have been observed from repeat seafloor surveys of sandy proximal submarine channels in lakes (Fricke et al., 2015), estuarine settings (Normandeau et al., 2014), submarine deltas (Conway et al., 2012; Casalbore et al., 2017), deep-sea canyons (Smith et al., 2005, 2007; Paull et al., 2018) and volcanic islands (Chiocci et al., 2013; Casalbore et al., 2014; Clare et al., 2018). The repetition of erosion and deposition that occurs during the upstream-migration of these crescentic bedforms ensures that the stratigraphic completeness of the submarine channel deposits will be low in these highly active and bypass-dominated settings. Such sandy-floored channels may therefore be relatively poor for reconstructing event-histories (particularly where aggradation rates are low), and can render core-to- core correlation impossible, even within distances of a few tens of metres (Hage et al., 2018).

4.5.4.2 Implications for larger muddy submarine channels

Similar scale upstream-migrating bedforms do not appear to typify larger mud-dominated systems. However, longer wavelength (c. 500 m) bedforms (equivalent to the 'large-scale' bedforms of Symons et al., 2016) that are inferred to have migrated upstream have been observed in sites such as the deep-sea Amazon Fan (Normark et al., 2002). As the resolution of bathymetric data is a function of water depth, it is possible that this has precluded identification of bedforms in most deep-water sites (Symons et al., 2016). Thus, it is unclear as to precisely how well our findings may relate to the world's largest muddy submarine channels (e.g. Amazon, Indus and Congo).

Recent direct monitoring of turbidity currents in the upper reaches of the offshore Congo Canyon, demonstrated that sub-annually recurring turbidity currents are capable of eroding seafloor sediment, which is then transported further down-canyon (Azpiroz-Zabala et al., 2017). Comparison of this flow monitoring data with sediments acquired from seafloor coring indicated that the depositional record under-represents the frequency of turbidity currents by at least an order of magnitude in the axis of the muddy Congo Canyon. In similarly-active muddy systems, stratigraphic completeness is thus unlikely to be high in the channel axis, but how this varies across and down the system is also unclear. Until high-resolution time-lapse data are available, we hypothesize that accumulation of mud may shield underlying deposits from subsequent erosion, and that areas of low stratigraphic completeness may be less extensive in muddy systems. This may promote a higher stratigraphic completeness than that observed in proximal sandy settings, such as at Squamish Delta. This current uncertainty underlines the need for more repeat seafloor surveys in a wider range of active settings in order to better constrain the relative controls played by substrate, system scale and aggradation rate on stratigraphic completeness.

4.6 Conclusions

We report one of the most detailed time-lapse studies of any turbidity current system. Through combining flow monitoring, repeat bathymetric surveys and core sampling, we revealed how three active submarine channels build stratigraphic architecture. In this setting, the effects of upstream-migrating bedforms ensure that stratigraphic completeness is generally low (even in the terminal lobes of the system), because of the competing effects of deposition and erosion. Other less-frequent events, such as delta- lip collapses and incision at the down-slope transition to the lobe, can exert a more profound influence on what is recorded in the depositional record (or not). Short lived, more powerful and infrequent events can exert varied effects: delta-lip collapses may be largely preserved, while canyon-flushing flows may remove significant thicknesses of sediment. These insights into the stratigraphic completeness of active submarine channels demonstrate that one should expect a high degree of incompleteness in similar systems. Frequency of flows, aggradation rate and the extent of variation in magnitude of events all play important roles and dictate exactly how incomplete

the ultimate geological record will be. Perhaps most importantly, we have demonstrated how repeat surveys can be used to monitor the stratigraphic evolution of submarine systems. The emergence of autonomous survey platforms now enables multiple repeat, high resolution surveys, requiring limited human effort, and opens up exciting new opportunities to understand how a much wider range of offshore systems evolve and provide calibration for numerical models.

Figures presented as a supplement to the published paper

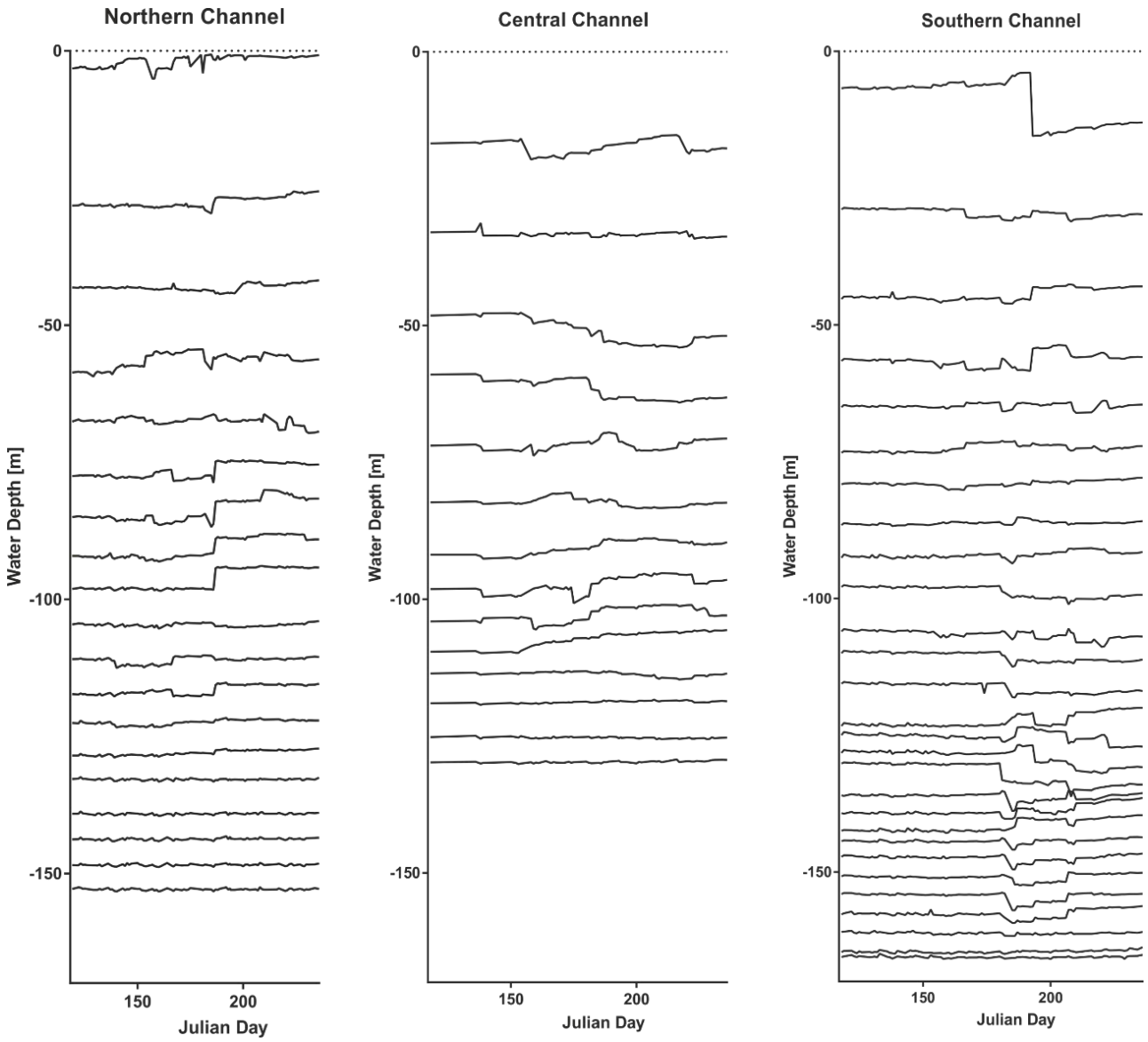

Figure S1: Seafloor elevation changes through time, taken at 100 m interval along single points of the thalweg for each of the three channels at the Squamish prodelta

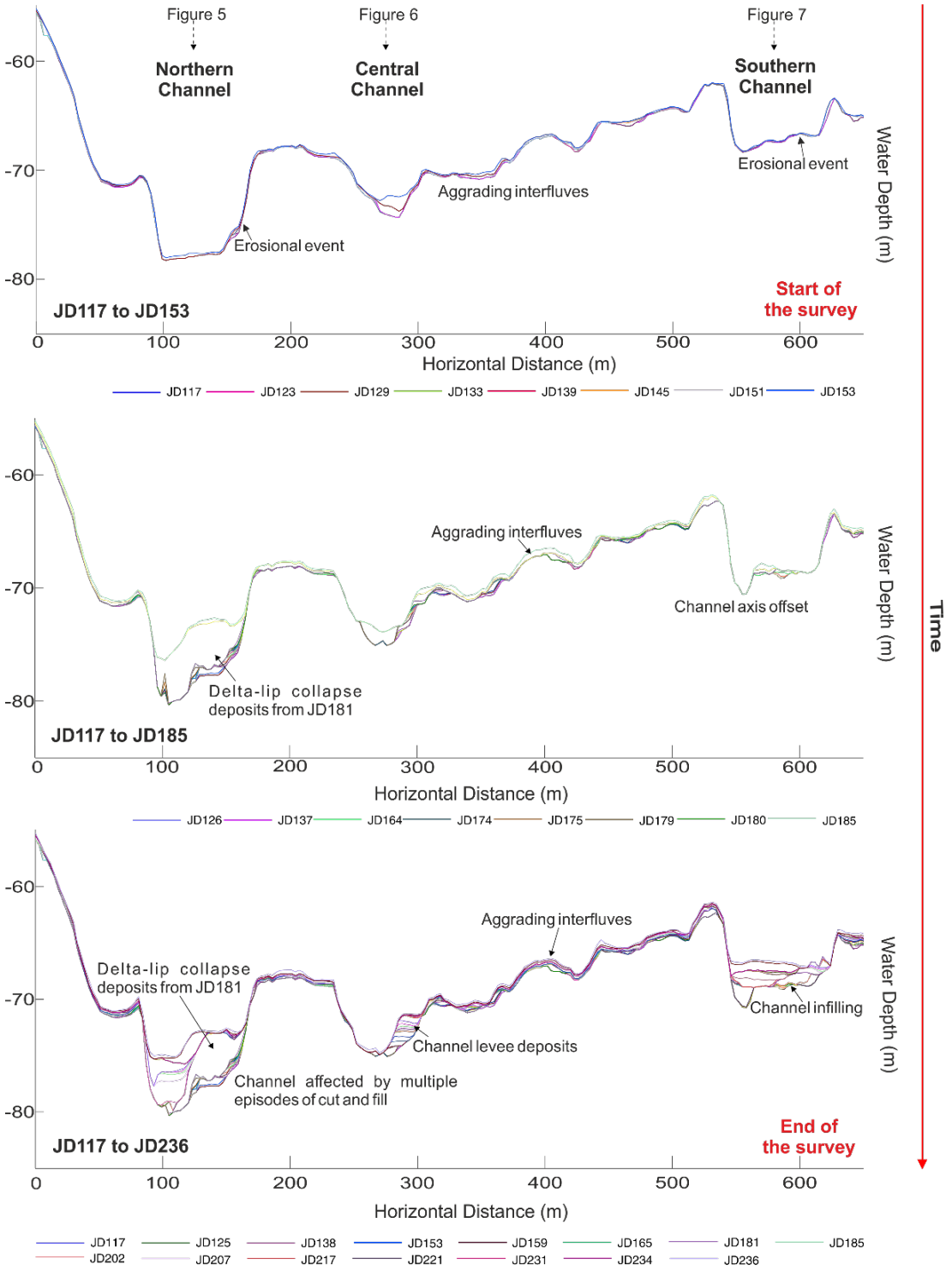

Figure S2: Across channel profile B (see Figure 4.2-D in the main text for the location of the profile; vertical exaggeration: 9x)

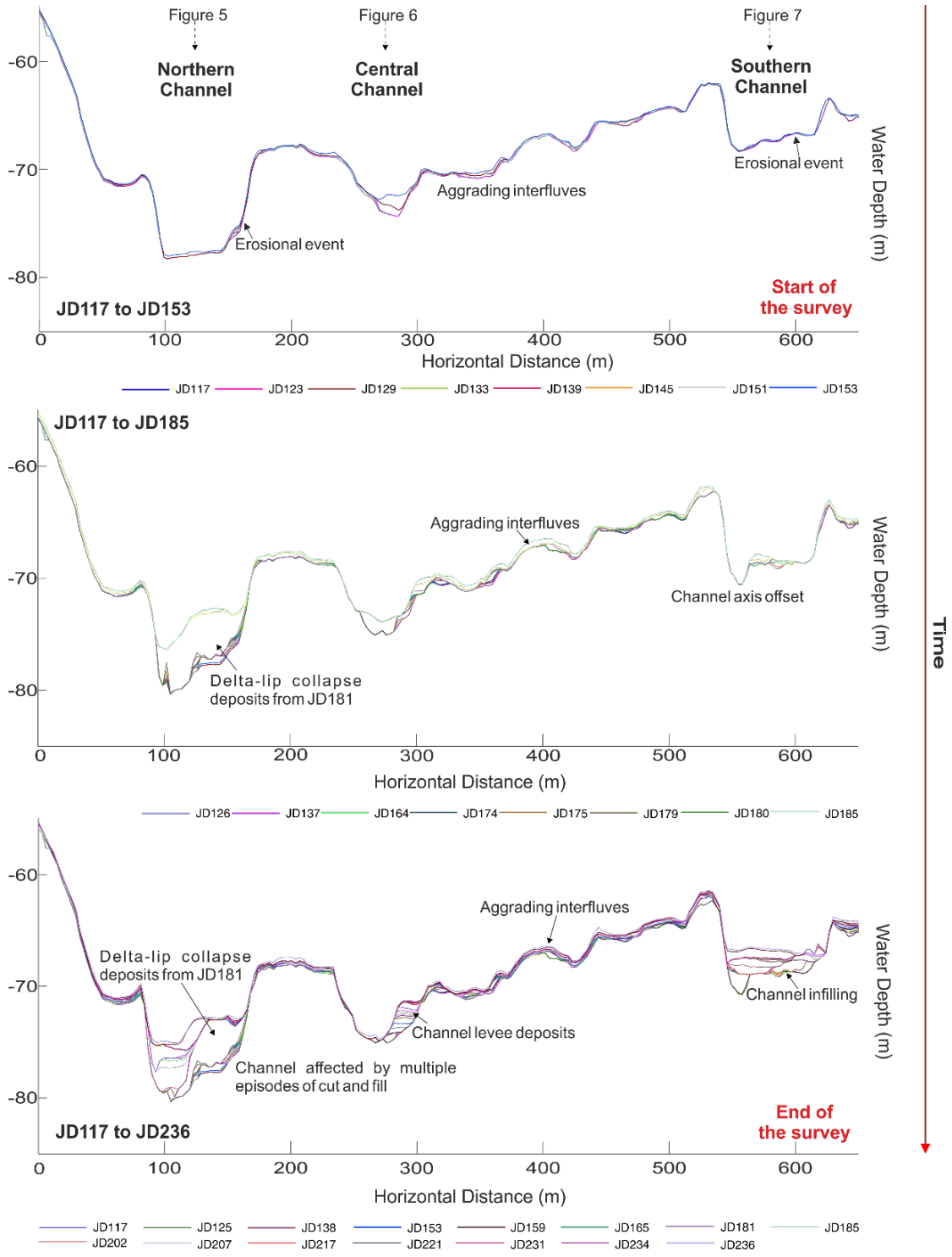

Figure S3: Across channel profile C (see Figure 4.2-D in the main text for the location of the profile; vertical exaggeration: 9x)

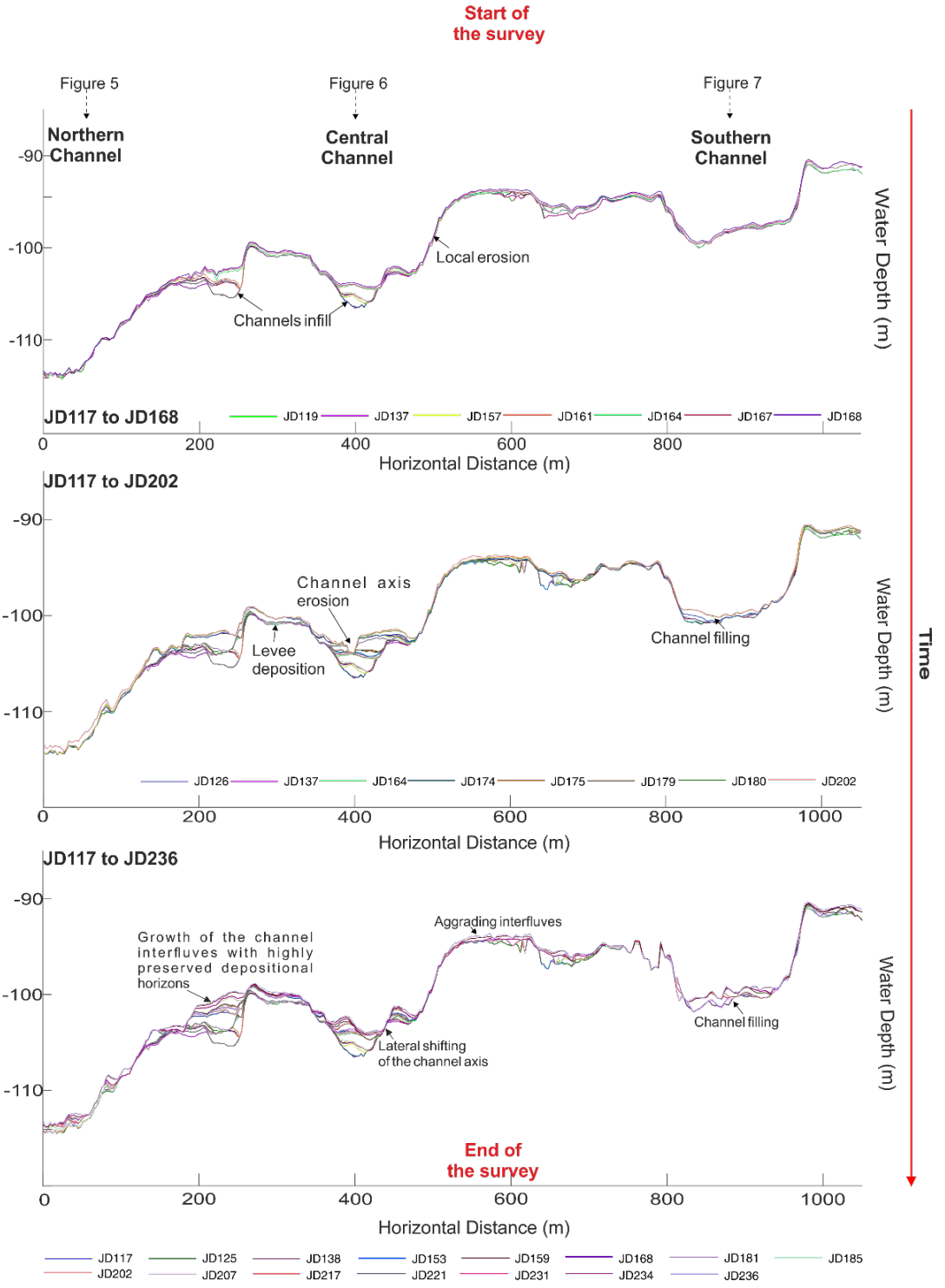

Figure S4: Across channel profile D (see Figure 4.2-D in the main text for the location of the profile; vertical exaggeration: 12x)

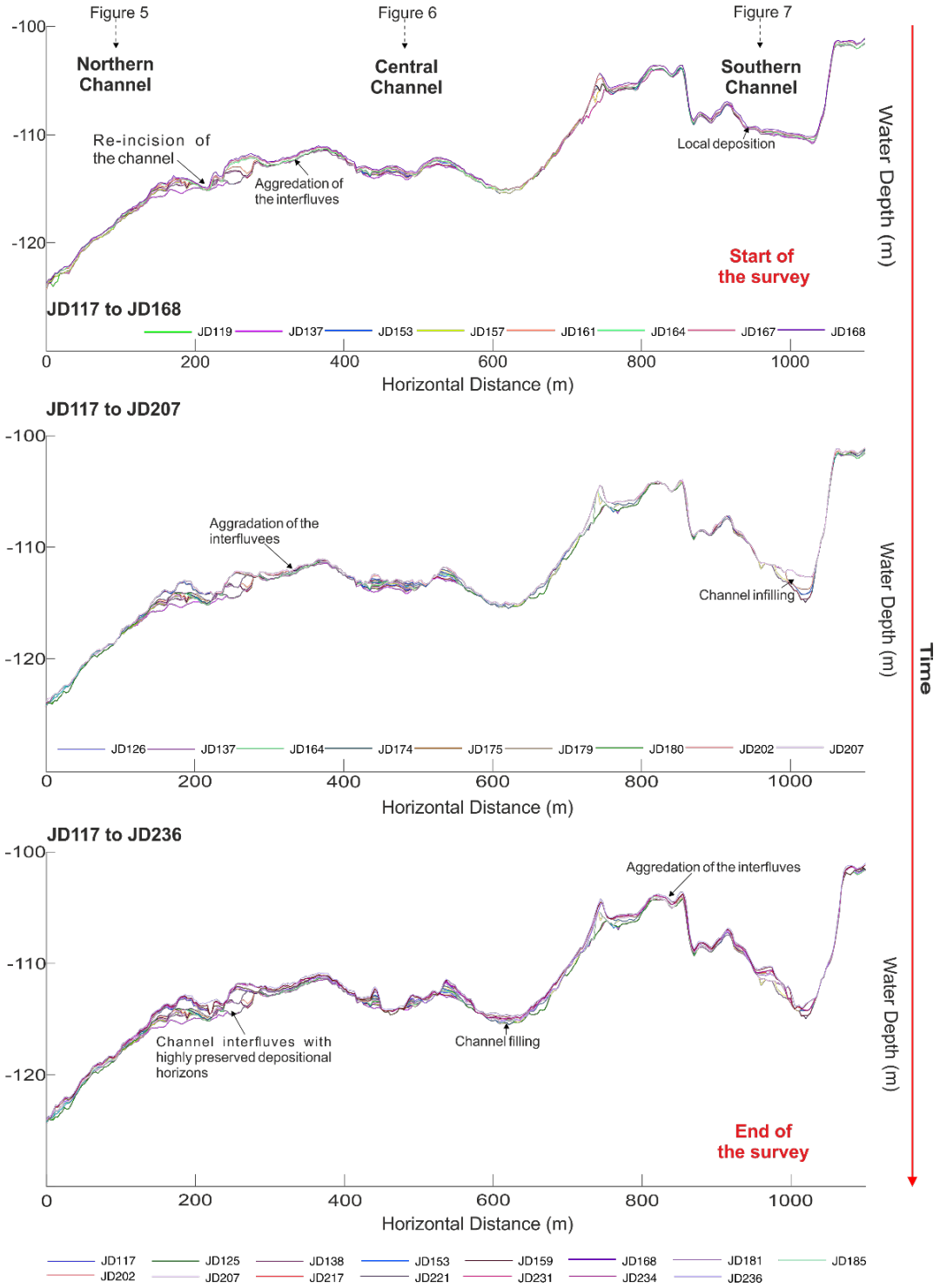

Figure S5: Across channel profile E (see Figure 4.2-D in the main text for the location of the profile; vertical exaggeration: 14.5x)

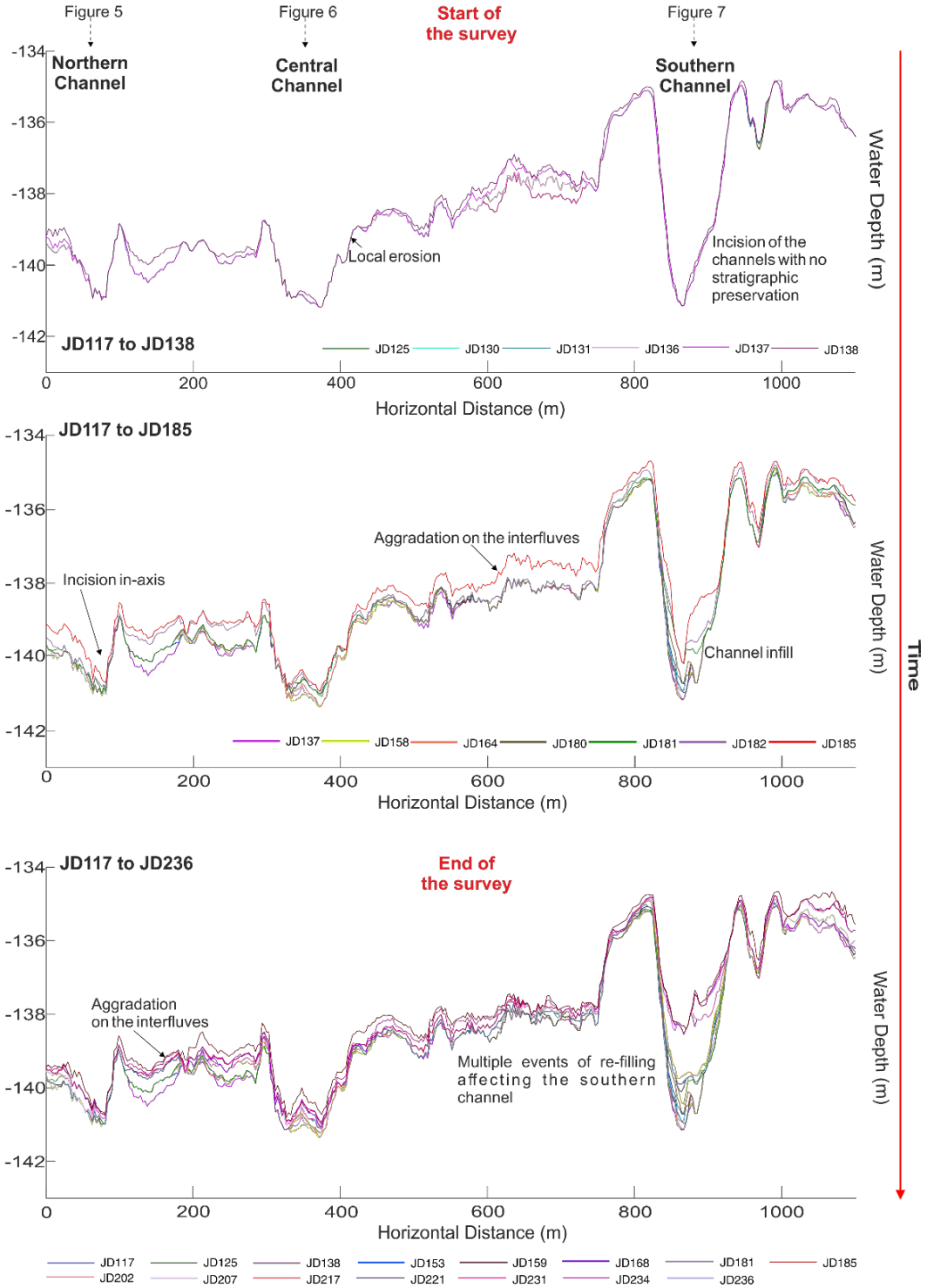

Figure S6: Across channel profile G (see Figure 4.2-D in the main text for the location of the profile; vertical exaggeration: 48x)

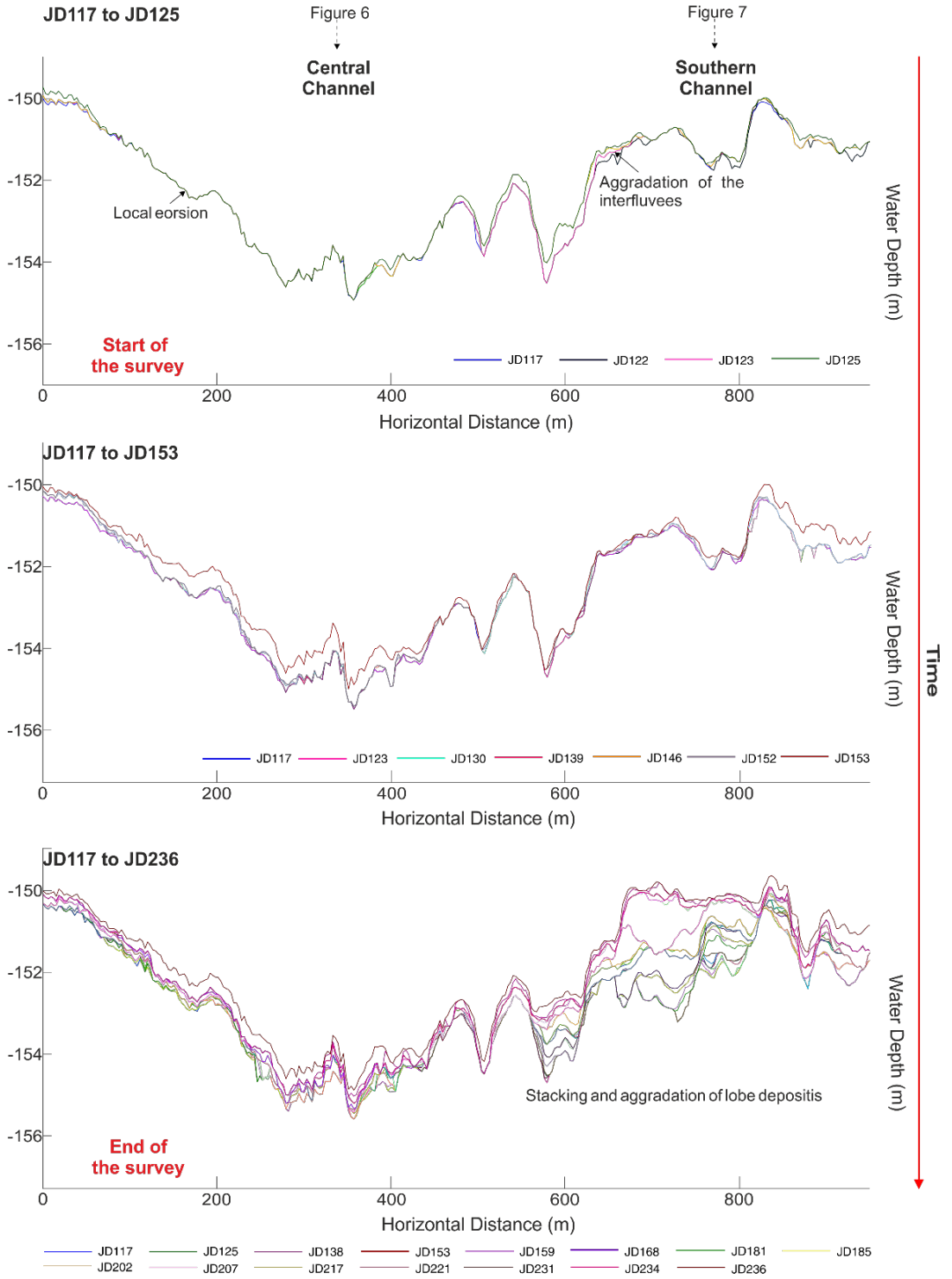

Figure S7: Across channel profile H (see Figure 4.2-D in the main text for the location of the profile; vertical exaggeration: 47.5x)

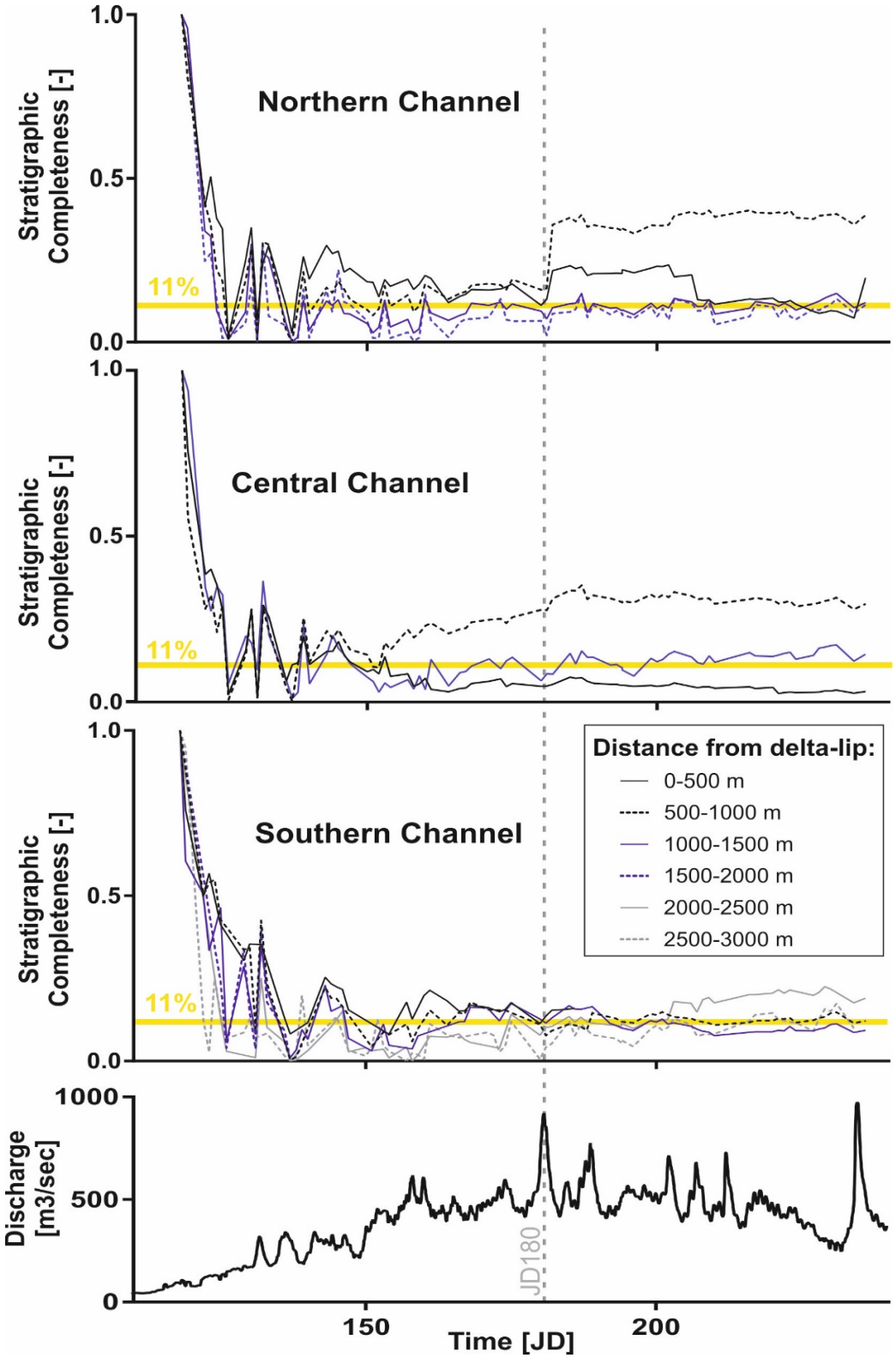

Figure S8: River discharge rata and evolution of stratigraphic completeness over time along the three channel at the Squamish prodelta

Animated videos presented in the online material as follows:

Animated videos MS1 to MS18 presented in the online material and available at this link https://doi.org/10.1016/j.epsl.2019.03.033

- Movie S1_NorthernChannel.avi – Time-lapse animation of stratigraphic evolution of the Northern Channel
- Movie S2_NorthChannelProximal.avi – Time-lapse animation of stratigraphic evolution of proximal to medial parts of Northern Channel
- Movie S3_NorthChannelDistal.avi – Time-lapse animation of stratigraphic evolution of medial to distal parts of Northern Channel
- Movie S4_CentralChannel.avi – Time-lapse animation of stratigraphic evolution of the Central Channel
- Movie S5_CentralChannelProximal.avi – Time-lapse animation of stratigraphic evolution of proximal to medial parts of Central Channel
- Movie S6_CentralChannelDistal.avi – Time-lapse animation of stratigraphic evolution of medial to distal parts of Central Channel
- Movie S7_SouthChannel.avi – Time-lapse animation of stratigraphic evolution of the Southern Channel
- Movie S8_SouthChannelProximal.avi – Time-lapse animation of stratigraphic evolution of proximal to medial parts of Southern Channel
- Movie S9_SouthChannel_LTZ.avi – Time-lapse animation of stratigraphic evolution of the channel lobe transition zone of Southern Channel
- Movie S10_SouthChannel_LTZ_Zoom - Time-lapse animation of stratigraphic evolution of the channel lobe transition zone of Southern Channel – zoom in
- Movie S11_A.avi- Time-lapse animation of stratigraphic evolution of across-profile A
- Movie S12_B.avi- Time-lapse animation of stratigraphic evolution of across-profile B
- Movie S13_C.avi- Time-lapse animation of stratigraphic evolution of across-profile C
- Movie S14_D.avi- Time-lapse animation of stratigraphic evolution of across-profile D
- Movie S15_E.avi- Time-lapse animation of stratigraphic evolution of across-profile E
- Movie S16_F.avi- Time-lapse animation of stratigraphic evolution of across-profile F
- Movie S17_G.avi- Time-lapse animation of stratigraphic evolution of across-profile G
- Movie S18_H.avi- Time-lapse animation of stratigraphic evolution of across-profile H

Chapter 5
Conclusions

5.1 Revisiting the thesis aims

The overarching aim of this thesis was to better understand how the velocity structure of turbidity currents varies across different scales and how this is reflected in nature in terms of their deposits and the shapes that they leave on the sea floor. To fulfill this objective, I have used observations of turbidity currents in action from multiple systems worldwide, bedforms across extensive reaches of submarine canyons offshore East Africa, and from observing how repeated turbidity currents build and modify stratigraphy at the active Squamish submarine delta, British Columbia. The findings presented in this thesis provide new insights into turbidity currents and I conclude that while turbidity current flow behaviour, and the bedforms that these flows create, appear to occur along a continuum, the deposits that they leave behind may disproportionately preserve the evidence of the largest, least frequent events.

In this thesis, I have documented the highly variable nature of turbidity currents, as revealed by direct monitoring from multiple sites worldwide (Chapter 2), that is manifested on the seafloor as dune-scale bedforms to large erosional scours in Mozambique (Chapter 3), and how the dynamic interplay of depositional and erosion in highly active systems such as the Squamish delta can both build and wipe out their stratigraphic record (Chapter 4). These various studies demonstrate that there appears to be a general continuity in turbidity current behaviour, as revealed by collation of global monitoring datasets (Chapter 2) and the identification of a previously 'missing' medium-scale of bedforms detected along the continental slope offshore East Africa (Chapter 3). The various types of flow on that continuum likely explain the variations we see in stratigraphic completeness at the Squamish Delta, where the highest velocity flows, that are capable of transporting sand, are presumably most responsible for the erosion (and thus low stratigraphic completeness) within the axes of the submarine channels and forming the deepest scours.

5.2 Answering the initial science questions

5.2.1 Is there a continuum in the velocity structure of turbidity currents, and what controls that behaviour? (Chapter 2)

The number of turbidity current monitoring studies has grown rapidly over the past decade and Chapter 2 provides a step-forward in investigating key similarities and differences between a compilation of direct flow measurements. The analysis of the temporal evolution of the maximum velocity of turbidity currents observed at different sites worldwide reveals two end-member flow states. The analysis shows that the events either feature a rapid peak in

velocity followed by an exponential decay or, flows continue at a plateau-like, near constant velocity that can last for days. In Chapter 2, it is suggested that rather than triggers or system input type, flow structure is primarily governed by the grain size of the sediment that is available for incorporation into the flow.

Future research: Whether the data gathered to date captures the full diversity of turbidity currents worldwide remains an open question, however; thus providing the motivation to ensure under-represented systems (e.g. muddy and carbonate-dominate systems) are monitored in future studies. Deployment of ADCP moorings in systems such as those in carbonate-dominated margins, such as canyons in the Bahama Banks would determine how active the submarine canyons are, and whether the flows behave in a similar manner to those observed in Chapter 2.

5.2.2 Is there a continuum in the dimensions of bedforms created on the seafloor by turbidity current, and what are we currently missing from deep-sea surveys? (Chapter 3)

Previously it was thought that flow modes were bimodal, because observations of turbidity current bedforms fell into two main dimensional classes. In that model small-scale bedforms were thought to be restricted to confined settings, while large-scale sediment waves occur in unconfined settings, and no intermediate size class exists. Chapter 3 presented a new morphometric analysis of bedforms dimensions using high resolution AUV bathymetry across two large submarine canyons that demonstrates a previously-unrecognised continuum between small, crescentic bedforms and large-scale sediment waves. The newly observed medium-scale bedforms relate to a type that is either transitional between small crescentic bedforms and large-scale sediment waves or are a steep stepped-form, known as a knickpoints that is increasingly observed in many other canyons and channels worldwide. Bedform dimensions can vary independently of water depth, but the identification of the smallest scale bedforms is hampered in increasing water depths.

Future research: High-resolution AUV surveys provide the means to fill fundamental gaps in our understanding of how canyons and channels are built and maintained, and to better constrain the nature of particulate transport into the deep sea. Future channel-scale surveys will allow us to investigate whether the intermediate scale of bedforms exists in other sites, and how common small-scale bedforms are in deep-water settings worldwide. Major submarine channel systems, such as the Amazon Channel remain un-surveyed in detail and this exposes a major gap in our understanding of deep-sea sediment transport that could be filled with such surveys.

5.2.3 How do turbidity currents build stratigraphy and how faithfully does that stratigraphy preserve a record of past flow behaviour? (Chapter 4)

Through combining flow monitoring, repeat bathymetric surveys and core sampling, Chapter 4 demonstrated that the completeness of the depositional record can be compromised by the effects of erosion by recurrent turbidity currents. In an extremely active systems such as the Squamish Delta, the analysis of repeat bathymetric surveys shows how erosion during the upstream-migration of bedforms ensure that stratigraphic continuity of the depositional record is generally low (even in the terminal lobes of the system). Less-frequent events, such as delta-lip collapses and incision at the down-slope transition to the lobe, exert a more profound influence on what is recorded in the depositional record; often removing the evidence of numerous smaller flows. Short-lived, more powerful and infrequent events can strongly affect the completeness of the depositional records. Delta-lip collapses are generally well preserved, while canyon-flushing flows can remove several metres of the previously formed stratigraphy. These insights into the stratigraphic completeness of active submarine channels demonstrate that one should expect a high degree of incompleteness in similar systems. Frequency of flows, aggradation rate and the extent of variation in magnitude of events all play important roles and dictate exactly how incomplete the ultimate geological record will be.

Future research: This is the first such study of stratigraphic completeness using repeated seafloor surveys in submarine channels. Similar studies should be performed in other systems to understand how grain size, flow type, system scale and other variables affect stratigraphic completeness and how it varies over different timescales. It is unclear how well our results from this sandy and relatively small-scale system will apply to muddy and large-scale systems, such as the Congo Canyon. Future repeat seafloor surveys, coupled with sediment cores will enable a similar analysis and test the hypotheses outlined in Chapter 4.

5.3 Broader implications

The outcomes of this thesis have broad relevance to a number of studies, such as understanding the nature of carbon and pollutant transport and the efficiency of their burial (e.g. Galy et al., 2007; Hage et al., 2020), but perhaps the most relevant application is in relation to geohazard assessment. Geohazard assessments for seafloor infrastructure such as telecommunications cables and pipelines requires an understanding of the frequency, magnitude (e.g. extent, velocity) and nature of turbidity currents (Bruschi et al., 2006). This thesis provides new insights into the global variability in flow velocity and duration, in particular in Chapter 2 identifying the physical controls on flow behaviour (i.e. grain size and slope gradient), which can now be used to inform pipeline and cable routes (e.g. avoid steep slopes and systems with coarse grain sizes, or design pipelines to withstand prolonged, low velocity impacts in muddy low relief systems). Determining the nature of larger turbidity currents (i.e. larger than those recorded during relatively short monitoring windows) also requires consideration in such hazard assessments. The nature of past flows can be inferred from bedform morphometrics, but as shown in Chapter 3 this may require high-resolution (e.g. AUV) bathymetric datasets. This new contribution shows how certain types of bedform (and hence types of flow that formed them) may be missing from bathymetric datasets that were acquired in deep water from vessel-mounted systems. An important message to take

from this study is the value of such high resolution datasets to better understand the variability of turbidity current activity. To assess the likely frequency of turbidity currents, geohazard assessments often analyse sediment cores, using age dating techniques to determine the emplacement time of event deposits (e.g. Goldfinger et al., 2007; Hunt et al., 2013). However, if successive flows erode sediment, this will affect the completeness of these sedimentary records. It is therefore important to assess whether certain events are better recorded than others, and which settings are better recorders of past geohazard activity. Chapter 4 provides the first attempt anywhere to do this in an active turbidity current system, concluding that many parts of the submarine channel systems on the Squamish delta feature very poorly preserved stratigraphy and are thus unsuitable for reconstruction of past event frequency and magnitude. However, large landslide events are better preserved, and guidance for future sampling is provided (e.g. levees and distal lobe provide the greatest stratigraphic completeness).

Reference List

Azpiroz-Zabala, M., Cartigny, M.J.B., Talling, P.J., Parsons, D.R., Sumner, E.J., Clare, M.A., Simmons, S.M., Cooper, C., Pope and E.L., 2017. Newly recognised turbidity current structure can explain prolonged flushing of submarine canyons. Science Advances: 3(10), e1700200. DOI: 10.1126/sciadv.1700200

Armitage, D. A., Romans, B. W., Covault, J. A., & Graham, S. A., 2009. The influence of mass-transport-deposit surface topography on the evolution of turbidite architecture: The Sierra Contreras, Tres Pasos Formation (Cretaceous), southern Chile. Journal of Sedimentary Research, 79(5), 287-301

Baas, J.H., McCaffrey, W.D., Haughton, P.D. and Choux, C., 2005. Coupling between suspended sediment distribution and turbulence structure in a laboratory turbidity current. Journal of Geophysical Research: Oceans, 110(C11)

Bagnold, R.A., 1962. Auto-suspension of transported sediment; turbidity currents. Proceedings of the Royal Society London, 265, 315–319. https://doi.org/10.1098/rspa.1962.0012

Bailey, L.P., Clare, M.A., Rosenberger, K.J., Cartigny, M.J., Talling, P.J., Paull, C.K., Gwiazda, R., Parsons, D.R., Simmons, S.M., Xu, J. and Haigh, I.D., 2021. Preconditioning by sediment accumulation can produce powerful turbidity currents without major external triggers. Earth and Planetary Science Letters, 562, p.116845

Barrell, J., 1917. Rhythms and the measurements of geologic time. Bulletin of the Geological Society of America, 28(1), 745-904

Bernhardt, A., Melnick, D., Hebbeln, D., Lückge, A., Strecker, M. R., 2015. Turbidite paleoseismology along the active continental margin of Chile–Feasible or not? Quaternary Science Reviews, 120, 71-92

Biscara, L., Hanquiez, V., Leynaud, D., Marieu, V., Mulder, T., Gallissaires, J. M., & Garlan, T., 2012. Submarine slide initiation and evolution offshore Pointe Odden, Gabon—Analysis from

Bongo-Passi, G., 1984. Contribution a` l'e´tude lithostratigraphique, mineralogique etge´ochimique du delta sous-marin profound du fleuve Congo. Universite´ de Toulouse, 215

Bouma, A., 1964. Turbidites. In Developments in sedimentology. Vol. 3, pp. 247-256. Elsevier

Brooks, H. L., Hodgson, D. M., Brunt, R. L., Peakall, J., Flint, S. S., 2017. Exhumed lateral margins and increasing flow confinement of a submarine landslide complex. Sedimentology

Bruschi, R., Bughi, S., Spinazzè, M., Torselletti, E. and Vitali, L., 2006. Impact of debris flows and turbidity currents on seafloor structures. Norwegian Journal of Geology/Norsk Geologisk Forening, 86(3).

Burger, R.L., Fulthorpe, C.S. and Austin Jr, J.A., 2001. Late Pleistocene channel incisions in the southern Eel River Basin, northern California: implications for tectonic vs. eustatic influences on shelf sedimentation patterns. Marine Geology, 177(3-4), pp.317-330

Campbell, K.J., Kinnear, S. and Thame, A., 2015. AUV technology for seabed characterization and geohazards assessment. The Leading Edge, 34(2), pp.170-178

Canals, M., Puig, P., de Madron, X. D., Heussner, S., Palanques, A., & Fabres, J., 2006. Flushing submarine canyons. Nature, 444(7117), 354

Cantero, M.I., Cantelli, A., Pirmez, C., Balachandar, S., Mohrig, D., Hickson, T.A., Yeh, T., Naruse, H. and Parker, G., 2012. Emplacement of massive turbidites linked to extinction of turbulence in turbidity currents. Nature Geoscience, 5, 42–45. http://doi.org/10.1038/ngeo1320

Carter, L., Gavey, R., TALLING, P.J. and Liu, J.T., 2014. Insights into submarine geohazards from breaks in subsea telecommunication cables. Oceanography, 27(2), pp.58-67

Cartigny, M.J.B, Postma, G., van den Berg, J. H.,. Mastbergen, D., 2011. A comparative study of sediment waves and cyclic steps based on geometries,internal structures and numerical modeling. Marine Geology 280, 40-56

Cartigny, M.J.B., 2013. Morphodynamics of supercriticalhigh-density turbidity currents. Utrecht Studies in EarthSciences, 10, 153 pp

Cartigny, M.J., Ventra, D., Postma, G. and van Den Berg, J.H., 2014. Morphodynamics and sedimentary structures of bedforms under supercritical-flow conditions: new insights from flume experiments. Sedimentology, 61(3), pp.712-748

Carvajal, C., Paull, C.K., Caress, D.W., Fildani, A., Lundsten, E., Anderson, K., Maier, K.L., McGann, M., Gwiazda, R. and Herguera, J.C., 2017. Unraveling the channel–lobe transition zone with high-resolution AUV bathymetry: Navy Fan, offshore Baja California, Mexico. Journal of Sedimentary Research, 87(10), pp.1049-1059

Casalbore, D., Ridente, D.; Bosman, A.; Chiocci, F.L., 2017. Depositional and erosional bedforms in Late Pleistocene-Holocene pro-delta deposits of the Gulf of Patti (southern Tyrrhenian margin, Italy). Marine Geology, 385, 216-227

Casalbore D, Bosman A, Ridente D, Chiocci F., 2016. Coastal and submarine landslides in the tectonically-active Tyrrhenian Calabrianmargin (Southern Italy): examples and geohazard implications. In: Krastel S (ed) Submarine mass movements and their consequences, vol 37, Advances in Natural and Technological Hazards Research. Springer, Heidelberg, pp 261–269. doi:10.1007/978-3-319-00972

Casalbore, D., Romagnoli, C., Bosman, A., Chiocci, F. L. 2014. Large-scale seafloor waveforms on the flanks of insular volcanoes (Aeolian Archipelago, Italy), with inferences about their origin. Marine Geology, 355, 318-329

Casalbore, D., Chiocci, F.L., Scarascia Mugnozza, G., Tommasi, T., Sposato, A., 2011. Flash-flood hyperpycnal flows generating shallow-water landslides at Fiumara mouths in

Western Messina Strait (Italy). Marine Geophysics Research, 27, 32:257

Cattaneo, A., Babonneau, N., Ratzov, G., Dan-Unterseh, G., Yelles, K., Bracène, R. & Déverchère, J., 2012. Searching for the seafloor signature of the 21 May. 2003 Boumerdès earthquake offshore central Algeria. Natural Hazards and Earth System Sciences, 12(7), 2159-2172.

Cattaneo, A., Babonneau, N., Ratzov, G., Dan-Unterseh, G., Yelles, K., Bracène, R., and Déverchère, J. 2012. Searching for the seafloor signature of the 21 May 2003 Boumerdès earthquake offshore central Algeria. Natural Hazards and Earth System Sciences, 12(7), 2159-2172.

Chiarella, D., Longhitano, S.G, Tropeano, M. 2017. Types of mixing and heterogeneities in siliciclastic-carbonate sediments. Marine and Petroleum Geoscience, 88, 617-627. https://doi.org/10.1016/j.marpetgeo.2017.09.010

Chiocci, F. L., Ronagnoli, C., Casalbore, D., Sposato, A., Martorelli, E., Alonso, B., Casas, D., Conte, A.M., Di bella, L., Ercilla, G., Estrada, F., Falese, F., Farran, M., Forleo, V., Frezza, V., Hipolito, A., Lebani, A., Maisto, F., Pacheco, J., Pimental, A., Quartau, R., Roque, C., Sampio, I., Santorp, P.C., Tempere, F., 2013, Bathy-morphological setting of Terceira Island (Azores) after the FAIVI cruise, J. Maps, 9(4), 590–595

Clare, M., Lintern, D.G., Rosenberger, K., Hughes Clarke, J.E., Gwiazda, R., Cartigny, M.J., Talling, P.J., Perera, D., Xu, J., Parsons, D., Silva Jacinto, R. and Apprioual, R., 2020. Lessons learned from monitoring of turbidity currents and guidance for future platform designs. Geological Society, London, Special Publications. https://doi.org/10.1144/SP500-2019-173

Clare, M., Le Bas, T., Price, D., Hunt, J., Sear, D., Cartigny, M., Vellinga, A., Symons, W., Firth, C. and Cronin, S., 2018. Complex and cascading triggering of submarine landslides and turbidity currents at volcanic islands revealed from integration of high-resolution onshore and offshore surveys. Frontiers in Earth Science, https://doi.org/10.3389/feart.2018.00223

Clare, M., Vardy, M., Cartigny, M., Talling, P., Himsworth, M., Dix, J., Belal, M., 2017. Direct monitoring of active geohazards: emerging geophysical tools for deep-water assessments. Near Surface Geophysics, 15(4), 427-444

Clare, M. A., Clarke, J. H., Talling, P. J., Cartigny, M. J. B., & Pratomo, D. G., 2016. Preconditioning and triggering of offshore slope failures and turbidity currents revealed by most detailed monitoring yet at a fjord-head delta. Earth and Planetary Science Letters, 450, 208-220

Clark, J. D., & Pickering, K. T., 1996. Architectural elements and growth patterns of submarine channels: application to hydrocarbon exploration. AAPG bulletin, 80(2), 194-220

Clark, J.D., Kenyon, N.H. and Pickering, K.T., 1992. Quantitative analysis of the geometry of submarine channels: implications for the classification of submarine fans. Geology, 20(7), pp.633-636

Clarke, J.E.H., Shor, A.N., Piper, D.J. and Mayer, L.A., 1990. Large-scale current-induced erosion and deposition in the path of the 1929 Grand Banks turbidity current. Sedimentology, 37(4), pp.613-629.

Coffin, M.F., Rabinowitz, P.D., 1987. Reconstruction of Madagascar and Africa: evidence from the Davie Fracture Zone and Western Somali Basin. J. Geophys. Res. Solid Earth 92 (B9), 9385–9406

Coffin, M.F., Rabinowitz, P.D., 1992. The Mesozoic East African and Madagascan conjugate continental margins: stratigraphy and tectonics. In: Watkins, J.S., Zhiqiang, F., McMillen, K.J. (Eds.), Geology and Geophysics of Continental Margins, AAPG Memoir 53. The American Association of Petroleum Geologists, Tulsa, Oklahoma, U.S.A., pp. 207–240

Conway, K. W., Barrie, J. V., Picard, K., & Bornhold, B. D., 2012. Submarine channel evolution: active channels in fjords, British Columbia, Canada. Geo-Marine Letters, 32(4), 301-312

Cooper, C.K., Andrieux, O. and Wood, J., 2013. Turbidity Current Measurements in the Congo Canyon. In Offshore Technology Conference

Corella, J. P., Loizeau, J. L., Kremer, K., Hilbe, M., Gerard, J., Le Dantec, N., & Girardclos, S., 2016. The role of mass-transport deposits and turbidites in shaping modern lacustrine deepwater channels. Marine and Petroleum Geology, 77, 515-525

Covault, J.A., Sylvester, Z., Hubbard, S.M., Jobe, Z.R. and Sech, R.P., 2016. The stratigraphic record of submarine-channel evolution. The Sedimentary Record, 14(3), pp.4-11

Covault, J.A., Kostic, S., Paull, C.K., Sylvester, Z. and Fildani, A., 2017. Cyclic steps and related supercritical bedforms: building blocks of deep-water depositional systems, western North America. Marine Geology, 393, pp.4-20.

Covault, J.A., Kostic, S., Paull, C.K., Ryan, H.F. and Fildani, A., 2014. Submarine channel initiation, filling and maintenance from sea-floor geomorphology and morphodynamic modelling of cyclic steps. Sedimentology, 61(4), pp.1031-1054.

Crosby, B. T., & Whipple, K. X., 2006. Knickpoint initiation and distribution within fluvial networks: 236 waterfalls in the Waipaoa River, North Island, New Zealand. Geomorphology, 82(1-2), 16-38

Daly, R. A., 1936. 'Origin of submarine canyons', American Journal of Science (186), 401–420. URL: http://dx.doi.org/10.2475/ajs.s5-31.186.401

Damuth, J.E., Flood, R.D., Kowsmann, R.O., Belderson, R.H. and Gorini, M.A., 1988. Anatomy and growth pattern of Amazon deep-sea fan as revealed by long-range side-scan sonar (GLORIA) and high-resolution seismic studies. AAPG bulletin, 72(8), pp.885-911

de Leeuw, J., Eggenhuisen, J.T. and Cartigny, M.J., 2018. Linking submarine channel–levee facies and architecture to flow structure of turbidity currents: insights from flume tank experiments. Sedimentology, 65(3), pp.931-951

Dennieloua, B., Drozb, L., Babonneaub, N., Jacqa, C., Bonnela, C., Picota, M., Le Saouta, M., Saouta, Y., Bezd, M., Savoyea,B., Olue, K. and Rabouillef, C., 2017. Morphology,

structure, composition and build-up processes of the active channel-mouth lobe complex of the Congo deep-sea fan with inputs from remotely operated underwater vehicle (ROV) multibeam and video surveys. Deep–Sea Research Part II, 142, 25–49. http://dx.doi.org/10.1016/j.dsr2.2017.03.010

Dorrell, R. M., Peakall, J., Sumner, E. J., Parsons, D. R., Darby, S. E., Wynn, R. B., Tezcan, D., 2016. Flow dynamics and mixing processes in hydraulic jump arrays: Implications for channel-lobe transition zones. Marine Geology, 381, 181-193

Durkin, P. R., Hubbard, S. M., Holbrook, J., Boyd, R., 2018. Evolution of fluvial meander-belt deposits and implications for the completeness of the stratigraphic record. Bullettin of the Geological Society of America Bulletin, 130(5–6), 721–739. https://doi.org/10.1130/B31699.1

Englert, R.G., Hubbard, S.M., Cartigny, M.J., Clare, M.A., Coutts, D.S., Hage, S., Hughes Clarke, J., Jobe, Z., Lintern, D.G., Stacey, C. and Vendettuoli, D., 2020. Quantifying the three-dimensional stratigraphic expression of cyclic steps by integrating seafloor and deep-water outcrop observations. Sedimentology

Farre, J., McGregor, B., Ryan, W. and Robb. J., 1983. Breaching of the shelfbreak: passage from youthful to mature phase in submarine canyon evolution. In: The Shelfbreak: Critical Interface on Continental Margin (eds. Stanley, D. and Moore, G), 25-39, Special Publication no. 33, Society of Economic Palaeontologists and Mineralogists

Fricke, A. T., Sheets, B. A., Nittrouer, C. A., Allison, M. A., Ogston, A. S., 2015. An examination of Froude-supercritical flows and cyclic steps on a subaqueous lacustrine delta, Lake Chelan, Washington, USA. Journal of Sedimentary Research, 85(7), 754-767

Fox, P.J., Heezen, B.C. and Harian, A.M., 1968. Abyssal anti-dunes. Nature, 220(5166), pp.470-472

Fuhrmann, A., Kane, I.A., Clare, M.A., Ferguson, R.A., Schomacker, E., Bonamini, E. and Contreras, F.A., 2020. Hybrid turbidite-drift channel complexes: An integrated multiscale model. Geology, 48(6), pp.562-568

Fonnesu, M., Palermo, D., Galbiatia, M., Marchesini, M., Bonaminia, E., Bendias, D., 2020. A new world-class deep-water play-type, deposited by the syndepositional interaction of turbidity flows and bottom currents: The giant Eocene Coral Field in northern Mozambique. Marine and Petroleum Geology 111, 179–201. https://doi.org/10.1016/j.marpetgeo.2019.07.047

Forel, F.A., 1888. Le ravin sous-lacustre du Rhône dans le lac Léman Bull. Soc. Vaud. Sci. Nat., 23 (1888), pp. 85-107

Gales, J.A., Talling, P.T., Cartigny, M.J.B., Hughes Clarke, Lintern, G., Stacey, C. and Clare, M.A., 2019. What controls submarine channel development and the morphology of deltas entering deep-water fjords? Earth Surface Process Landforms, 44, 535–551. https://doi.org/10.1002/esp.4515

Galy, V., France-Lanord, C., Beyssac, O., Faure, P., Kudrass, H., & Palhol, F., 2007. Efficient

organic carbon burial in the Bengal fan sustained by the Himalayan erosional system. Nature, 450(7168), 407

Ge, Z., Nemec, W., Gawthorpe, R.L., and Hansen, E.W.M., 2017. Response of unconfined turbidity current to normal-faulttopography. Sedimentology, 64, 932–959

Girardclos S, Hilbe M, Corella JP, Loizeau JL, Kremer K, DelSontro T, Arantegui A, Moscariello A, Arlaud F, Akhtman Y, Anselmetti F, Lemmin U (2012) Searching the Rhone delta channel inLake Geneva since Franc¸ois-Alphonse Forel. Arch Sci 65:103–118

Goldfinger, C., Morey, A.E., Nelson, C.H., Gutiérrez-Pastor, J., Johnson, J.E., Karabanov, E., Chaytor, J., Eriksson, A. and Party, S.S., 2007. Rupture lengths and temporal history of significant earthquakes on the offshore and north coast segments of the Northern San Andreas Fault based on turbidite stratigraphy. Earth and Planetary Science Letters, 254(1-2), pp.9-27

Green, A., 2011. Submarine canyons associated with alternating sediment starvation and shelf-edge wedge development: Northern KwaZulu-Natal continental margin. Marine Geology, 284, 114-126

Guiastrennec-Faugas, L., Gillet, H., Peakall, J., Dennielou, B., Gaillot, A. and Jacinto, R.S., 2021. Initiation and evolution of knickpoints and their role in cut-and-fill processes in active submarine channels. Geology, 49(3), pp.314-319

Gwiazda, R., Paull, C.K., Ussler III, W. and Alexander, C.R., 2015. Evidence of modern fine-grained sediment accumulation in the Monterey Fan from measurements of the pesticide DDT and its metabolites. Marine Geology, 363, 125-133

Hage, S., Cartigny, M.J., Sumner, E.J., Clare, M.A., Hughes Clarke, J.E., Talling, P.J., Lintern, D.G., Simmons, S.M., Silva Jacinto, R., Vellinga, A.J. and Allin, J.R., 2019. Direct monitoring reveals initiation of turbidity currents from extremely dilute river plumes. Geophysical Research Letters, 46. https://doi.org/10.1029/2019GL084526

Hage, S., Cartigny, M.J.B., Clare, M.A., Sumner, E.J., Vendettuoli, D., Hughes Clarke, J.E., Hubbard, S.M., Talling, P.J., Lintern, D.G., Stacey, C.D., Englert, R.G., Vardy, M.E., Hunt, J.E., Yokokawa, M., Parsons, D.R., Hizzett, J.L., Azpiroz-Zabala, M., Vellinga, A.J., 2018. How to recognise crescentic bedforms formed by supercritical tur-bidity currents in the geologic record: insights from active submarine channels. Geology. https://doi .org /10 .1130 /G40095 .1

Hage, S., Galy, V.V., Cartigny, M.J.B., Acikalin, S., Clare, M.A., Gröcke, D.R., Hilton, R.G., Hunt, J.E., Lintern, D.G., McGhee, C. A., Parsons, D.R., Stacey, C.D., Sumner, E.J. and Talling, 2020. Efficient preservation of young terrestrial organic carbon in sandy turbidity current deposits. Geology, 48. https://doi.org/10.1130/G47320.1

Hamilton, P. B., Strom, K., Hoyal, D. C., 2013. Autogenic incision-backfilling cycles and lobe formation during the growth of alluvial fans with supercritical distributaries. Sedimentology, 60(6), 1498-1525

Haughton, P.J., Davis, C., McCaffrey, W. and Barker, S., 2009. Hybrid sediment gravity flow

deposits – Classification, origin and significance. Marine and Petroleum Geology, 26, 1900–1918. https://doi.org/10.1016/j.marpetgeo.2009.02.012

Heerema, C., Talling, P.J., Cartigny, M.J.B., Paull, C., Bailey, L., Simmons, S., Parsons, D.R., Clare, M.A., Gwiazda, R., Lundsten, E., Anderson, K., Maier, K.L., Xu, J.P., Sumner, E.J., Rosenburger, K., Gales, J., McGann, M., Carter, L., Pope, E. and Monterey Coordinated Canyon Experiment (CCE) Team, 2020. What determines the downstream evolution of turbidity currents? Earth and Planetary Science Letters, 532, 116023. https://doi.org/10.1594/IEDA/324529

Heezen, B.C., Menzies, R.J., Schneider, R.J., Ewing, W.M. and Granelli, N.C.L., 1964. Congo submarine canyon. AAPG bulletin, 48(7), pp.1126-1149

Heijnen, M.S., Clare, M.A., Cartigny, M.J.B., Talling, P.J., Hage, S., Lintern, D.G., Stacey, C., Parsons, D.R., Simmons, S.M., Chen, Y., Sumner, E.J., Dix J.K. and Hughes Clarke, J.E., 2020. Rapidly-migrating and internally-generated knickpoints can control submarine channel evolution. Nature Communications, Vol. 11, 3129

Hickin, E.J., 1989. Contemporary Squamish River sediment flux to Howe Sound, British Columbia. Canadian Journal Earth Science, 26, 1953-1963

Hill, P.R., Conway, K., Lintern, D.G., Meulé, S., Picarda, K. and Barriea, J.V., 2008. Sedimentary processes and sediment dispersal in the southern Strait of Georgia, BC, Canada. Marine Environmental Research, Volume 66, Supplement, S39-S48

Hizzett, J.L., Hughes Clarke, J.E., Sumner, E.J., Cartigny, M.J.B., Talling, P.J. and Clare, M.A., 2018. Which triggers produce the most erosive, frequent and longest runout turbidity currents on deltas? Geophysical Research Letters, 45, 855–863. https://dx.doi.org/10.1002/2017GL075751

Hiscott, R.N., 1994. Loss of capacity, not competence, as the fundamental process governing deposition from turbidity currents. Journal of Sedimentary Research, 64(2a), pp.209-214

Hofstra, M., Hodgson, D.M., Peakall, J. and Flint, S.S., 2015. Giant scour-fills in ancient channel-lobe transition zones: Formative processes and depositional architecture. Sedimentary Geology, 329, pp.98-114

Hodson, J.M. and Alexander, J., 2010. The effects of grain-density variation on turbidity currents and some implications for the deposition of carbonate turbidites. Journal of Sedimentary Research, 80(6), pp.515-528.

Howarth, J.D., Orpin, A.R., Kaneko, Y., Strachan, L.J., Nodder, S.D., Mountjoy, J.J., Barnes, P.M., Bostock, H.C., Holden, C., Jones, K., and Cagatay, M.N., 2021. Calibrating the marine turbidite paloeoseismometer using the 2016 Kaikoura earthquake. Nature Geoscience, V.14, 161-167. https://doi.org/10.1038/s41561-021-00692-6

Hubbard, S.M., Jobe, Z.R., Romans, B.W., Covault, J.A., Sylvester, Z. and Fildani, A., 2020. The stratigraphic evolution of a submarine channel: Linking seafloor dynamics to depositional products. Journal of Sedimentary Research, 90(7), pp.673-686

Hubbard, S.M., Covault, J.A., Fildani, A. and Romans, B.W., 2014. Sediment transfer and

deposition in slope channels: Deciphering the record of enigmatic deep-sea processes from outcrop. GSA Bulletin, 126(5-6), pp.857-871

Hughes, D. J., Shimmield, T. M., Black, K. D., and Howe, J. A., 2015. Ecological impacts of large-scale disposal of mining waste in the deep sea. Scientific Reports. 5:9985. doi: 10.1038/srep09985

Hughes Clarke, J.E., 2018. Multibeam echosounders. In Submarine geomorphology (pp. 25-41). Springer, Cham

Hughes Clarke, J.E., 2016. First wide-angle view of channelized turbidity currents links migrating cyclic steps to flow characteristics. Nature Communication, 7, 11896. https://doi.org/10.1038/ncomms11896

Hughes Clarke, J.E., Brucker, S., Muggah, J., Hamilton, T., Cartwright, D., Church, I., and Kuus, P., 2012. Temporal progression and spatial extent of mass wasting events on the Squamish prodelta slope. In Landslides and engineered slopes: protecting society through improved understanding (pp. 1091-1096). Taylor and Francis Group London

Hughes Clarke, J.E., Brucker, S., Muggah, J., Church, I., Cartwright, D., 2011. The Squamish Delta Repetitive Survey Program: A simultaneous investigation of prodeltaic sedimentation and integrated system accuracy. From U.S. Hydrographic Conference. Conference Paper.

Hughes Clarke, J.E., Marques, C.R.V., Pratomo, D., 2014. Imaging active mass-wasting and sediment flows on a fjord delta, Squamish, British Columbia. In: Subma-rine Mass Movements and Their Consequences, vol. 37. Springer International Publishing, pp. 249–260.

Hughes Clarke, J.E., Garden, J.V., Torresan, M., Mayer, L., 1998. The limits of spatial resolution achievable using a 30kHz multibeam sonar: model predictions and field results. IEEE Oceanic Engineering Society. OCEANS'98. Conference Proceedings (Cat. No.98CH36259)

Hughes Clark, J.E., Shor, A.,N., Piper, D.J., Mayer, L.A., 1990. Large-scale current-induced erosion and deposition in the path of Grand Banks turbidity currents. Sedimentology, 37, 613-629

Hunt, J.E., Wynn, R.B., Talling, P.J. and Masson, D.G., 2013. Frequency and timing of landslide-triggered turbidity currents within the Agadir Basin, offshore NW Africa: Are there associations with climate change, sea level change and slope sedimentation rates?. Marine Geology, 346, pp.274-291.

Huvenne, V.A., Tyler, P.A., Masson, D.G., Fisher, E.H., Hauton, C., Hühnerbach, V., Le Bas, T.P. and Wolff, G.A., 2011. A picture on the wall: innovative mapping reveals cold-water coral refuge in submarine canyon. PloS one, 6(12), p.e28755

Imran, J., Khan, S.M., Pirmez, C. and Parker, G., 2017. Froude scaling limitations in modeling of turbidity currents. Environmental Fluid Mechanics, 17(1), pp.159-186

Inman, D.L., Nordstrom, C.E. and Flick, R.E., 1976. Currents in submarine canyons: An air-

sea-land interaction. Annual Review of Fluid Mechanics, 8 (1), 275-310

Jobe, Z. R., Howes, N., Romans, B. W., & Covault, J. A., 2018. Volume and recurrence of submarine-fan-building turbidity currents. The Depositional Record

Jobe, Z., Sylvester, Z., Pittaluga, M. B., Frascati, A., Pirmez, C., Minisini, D., Cantelli, A., 2017. Facies architecture of submarine channel deposits on the western Niger Delta slope: Implications for grain-size and density stratification in turbidity currents. Journal of Geophysical Research: Earth Surface, 122(2). https://doi.org/10.1002/2016JF003903

Kane, I.A., Clare, M.A., 2019. Dispersion, Accumulation, and the ultimate fate of microplastics in deep-marine environments: a review and futuredDirections. Frontiere Earth Science https://doi.org/10.3389/feart.2019.00080

Kane, I.A., Pontén, A.S., Vangdal, B., Eggenhuisen, J.T., Hodgson, D.M. and Spychala, Y.T., 2017. The stratigraphic record and processes of turbidity current transformation across deep-marine lobes. Sedimentology, 64(5), pp.1236-1273

Kao, S. J., Dai, M., Selvaraj, K., Zhai, W., Cai, P., Chen, S. N., and Syvitski, J. P., 2010. Cyclone-driven deep sea injection of freshwater and heat by hyperpycnal flow in the subtropics. Geophysical Research Letters, 37(21)

Khripounoff, A., Vangriesheim, A., Crassous, P. and Etoubleau, J., 2009. High frequency of sediment gravity flow events in the Var submarine canyon (Mediterranean Sea). Marine Geology, 263 (1-4), 1-6

Khripounoff, A., Crassous, P., Bue, N.L., Dennielou, B. and Jacinto, R.S., 2012. Different types of sediment gravity flows detected in the Var submarine canyon (northwestern Mediterranean Sea). Progress in Oceanography, 106, 138-153

Klaucke, I., Savoye, B., Cochonat, P., 2000. Patterns abd processes of sediments dispersal on the continental slope off Nice, SE France. Marine Geology, 162, 405-422

Kelner, M., Migeon, S., Tric, E., Couboulex, F., Dano, A. and Lebourg, T., 2016. Frequency and triggering of small-scale submarine landslides on decadal timescales: analysis of 4D bathymetric data from the continental slope offshore Nice (France). Marine Geology 379, 281–297

Kneller, B.C. and Branney, M.J., 1995. Sustained high-density turbidity currents and the deposition of thick massive sands. Sedimentology, 42, 607–616

Komar, P.D., 1973. Continuity of turbidity current flow and systematic variations in deep-sea channel morphology. Geological Society of America Bulletin, 84(10), pp.3329-3338

Kostic, S., 2014. Upper flow regime bedforms on levees and continental slopes: Turbidity current flow dynamics in response to fine-grained sediment waves. Geosphere, 10(6), pp.1094-1103

Kostic, S., & Parker, G. 2006. The response of turbidity currents to a canyon–fan transition: internal hydraulic jumps and depositional signatures. Journal of Hydraulic Research, 44(5), 631-653.

Kostic, S., Sequeiros, O., Spinewine, B., & Parker, G., 2010. Cyclic steps: A phenomenon of supercritical shallow flow from the high mountains to the bottom of the ocean. Journal of Hydro-environment Research, 3(4), 167-172

Kuenen, P.H., 1964. Deep-sea sands and ancient turbidites. In Developments in sedimentology (Vol. 3, pp. 3-33). Elsevier

Kuenen, P.H., 1966. Experimental turbidite lamination in a circular flume. The Journal of Geology, 74(5, Part 1), pp.523-545

Lang, J., Brandes, C., & Winsemann, J., 2017. Erosion and deposition by supercritical density flows during channel avulsion and backfilling: Field examples from coarse-grained deepwater channel-levée complexes (Sandino Forearc Basin, southern Central America). Sedimentary geology, 349, 79-102

Leeder, M. 1999. Sedimentology and Sedimentary Basins: From Turbulence to Tectonics. Oxford: Blackwell

Lintern, D.G., Hill, P.R., and Stacey, C., 2016. Powerful unconfined turbidity current captured by cabled observatory on the Fraser River delta slope, British Columbia, Canada. Sedimentology, 63 (5), 1041-1064. Chicago

Lowe, D.R., 1979 b. Sediment gravity flows: their classification and some problems of application to natural flows and deposits, Soc. Econ. Paleontologists Mineralogists Special Publication, 27, 75-82

Lowe, D.R., 1982. Sediment gravity flows; II, depositional models with special reference to the deposits of high-density turbidity currents. Journal of Sedimentary Petrology, 52, 279–297

Macdonald, H.A., Wynn, R.B., Huvenne, V.A., Peakall, J., Masson, D.G., Weaver, P.P. and McPhail, S.D., 2011. New insights into the morphology, fill, and remarkable longevity (> 0.2 my) of modern deep-water erosional scours along the northeast Atlantic margin. Geosphere, 7(4), pp.845-867

Mahanjane, E., Franke, D., 2014. The Ruvuma deep-water fold-and-thrust belt, offshore Mozambique. Tectonophsyics 614, 91–99

Mahon, R. C., Shaw, J. B., Barnhart, K. R., Hobley, D. E., and McElroy, B. 2015. Quantifying the stratigraphic completeness of delta shoreline trajectories. Journal of Geophysical Research: Earth Surface, 120(5), 799-817

Maier, K.L., Paull, C.K., Caress, D.W., Anderson, K., Nieminski, N.M., Lundsten, E.,Erwin, B.E., Gwiazda, R., Fildani, A., 2020. Submarine-fan development revealed by integrated high-resolution datasets from la Jolla Fan, Offshore California, U.S.A. Journal of Sedimentary Research, 2020, v. 90, 468–479 Current Ripples DOI: http://dx.doi.org/10.2110/jsr.2020.22

Maier, K.L., Gales, J.A., Paull, C.K., Rosenberger, K., Talling, P.J., Simmons, S.M., Gwiazda, R., McGann, M., Cartigny, M.J., Lundsten, E. and Anderson, K., 2019. Linking direct measurements of turbidity currents to submarine canyon-floor deposits. Frontiers in

Earth Science, 7, p.144

Maier, K.L., Rosenberger, K., Paull, C.K., Gwiazda, R., Gales, J., Lorenson, T., Barry, J.P., Talling, P.J., McGann, M., Xu, J. and Lundsten, E., 2019b. Sediment and organic carbon transport and deposition driven by internal tides along Monterey Canyon, offshore California. Deep Sea Research Part I: Oceanographic Research Papers, 103-108

Maier, K.L., Brothers, D.S., Paull, C.K., McGann, M., Caress, D.W. and Conrad, J.E., 2017. Records of continental slope sediment flow morphodynamic responses to gradient and active faulting from integrated AUV and ROV data, offshore Palos Verdes, southern California Borderland. Marine Geology, 393, pp.47-66

Mastbergen, D., van den Ham, G., Cartigny, M., Koelewijn, A., de Kleine M. and Clare M., 2016. Multiple flow slide experiment in the Westerschelde Estuary, The Netherlands. In: Submarine Mass Movements and Their Consequences, pp. 241–249. Springer International Publishing

Maselli, V., Kroon, D., Iacopini, D., Wade, B.S., Pearson, P.N., de Haas, H., 2020. Impact of the East African Rift System on the routing of the deep-water drainage network offshore Tanzania, western Indian Ocean. Basin Research, Volume 32, Issue 5, p. 789 - 803

Mayer, L.A., 2006. Frontiers in seafloor mapping and visualization. Marine Geophysical Researches 27, 7–17. DOI 10.1007/s11001-005-0267-x

McCave, I.N., 2017. Formation of sediment waves by turbidity currents and geostrophic flows: A discussion. Marine Geology, 390, pp.89-93

Middleton, G.V., 1966. Experiments on density and turbidity currents. I. Motion of the head. Canadian Journal of Earth Science, 3, 523-546

Middleton, G.V. and Hampton, M.A., 1976. Subaqueous sediment transport and deposition by sediment gravity flows, in Stanley, D. J., and Swift, D. J. P., eds., Marine Sediment Transport and Environmental Management. New York, Wiley, 197-218

Mitchell, N.C., 2006. Morphologies of knickpoints in submarine canyons. GSA Bulletin, 118(5-6), pp.589-605

Mohrig, D. and Marr, J.G., 2003. Constraining the efficiency of turbidity current generation from submarine debris flows and slides using laboratory experiments. Marine and Petroleum Geology, 20(6-8), pp.883-899

Moody, J. A., and Meade, R. H., 2014. Ontogeny of point bars on a river in a cold semi-arid climate. Bulletin of the Geological Society of America, 126(9–10), 1301–1316. https://doi.org/10.1130/B30992.1

Mountjoy, J.J., Howarth, J.D., Orpin,A.R., Barnes, P.M., Bowden, D.A., Rowden, A.A., Schimel, A.C.G., Holden, C., Horgan, H.J., Nodder, S.D., Patton, J.R., Lamarche, G., Gerstenberger, M., Micallef, A., Pallentin, A. and Kane, T., 2018. Earthquakes drive large-scale submarine canyon development and sediment supply to deep-ocean basins. Science Advances, 4, eaar3748

Mulder, T. and Cochonat, P., 1996. Classification of offshore mass movements. Journal of

Sedimentary Research, 66, 43–57

Mulder, T., Migeon, S., Savoye, B. and Faugères, J.C., 2001. Inversely graded turbidite sequences in the deep Mediterranean: a record of deposits from flood-generated turbidity currents?. Geo-Marine Letters, 21(2), pp.86-93

Mulder, T., Syvitskib, J.P.M., Migeonc, S., Fauge`resa, J.C. and Savoye, B., 2003. Marine hyperpycnal flows: initiation, behavior and related deposits. A review. Marine and Petroleum Geology, 20, 861–882. https://doi.org/10.1016/j.marpetgeo.2003.01.003

Mutti, E. and Normark, W.R., 1987. Comparing examples of modern and ancient turbidite systems: problems and concepts. In Marine clastic sedimentology (pp. 1-38). Springer, Dordrecht.Nakajima, T., & Itaki, T. (2007). Late Quaternary terrestrial climatic variability recorded in deep-sea turbidites along the Toyama Deep-Sea Channel, central Japan Sea. Palaeogeography, Palaeoclimatology, Palaeoecology, 247(1-2), 162-179

Mutti, E., Tinterri, R., Benevelli, G., di Biase, D. and Cavanna, G., 2003. Deltaic, mixed and turbidite sedimentation of ancient foreland basins. Marine and Petroleum Geology, 20 (6-8), 733-755

Nakajima, T., 2002. Laboratory experiments and numerical simulation of sediment-wave formation by turbidity currents. Marine Geology, 192(1-3), pp.105-121

Nash, I.F.J. and Roberts, P.M., 2011, January. MEIDP-The deep sea gas route to India. In Offshore Technology Conference. Offshore Technology Conference

Normandeau, A., Lajeunesse, P., Poiré, A.G. and Francus, P., 2016. Morphological expression of bedforms formed by supercritical sediment density flows on four fjord-lake deltas of the south-eastern Canadian Shield (Eastern Canada). Sedimentology, 63(7), pp.2106-2129

Normandeau, A., Lajeunesse, P., St-Onge, G., Bourgault, D., Drouin, S. S. O., Senneville, S., and Bélanger, S., 2014. Morphodynamics in sediment-starved inner-shelf submarine canyons (Lower St. Lawrence Estuary, Eastern Canada). Marine Geology, 357, 243-255

Normark, W. R., Piper, D. J., Posamentier, H., Pirmez, C., and Migeon, S., 2002. Variability in form and growth of sediment waves on turbidite channel levees. Marine Geology, 192(1-3), 23-58

Ono, K., and Björklund, P., 2018. Froude supercritical flow bedforms in deepwater slope channels? Field examples in conglomerates, sandstones and fine-grained deposits. Sedimentology, 65(3), 639-669

Orange, D.L., Teas, P.A. and Decker, J., 2010. Multibeam backscatter-insights into marine geological processes and hydrocarbon seepage. Offshore Technology Conference

Pantin, H. M., 1979. Interaction between velocity and effective density in turbidity flow: phase-plane analysis, with criteria for autosuspension. Marine Geology, 31(1-2), 59-99

Paola, C., Ganti, V., Mohrig, D., Runkel, A. C., and Straub, K. M., 2018. Time Not Our Time: Physical Controls on the Preservation and Measurement of Geologic Time. Annual Review of Earth and Planetary Sciences, 46, 409-438

Paola, C., Straub, K., Mohrig, D., Reinhardt, L., 2009. The “unreasonable effectiveness” of stratigraphic and geomorphic experiments. Earth Science Reviews 97 (1-4), 1-43

Parker, G., 1982. Conditions for the ignition of catastrophically erosive turbidity currents. Marine Geology, 46(3-4), 307-327

Parker, G., Fukushima, Y. and Pantin, H.M., 1986. Self-accelerating turbidity currents. Journal of Fluid Mechanisms, 171, 145. https://doi.org/10.1017/S002211208600140

Paull, C.K., Talling, P.J., Maier, K.L., Parsons, D., Xu, J., Caress, D.W., Gwiazda, R., Lundsten, E.M., Anderson, K., Barry, J.P., Chaffey, M., O’Reilly, T., Rosenberger, K.J., Gales, J.A., Kieft, B., McGann, M., Simmons, S.M., McCann, M., Sumner, E.J., Clare, M.A. and Cartigny, M.J., 2018. Powerful turbidity currents driven by dense basal layers. Nature Communications, 9, 4114. https://doi.org/10.1038/s41467-018-06254-6

Paull, C.K., Caress, D.W., Lundsten, E., Gwiazda, R., Anderson, K., McGann, M., Conrad, J., Edwards, B. and Sumner, E.J., 2013. Anatomy of the La Jolla submarine canyon system; offshore Southern California. Marine Geology, 335, pp.16-34

Paull, C.K., Caress, D.W., Ussler, W., Lundsten, E. and Meiner-Johnson, M., 2011. High-resolution bathymetry of the axial channels within Monterey and Soquel submarine canyons, offshore central California. Geosphere, 7(5), pp.1077-1101

Paull, C.K., Ussler III, W., Caress, D.W., Lundsten, E., Covault, J.A., Maier, K.L., Xu, J. and Augenstein, S., 2010a. Origins of large crescent-shaped bedforms within the axial channel of Monterey Canyon, offshore California. Geology, 6(6), pp.755-774

Paull, C.K., Mitts, P., Ussler III, W., Keaten, R. and Greene, H.G., 2005. Trail of sand in upper Monterey Canyon: offshore California. Geological Society America Bulletin,117, 1134–1145

Paull, C.K., Greene, H.G., Ussler, W., III, and Mitts, P.J., 2002, Pesticides as tracers of sediment transport through Monterey Canyon: Geo-Marine Letters, v. 22, p. 121–126

Piper, D.J. and Savoye, B., 1993. Processes of late Quaternary turbidity current flow and deposition on the Var deep-sea fan, north-west Mediterranean Sea. Sedimentology, 40(3), pp.557-582

Piper, D.J. and Normark, W.R., 2009. Processes that initiate turbidity currents and their influence on turbidites: a marine geology perspective. Journal of Sedimentary Research, 79(6), pp.347-362

Pohl, F., Eggenhuisen, J.T., Kane, I.A. and Clare, M.A., 2020. Transport and burial of microplastics in deep-marine sediments by turbidity currents. Environmental science & technology, 54(7), pp.4180-4189

Pope, E.L., Talling, P.J., Carter, L., Clare, M.A., Hunt, J.E., 2017. Damaging sediment density flows triggered by tropical cyclones. Earth Planet. Sci. Lett. 458, 161–169

Postma, G., 1986. Classification for sediment gravity-flow deposits based on flow conditions during sedimentation. Geology, 14, 291-294

Postma, G. and Cartigny, M.J., 2014. Supercritical and subcritical turbidity currents and their deposits—A synthesis. Geology, 42(11), pp.987-990

Prior, D.B., Bornhold, B.D., Wiseman, W.J. and Lowe, D.R., 1987. Turbidity current activity in a British Columbia fjord. Science, 237 (4820), 1330-1333

Ramsay, P, 1995. 9000 years of sea-level change along the southern African coastline. Quaternary International, 31, 71-75

Rabouille, C., Baudin, F., Dennielou, B. and Olu, K., 2017. Organic carbon transfer and ecosystem functioning I the terminal lobes of the Congo deep-sea fan: outcomes of the Congolobe project. Deep-Sea Research Part II, 142, 1-6. http://dx.doi.org/10.1016/j.dsr2.2017.07.006

Reesink, A. J. H., Van den Berg, J. H., Parsons, D. R., Amsler, M. L., Best, J. L., Hardy, R. J., & Szupiany, R. N., 2015. Extremes in dune preservation: controls on the completeness of fluvial deposits. Earth-science reviews, 150, 652-665

Reesink, C.V., Teasdale, J.P., and Mahanjane, E.S., 2016. Insight into the East Coast of Africa from a new tectonic model of the early Indian Ocean, in Nemčok, M., et al., eds., Transform Margins: De-velopment, Controls and Petroleum Systems: Geo-logical Society [London] Special Publication 431, p. 299–322, https://doi .org/10.1144/SP431.12

Reeves, C. V., Teasdale, J. P. and Mahanjane, E. S., 2016. Geological Society, London, Special Publications, 431, 299-322, https://doi.org/10.1144/SP431.12

Rohling, E. J., Grant, K., Bolshaw, M., Roberts, A. P., Siddal, M., Hemleben, C., and Kucera, M., 2009. Antarctic temperature and global sea level closely coupled over the past five glacial cycles. Nature Geoscience, 2(7), 500-504

Sadler, P. M., 1981. Sediment accumulation rates and the completeness of stratigraphic sections. The Journal of Geology, 89(5), 569-584

Salinas, J.S., Balachandar, S., Shringarpure, M., Fedele, J., Hoyal, D., Zuñiga, S. and Cantero, M.I., 2021. Anatomy of subcritical submarine flows with a lutocline and an intermediate destruction layer. Nature Communications, 12(1), pp.1-11

Salman, G., and Abdula, I., 1995. Development of the Mozambique and Ruvuma sedimentary basins, offshore Mozambique: Sedimentary Geology, v. 96, p. 7–41, https://doi .org/10.1016/0037-0738(95)00125-R

Savoye, B., Babonneau, N., Dennielou, B. and Bez, M., 2009. Geological over view of the Angola–Congo margin, the Congo deep-sea fan and its submarine valleys. Deep-Sea Research II, 56, 2169–2182. doi:10.1016/j.dsr2.2009.04.001

Schlünz, B., Schneider, R.R., 2000. Transport of terrestrial organic carbon to oceans by rivers: re-estimating flux- and burial rates. Int Journ Earth Science, 88, 599-606

Schwenk, J., Khandelwal, A., Fratkin, M., Kumar, V., and Foufoula-Georgiou, E., 2017. High spatiotemporal resolution of river planform dynamics from Landsat: The RivMAP toolbox and results from the Ucayali River. Earth and Space Science, 4(2), 46–75. Retrieved from http://doi.wiley.com/10.1002/2016EA000196

Sequeiros, O.E., 2012. Estimating turbidity current conditions from channel morphology: A Froude number approach. Journal of Geophysical Research: Oceans, 117(C4)

Silva, T.A., Girardclos, S., Stutenbecker, L., Bakker, M., Costa, A., Schlunegger, F., Lane, S.N., Molnar, P. and Loizeau, J-L., 2018. The sediment budget and dynamics of a delta-canyon-lobe system over the Anthropocene timescale: The Rhone River Delta, Lake Geneva (Switzerland/France). Sedimentology. https://doi.org/10.1111/sed.12519

Simmons, S.M., Azpiroz-Zabala, M., Cartigny, M. J. B., Clare, M. A., Cooper, C., Parsons, D. R., Pope, E. L., Sumner, E. J. and Talling, P. J., 2020. Novel acoustic method provides first detailed measurements of sediment 1 concentration structure within submarine turbidity currents. Geophysical Research: Oceans, 125, e2019JC015904. https://doi.org/10.1029/2019JC015904

Smith, D. P., Kvitek, R., Iampietro, P. J., and Wong, K., 2007. Twenty-nine months of geomorphic change in upper Monterey Canyon (2002–2005). Marine Geology, 236(1-2), 79-94

Smith, D.P., Ruiz, G., Kvitek, R., Iampietro, P., 2005. Semiannual patterns of erosion and deposition in upper Monterey Canyon from serial multibeam bathymetry. Geological Society of America Bulletin, 117 (9-10), 1123–1133

Spinewine, B., Sequeiros, O.E., Garcia, M.H., Beaubouef, R.T., Sun, T., Savoye, B. and Parker, G., 2009. Experiments on wedge-shaped deep sea sedimentary deposits in minibasins and/or on channel levees emplaced by turbidity currents. Part II. Morphodynamic evolution of the wedge and of the associated bedforms. Journal of Sedimentary Research, 79(8), pp.608-628

Stacey C.D., Hill, P.H., Talling P.J., Enkin, R.J., Hughes Clarke, J., Lintern, D.G., 2018: How turbidity currents frequency and character varies down a delta-fjord system: Combining direct monitoring, deposits and seismic data. Sedimentology

Stevenson, C.J., Feldens, P., Georgiopoulou, A., Schönke, M., Krastel, S., Piper, D.J., Lindhorst, K. and Mosher, D., 2018. Reconstructing the sediment concentration of a giant submarine gravity flow. Nature communications, 9(1), pp.1-7

Stow, D.A.V., Hernández-Molina, F.J., Llave, E., Sayago-Gil, M., Díaz del Río, V., Branson, A., 2009. Bedform-velocity matrix: The estimation of bottom current velocity from bedform observations. Geology, v. 37, no. 4, 327–330. doi: 10.1130/G25259A.1; 1 figure; Data Repository item 2009085.

Strauss, D., & Sadler, P. M., 1989. Stochastic models for the completeness of stratigraphic sections. Mathematical Geology, 21(1), 37-59

Straub, K. M., & Esposito, C. R., 2013. Influence of water and sediment supply on the stratigraphic record of alluvial fans and deltas: Process controls on stratigraphic completeness. Journal of Geophysical Research: Earth Surface, 118(2), 625-637

Sumner, E.J. and Paull, C.K., 2014. Swept away by a turbidity current in Mendocinosubmarine canyon, California. Geophys. Res. Lett., 41,7611–7618,

doi:10.1002/2014GL061863

Syahnur, Y. and Jaya, K.A., 2016. Geomatics best practices in Saka Indonesia Pangkah Limited (Case Study: Ujung Pangkah Pipeline Integrity). 2015 Indonesian Petroleum Association Convention

Sylvester, Z., Pirmez, C., & Cantelli, A., 2011. A model of submarine channel-levee evolution based on channel trajectories: Implications for stratigraphic architecture. Marine and Petroleum Geology, 28(3), 716–727. Retrieved from http://dx.doi.org/10.1016/j.marpetgeo.2010.05.012

Symons, W.O., Sumner, E.J., Talling, P.J., Cartigny, J.B., Clare, M.A., 2016. Large-scale sediment waves and scours on the modern seafloor and their implications for the prevalence of supercritical flows. Marine Geology, 371, 130–148, http://dx.doi.org/10.1016/j.margeo.2015.11.009

Symons, W.O., Sumner, E.J., Paull, C.K., Cartigny, M.J., Xu, J.P., Maier, K.L., Lorenson, T.D. and Talling, P.J., 2017. A new model for turbidity current behavior based on integration of flow monitoring and precision coring in a submarine canyon. Geology, 45(4), pp.367-370

Syvitski, J.P.M, Smith, J.N., Calabrese, E.A., Boudreau, B.P., 1988. Basin sedimentation and the growth of prograding deltas. Journal of Geophysical Research, 93 (No. C6), 6895-6908

Stow, D.V., Bowen, A.J., 1980. A physical model for the transport and sorting of fine-grained sediment by turbidity currents. Sedimentolgy, 27, 31-46

Talling, P. J., Wynn, R. B., Masson, D. G., Frenz, M., Cronin, B. T., Schiebel, R., and Amy, L. A., 2007. Onset of submarine debris flow deposition far from original giant landslide. Nature, 450, 541-544

Talling, P.J., Masson, D.G., Sumner, E.J. and Malgeisni, G., 2012. Subaqueous sediment density flows: Depositional processes and deposit types. Sedimentology. https://doi.org/10.1111/j.1365-3091.2012.01353.x

Talling, P.J., Paull, C.K., and Piper, D.J., 2013. How are subaqueous sediment density flows triggered, what is their internal structure and how does it evolve? Direct observations from monitoring of active flows. Earth-Science Reviews, 125, 244-287

Talling, P. J., 2014. On the triggers, resulting flow types and frequencies of subaqueous sediment density flows in different settings. Marine Geology, 352, 155-182

Talling, P. J., Allin, J., Armitage, D. A., Arnott, R. W., Cartigny, M. J., Clare, M. A., and Hill, P. R., 2015. Key Future Directions For Research On Turbidity Currents and Their Deposits. Journal of Sedimentary Research, 85(2), 153-169

Trabucho-Alexandre, J., 2014. More gaps than shale: erosion of mud and its effect on preserved geochemical and palaeobiological signals. From: Smith, D. G., Bailey, R. J., Burgess, P. M. & Fraser, A. J. (eds) Strata and Time: Probing the Gaps in Our Understanding. Geological Society, London, Special Publications, 404, http://dx.doi.org/10.1144/SP404.10

Tubau, X., Paull, C.K., Lastras, G., Caress, D.W., Canals, M., Lundsten, E., Anderson, K., Gwiazda, R. and Amblas, D., 2015. Submarine canyons of Santa Monica Bay, Southern California: variability in morphology and sedimentary

Van der Mark, C.F. and Blom, A., 2007. A new and widely applicable tool for determining the geometric properties of bedforms. SSN 1568-4652, CE&M research report 2007R-003/WEM-002

Van der Mark, C.F., Blom, A. and Hulscher, S. J. M. H., 2008. Quantification of variability in bedform geometry. Journal of Geophysical Research, Vol. 113, F03020, doi:10.1029/2007JF000940, 2008

Van den Berg, J. H., Martinius, A. W., and Houthuys, R., 2017. Breaching-related turbidites in fluvial and estuarine channels: Examples from outcrop and core and implications to reservoir models. Marine and Petroleum Geology, 82, 178-205

Vellinga, A.J., Cartigny, M.J.B., Hansen, E.W.M., Talling, P.J., Clare, M.A., Sumner, E.J., 2016. Process-based modelling of turbidity currents: from computational fluiddynamics to depositional signature. Conference Paper. DOI: 10.3997/2214-4609.201600374

Vellinga, A.J., Cartigny, M.J.B., Eggenhuisen, J.T., and Hansen, E.W., 2018. Morphodynamics and depositional signature of lowaggradation cyclic steps: New insights from a depth-resolved numerical model. Sedimentology 65, 540–560

Vendettuoli, D. 2016. What is the depositional and architectural signature of turbidity current activity? New insights from the most extensive dataset yet recorded. (Unpublished master's thesis). Royal Holloway University of London, Egham

Vendettuoli, D., Clare, M.A., Hughes Clarke, J.E., Vellinga, A., Hizzet, J., Hage, S., Cartigny, M.J.B., Talling, P.J., Waltham, D., Hubbard, S.M., Stacey, C., Lintern, D.G., 2019. Daily bathymetric surveys document how stratigraphy is built and its extreme incompleteness in submarine channels. Earth Planet. Sci. Lett. 515, 231–247

Whittaker, A.C. and Boulton, S.J., 2012. Tectonic and climatic controls on knickpoint retreat ratesand landscape response times. Journal of Geophysical Reasearch, Vol. 117, doi:10.1029/2011JF002157

Wood, J. D., 2013. Ocean Current Measurements at the Elang-1 Location, Cenderawasih Bay, Eastern West Papua, Indonesia, July 2012 to December 2013. Ocean Data Technologies, Inc. technical report prepared for Niko Resources Ltd., Jakarta, Indonesia

Wynn, R.B., Weaver, P.P., Ercilla, G., Stow, D.A. and Masson, D.G., 2000. Sedimentary processes in the Selvage sediment-wave field, NE Atlantic: new insights into the formation of sediment waves by turbidity currents. Sedimentology, 47(6), pp.1181-1197

Wynn, R.B. and Stow, D.A.V., 2002. Classification and characterisation of deep-water sediment waves. Marine Geology, 192, 7–22

Wynn, R.B., Kenyon, N.H., Masson, D.G., Stow, D.A. and Weaver, P.P., 2002. Characterization and recognition of deep-water channel-lobe transition zones. AAPG bulletin, 86(8), pp.1441-1462

Wynn, R. B., Piper, D. J., & Gee, M. J., 2002. Generation and migration of coarse-grained sediment waves in turbidity current channels and channel–lobe transition zones. Marine Geology, 192(1-3), 59-78

Wynn, R.B., Huvenne, V.A., Le Bas, T.P., Murton, B.J., Connelly, D.P., Bett, B.J., Ruhl, H.A., Morris, K.J., Peakall, J., Parsons, D.R. and Sumner, E.J., 2014. Autonomous Underwater Vehicles (AUVs): Their past, present and future contributions to the advancement of marine geoscience. Marine Geology, 352, pp.451-468

Xu, J.P., Barry, J.P., Paull, C.K., 2013. Small-scale turbidity currents in a big submarine canyon. Geology, 41(2): 143-146. https://doi.org/10.1130/G33727.1

Xu, J.P. and Noble, M.A., 2004. In-situ measurements of velocity structure within turbidity currents. Geophysical research Letters, V.31, L09311, doi:10.1029/2004GL019718

Xu, J.P., Wong, F.L., Kvitek, R., Smith, D.P. and Paull, C.K., 2008. Sandwave migration in Monterey Submarine Canyon, Central California. Marine Geology 248, 193–212

Xu, J.P., 2010. Normalised velocity profiles of field-measured turbidity currents. Geology, 38(6), pp.563-566.

Xu, J.P. 2011. Measuring currents in submarine canyons: Technological and scientific progress in the past 30 years. Geosphere 7 (4): 868–876

Zeng, J., Lowe, D.R., Prior, D.B., WISEMAN JR, W.J. and Bornhold, B.D., 1991. Flow properties of turbidity currents in Bute Inlet, British Columbia. Sedimentology, 38(6), pp.975-996

Zhong, G. and Peng, X., 2021 Transport and accumulation of plastic litter in submarine canyons. The role of gravity flows. Geology, v. 49. https://doi.org/10.1130/G48536.